

Finite-size effects in high dimensional physical systems



A thesis submitted for the degree of
Doctor of Philosophy
at Monash University in 2018

Jens C. Grimm

Bachelor of Science, LMU Munich, 2011

Master of Science, LMU Munich, 2014

School of Mathematical Sciences

Monash University, Australia

June, 2018

Copyright notice

I certify that I have made all reasonable efforts to secure copyright permissions for third-party content included in this thesis and have not knowingly added copyright content to my work without the owner's permission.

© Jens C. Grimm (2018).

Abstract

This thesis consists of two parts.

In the main part, we will study finite-size effects on high-dimensional physical systems. It is well-known that models of critical phenomena typically possess an upper critical dimension, d_c , such that in dimensions $d \geq d_c$, their thermodynamic behaviour is governed by critical exponents taking simple mean-field values. In contrast to the simplicity of the thermodynamic behaviour, the theory of finite-size scaling in dimensions above d_c is surprisingly subtle, and remains the subject of ongoing debate. We address this long-standing debate, by introducing a *random-length* random walk model, which we then study rigorously. We prove that this model exhibits the same universal FSS behaviour previously conjectured for the self-avoiding walk and Ising model on finite boxes in high-dimensional lattices. Our results show that the mean walk length of the random walk model controls the scaling behaviour of the corresponding Green's function. We numerically demonstrate the universality of our rigorous findings by extensive Monte Carlo simulations of the Ising model and self-avoiding walk on five-dimensional hypercubic lattices with free and periodic boundaries.

In the second part, we will numerically compare the efficiency of various Markov-chain Monte Carlo algorithms for simulating the zero-field ferromagnetic Ising model. In particular, we will design an irreversible algorithm for the Ising model by using the lifting technique. Even though lifting is considered as a promising method to speed up Markov-chain Monte Carlo algorithms, it is an open question how it affects efficiency in specific examples. We will numerically study the dynamic critical behavior of an energy-like observable on both the complete graph and toroidal grids, and compare our findings with reversible worm algorithms. Our results show that the lifted algorithm improves the dynamic exponent of the energy-like observable on the complete graph, and leads to a significant constant improvement on high-dimensional toroidal grids.

Declaration

This thesis contains no material which has been accepted for the award of any other degree or diploma at any university or equivalent institution and that, to the best of my knowledge and belief, this thesis contains no material previously published or written by another person, except where due reference is made in the text of the thesis.



Jens C. Grimm

29/06/2018

Publications during enrollment

- Part 1, Section 3.2 is based on the article *Geometric Explanation of Anomalous Finite-Size Scaling in High Dimensions*, published in Phys. Rev. Lett. 118, 115701, 2017. The article was joint work with Youjin Deng, Eren M. Elçi, Timothy M. Garoni and Zongzheng Zhou.
- The main results from Chapter 3 and 4 (Part 1) are based on the article *Random-length random walks and finite-size scaling in high dimensions* which is available on arXiv:1809.00515 [cond-mat.stat-mech]. The article was joint work with Youjin Deng, Sheng Fang, Timothy M. Garoni and Zongzheng Zhou.
- Part 2 is based on the article *Lifted worm algorithm for the Ising model*, published in Phys. Rev. E 97, 042126, 2018. The article was joint work with Youjin Deng, Lijie Ding, Eren M. Elçi, Timothy M. Garoni, and Abraham Nasrawi.

*If you always do what you've
always done, you'll always be
where you've always been.*

Acknowledgments

- **Timothy M. Garoni:** First and foremost, I would like to thank my main supervisor Tim Garoni. Thank you very much for every single discussion in Melbourne, Newcastle, Kiama, Berlin, Lyon and Auckland. Thank you for your mentorship and guidance during the last three years in Australia. I enjoyed my PhD under your supervision very much. All the best for the future, boss.
- **Zongzheng Zhou (周宗政):** 谢谢你和我在澳大利亚和新西兰的美好时光，以及你对我博士第二年和第三年的支持。我非常享受和你的讨论。我希望你的家人一切顺利，并希望你能享受你的时光。
- **Youjin Deng (邓友金):** 您不仅是一个伟大的学者，而且有着一个不断前进的深刻个性。非常感谢您对我的支持。我希望您可以永远保持对科学的好奇和热忱。
- Many thanks to our collaborators **Andrea Collevocchio, Lijie Ding, Eren M. Elçi, Sheng Fang** and **Aby Nasrawi** for fruitful discussions and great support.
- **Lothar Ebeling-Brand:** Vielen Dank, dass Du mich während meiner Schulzeit für theoretische Physik begeistert hast. Dein stets sehr motivierender und herausfordernder Unterricht wird mir immer in besonderer Erinnerung bleiben.
- **John K. Chan:** Il est rare de rencontrer des gens réellement passionnés par leur travail, des gens qui poussent les choses au-delà de l'ordinaire. John est l'un d'entre eux. Merci beaucoup.
- **Kevin Leckey:** Barabende, Gaming, Crown Casino und der Melbourne Central Language Exchange werden immer Erlebnisse sein, an die ich mich gerne zurück erinnere. Es war eine super Zeit. Vielen Dank dafür, Kevin.
- **Alin R. Paraschiv and Daniela A. Lăcătuș:** Vă mulțumesc pentru ospitalitatea deosebită și conversațiile profunde despre absolut tot ce am discutat în universitate cât și în afară. Mi-a plăcut foarte mult să văd pasiunea pe care amândoi o aveți pentru cercetare, și sper ca întotdeauna să păstrați această curiozitate. Mult success pe viitor!
- **Özge M. Özçakır:** Beraber katıldığımız, Avustralya Açık, Golf, Monash Tower gibi etkinlikleri hep güzel hatırlayacağım. Hoşça geçirdiğimiz zamanlar için teşekkürler.

- **Sajjad and Sobhan Hosseini:** بابت پاب کرول، خاطرات ارزشمند بسیاری باهم داشتیم. گفتگوهای پرمعنا و میرزا قاسمی های بسیار ممنون و سپاسگذارم و آرزوی بهترین ها را برایتان دارم. آشنایی و دوستی با شما مایه سرافرازی من بود.
- **Sarah and Maryam Jabbari:** به خاطر همه لحظه های خاص و ارزشمندی که با هم سپری کردیم متشکرم. خوشحالم که گرسنگی نکشیدید و به سمت ماه پرواز کردید. آرزوی بهترینها برای شما در سوئد، استرالیا، آلمان و یا در هر کجای دنیا که آرزوهایتان شما را ببرد، دارم.
- **Nima Sadeghi:** سفرهایمان به رستوران های عالی در ملبورن به پایان رسید. مکالمه هایمان در انگلیش کانکت و سفرمان به مورنینگتون پنینشولا همیشه جزء بهترین خاطراتم خواهد بود. آرزوی بهترینها را برایتان دارم و بابت همه لحظات خوشی که با هم سپری کردیم ممنونم.
- **Abbas Raboonik:** بابت مکالمه هایمان داخل و خارج دانشگاه ممنونم و امیدوارم بهترین لحظات SanQ را در استرالیا سپری کنید. افشین امیدوارم همیشه اشتیاق برای فیزیک را حفظ کنی.
- **Oscar Rodríguez Trujillo:** Finalmente descubrí que no eres de Suramérica. Hablando en serio, mil gracias por las conversaciones que tuvimos. Te deseo lo mejor en tu futuro y disfruta de tu tiempo aquí en Australia.
- **Dhananjay Thiruvady:** Thank you, DJ, for our interesting, valuable and meaningful conversations. All the best for your future.
- Many thanks to my office mates in room 336 for providing a nice working environment. More generally, I would like to thank all math PhD students for fun discussions in the coffee kitchen.
- Many thanks to my mates from the Monash table tennis club. I would like to thank the club members and our team for great memories at the club, the Australian and Southern Uni Games in Perth, in Geelong and at the Gold Coast.
- Some outstanding persons. I would like to thank my friends **Henning P., Michael R., Roland B., Julian L., Fabian N., Patrick A., Tobias J., Markus K., Javier C., Peter K., and Lini B.** (Dankschwa!).
- Last but not least, thank you **Mum and Dad** for..... *everything*.

Contents

Introduction	1
I Finite-size Scaling above the upper critical dimension	1
1 Introduction	2
1.1 Literature Overview	2
1.2 Outline of Part 1	6
2 Models	8
2.1 Random-length Models	8
2.1.1 Why study Random-length Models?	8
2.1.2 Random-length Random Walk (RLRW)	9
2.1.3 Random-length Loop-erased Random Walk (RLLERW)	10
2.2 n-vector models	12
2.2.1 Ising model in a loop representation	12
2.2.2 Self-avoiding Walk in the variable length ensemble	13
2.3 Observables	13
2.4 Numerical details	14
3 FSS on hypercubic lattices with PBC	16
3.1 Random-length Random Walk	16
3.1.1 Preliminaries	18
3.2 Random-length Random Walk	18
3.2.1 Preliminaries	18
3.2.2 RLRW Green's function on \mathbb{Z}^d	19
3.2.3 RLRW Green's function on a box with PBC	24
3.2.4 Lemmas	34
3.3 SAW and Ising model at criticality	43

3.3.1	Two-point functions and susceptibility	44
3.3.2	Windings and unwrapped two-point functions	44
3.4	SAW and Ising model at pseudo-critical points	47
4	FSS on hypercubic lattices with FBC, RBC and HBC	55
4.1	RLRW on a box with RBC and HBC	56
4.1.1	Preliminaries	57
4.1.2	RLRW Green's function on a box with RBC and HBC	58
4.2	SAW and Ising model at criticality	63
4.3	SAW and Ising model at pseudo-criticality	64
5	Discussion	70
II	Lifted worm algorithm for the Ising model	76
1	Introduction	77
1.1	Outline	78
2	Worm algorithms	80
2.1	P-S Worm Algorithm	80
2.2	Irreversible Worm Algorithm	81
2.2.1	B-S type Worm Algorithm	81
2.2.2	Irreversible Worm Algorithm	84
3	Time scales and numerical setup	85
3.1	Time Scales in MCMC algorithms	85
3.2	Numerical Setup	86
4	Results	88
4.1	Toroidal grids	88
4.2	Complete graph	89
5	Outlook	93
A	Appendix	95

CONTENTS

A.1 Estimation with the Madras-Sokal automatic windowing algorithm and suppressed slow modes	95
A.2 Least square fitting a weighted exponential ansatz	96

Part I

Finite-size Scaling above the upper critical dimension

Introduction

1.1 Literature Overview

In critical phenomena, continuous phase transitions are characterized by a singular behaviour of the correlation length in the thermodynamic limit. Close to a critical point, physical observables exhibit a power-law behaviour with corresponding critical exponents. Important examples are the scaling of the correlation length $\xi \simeq |T - T_c|^{-\nu}$, the two-point function $g(\mathbf{x}) \simeq \|\mathbf{x}\|^{2-d+\eta}$, and the susceptibility $\chi \simeq |T - T_c|^{-\gamma}$.

Finite-size scaling (FSS) is a fundamental physical theory within statistical mechanics describing the asymptotic approach to the thermodynamic limit of finite systems in the neighbourhood of a critical phase transition [1, 2, 3]. Finite systems are characterized by three length scales; ξ , the linear system size L of the underlying lattice, and the microscopic length a which quantifies the range of interactions in the lattice. Close to a critical point, the finite-size scaling hypothesis [2] assumes that the microscopic length a can be neglected, and $\xi \approx L$. Within this framework, FSS allows the extraction of critical exponents from finite size data. As an illustration, the leading scaling behaviour of the susceptibility is given by $\chi \simeq |T - T_c|^{-\gamma} \simeq L^{\gamma/\nu}$.

It is well-known [4] that models of critical phenomena typically possess an upper critical dimension, d_c , such that in dimensions $d \geq d_c$, their thermodynamic behaviour is governed by critical exponents taking simple mean-field values. Important examples with $d_c = 4$ are the Ising model [5, 6, 7, 8, 9], the self-avoiding walk [10, 11] and the

Loop-Erased Random Walk [12].

In contrast to the simplicity of the thermodynamic behaviour, the theory of FSS on high-dimensional hypercubic lattices with either free and periodic boundary conditions is surprisingly subtle, and remains the subject of ongoing debate, see e.g. [34, 35, 30, 29, 32, 33] for the most recent work.

We first consider the debate on **periodic** boundaries. In 1982, Brezin [13] argued via renormalization group arguments that standard FSS fails above d_c by studying the lattice ϕ^4 Hamiltonian on a d -dimensional hypercubic lattice with periodic boundaries. This breakdown was explained in 1983 by Fisher and Privman [14, 15] by dangerous irrelevant variables in the renormalization group. In 1985, Binder *et al.* [16, 17] investigated the consequence of dangerous irrelevant variables on the scaling behaviour of the free energy for the Ising model, and numerically investigated the critical FSS behaviour of the renormalized coupling constant and the susceptibility. It was numerically observed that the susceptibility scales as $L^{d/2}$, in contrast to the standard mean-field scaling L^2 . This conjecture was supported by studying linear systems up to $L = 7$. In the same year Brezin and Zinn-Justin [18] theoretically studied the continuous ϕ^4 field Hamiltonian via renormalization group on a d -dimensional hypercubic lattice with periodic boundaries, and calculated the renormalized coupling constant at criticality. The value for the renormalized coupling constant in [18] deviated significantly from both the numerical result in [16, 17] and another numerical study by Rickwardt *et al.* [19] who were able to study linear system sizes up to $L = 17$. It was debated whether these discrepancies were caused by large finite-size effects in the Monte Carlo studies, or if the continuous ϕ^4 field Hamiltonian in [18] was insufficient to describe the behaviour of the Ising model above d_c . In 1996, Luijten and Blöte [20] reinvestigated the value of the renormalized coupling constant at criticality. Instead of studying the short-range Ising model in high dimensions, where it is computationally difficult to simulate large systems, Luijten and Blöte simulated models with ferromagnetic long-range interactions decaying with $\|\mathbf{x}\|^{-d-\sigma}$. It is known rigorously [21] that these long range Ising models have upper critical dimension $d_c = 2\sigma$. The numerical observations in [20] were in excellent agreement with the calculated value of g in [18]. It was concluded that the discrepancy with the former Monte Carlo results was caused by corrections to scaling.

In 1998, Chen and Dohm [22, 23, 24] provided new theoretical insights for the finite-size scaling theory on periodic boundaries above d_c . Chen and Dohm reinvestigated the theoretical predictions in [18] by comparing the scaling behaviour for the continuous ϕ^4 field Hamiltonian with the lattice ϕ^4 Hamiltonian of the $O(n)$ model

in the large n limit. It was theoretically argued, without using renormalization group arguments, that the susceptibility scales as L^{d-2} in the case of the continuous ϕ^4 field Hamiltonian, while it scales as $L^{d/2}$ in the case of the lattice ϕ^4 Hamiltonian. The latter result is in agreement with the theoretical predictions for the spherical model [13], the mean-spherical model [25] and also matches with the numerical observation for the susceptibility of the Ising model [17, 26]. It was concluded that the leading finite-size effects of spin systems on high-dimensional lattices with periodic boundaries are not correctly described by the continuous ϕ^4 field Hamiltonian studied in [18], and that the recent interpretations of Monte Carlo results in [16, 17, 19, 20] are therefore inconclusive. In [27], Binder *et al.* summarized the situation as follows ‘Thus we arrive at a rather disappointing state of affairs. Although for the ϕ^4 theory in $d = 5$ dimensions all exponents are known, including those of the corrections to scaling, and in principle very complete analytical calculations are possible, the existing theories clearly are not so good’.

In 2006, Papathanakos [28] reinvestigated the finite-size effects of the Ising model above d_c by using a geometric representation. As opposed to former studies, the results in [28] are mathematically rigorous. Instead of studying the Ising model as an interacting spin model, Papathanakos used so-called random-current and random-path representations [7, 8] which represent physical observables in terms of weighted averages over geometric objects. Using these representations, it was proved that the Ising two-point function satisfies

$$g(\mathbf{x}) \geq \begin{cases} c_1 \|\mathbf{x}\|^{-(d-2)}, & \|\mathbf{x}\| \leq c_2 L^{d/[2(d-2)]} \\ c_3 L^{-d/2}, & \|\mathbf{x}\| \geq c_2 L^{d/[2(d-2)]} \end{cases}$$

where c_1, c_2, c_3 are constants, and as a direct consequence that the susceptibility scales as

$$\chi \geq \text{const} \times L^{d/2}. \quad (1.1)$$

Moreover, it was conjectured that these equations also govern the correct asymptotic behaviour for $g(\mathbf{x})$ and χ . In recent years, the correct scaling of the two-point function has been reinvestigated [29, 30]. In contrast to the conjecture of Papathanakos, Kenna and Berche [29] argued by using a renormalization group argument that $g(\mathbf{x}) \asymp \|\mathbf{x}\|^{-d+2+\eta_Q}$ above d_c . Here, η_Q is a new critical exponent different to the standard exponent η . The need for a new exponent was refuted by Wittmann and Young [30] by analyzing the Fourier modes in the Ising model.

In recent years, the FSS behaviour of the Ising model on hypercubic lattices with

free boundaries has been the subject of ongoing debate. The debate primarily concerns the connection to the observed scaling behaviour on periodic boundaries at both the infinite-volume critical point and at pseudo-critical points. First, we consider the critical case. Lundow and Markström [31] numerically investigated the FSS behaviour of the susceptibility on five-dimensional hypercubic lattices by studying linear system sizes up to $L = 20$. It was numerically observed that $\chi \asymp L^2$, in agreement with the expected mean-field critical behaviour of the susceptibility, but in contrast to the FSS behaviour on hypercubic lattices with periodic boundaries. The scaling $\chi \asymp L^2$ on free boundaries was refuted by Berche *et al.* [32] who argued that the numerical observations in [31] are inconclusive since the effect of the boundary for the systems sizes simulated is too large. In particular, it was heuristically argued that χ does not exhibit the standard mean-field expectation $\chi \asymp L^2$ at criticality. This argument was numerically supported by studying linear system sizes up to $L = 51$. In a response, Lundow and Markström [33] reinvestigated the FSS behaviour of the susceptibility on free boundaries at criticality. In agreement with their former result in [31] and in contrast to [32], it was numerically observed that $\chi \asymp L^2$ by studying linear systems up to $L = 160$. This susceptibility scaling has been numerically confirmed by Wittmann and Young [30], and has been accepted as the correct scaling behaviour at criticality by Flores-Sola *et al.* in [35].

We now consider the scaling behaviour at pseudo-critical points. Berche *et al.* [32] numerically observed the anomalous scaling behaviour $\chi \asymp L^{d/2}$ on free boundaries at the pseudo-critical point T_L , defined to be the temperature which maximizes $\chi(T_L, L)$ ¹ in finite boxes with side length L . Moreover, it was numerically investigated how T_L scales with L (“shifting”), and how the width of χ at half height scales with L (“rounding”). It was numerically observed that the shift exponent is equal to 2 while the rounding exponent equals $d/2$. It was heuristically argued that this observation leads to different scaling behaviours of χ at criticality and at T_L . The scaling behaviour of $\chi(T_L, L)$ was re-investigated by Wittmann and Young in [30], and, more recently, by Lundow and Markström in [34]. Wittmann and Young [30] investigated the Fourier modes of the Ising model. It was theoretically argued that the anomalous FSS behaviour $\chi \asymp L^{d/2}$ originates from the $k = 0$ mode, while $\chi \asymp L^2$ for $k \neq 0$. This argument was supported by a numerical study with linear system sizes up to $L = 36$, and their results were in agreement with the finding $\chi \asymp L^{d/2}$ at T_L from [32]. In contrast to [32] and [30], Lundow and Markström [34] proposed a different scaling of the susceptibility by numerically studying the Ising model up to $L = 79$. It was numerically observed that $\chi(T_L, L)$ scales as L^2 , in agreement with the critical case

¹Strictly speaking, the modulus susceptibility $\bar{\chi}$, defined in Chap. 4, was maximized in [32].

on free boundaries.

In Part 1 of the thesis, we introduce a random-length random walk model (RLRW) to address the debate regarding the FSS behaviour of the Ising model on finite boxes with periodic and free boundary conditions above d_c . We prove that the mean walk length $\langle \mathcal{N} \rangle$ of this random walk model controls the scaling behaviour of the corresponding Green's function. Informed by this observation, we numerically investigate self-avoiding walks (SAW) which are in the same universality class as the Ising model above $d_c = 4$. We establish the FSS behaviour of the SAW mean walk length $\langle \mathcal{N}_{\text{SAW}} \rangle$ at both the infinite-volume critical point and at pseudo-critical points, and investigate the FSS behaviour of the SAW two-point function. Our central result is that if $\langle \mathcal{N}_{\text{RLRW}} \rangle$ is chosen to scale as $\langle \mathcal{N}_{\text{SAW}} \rangle$, then the SAW two-point function displays the same behaviour as the RLRW Green's function. This strongly suggests that the FSS behaviour of the SAW two-point function only depends on the boundary conditions through their effect on $\langle \mathcal{N} \rangle$. We numerically verify the universality of our observations for the two-point function of the Ising model.

1.2 Outline of Part 1

We now present an outline of Part 1.

- In Chapter 2, we define the investigated models and observables. We, moreover, introduce the algorithms used, and present our numerical methodology.
- In Chapter 3, we investigate finite-size effects on hypercubic lattices with *periodic* boundaries (PBC). Chapter 3 consists of the following sections:
 - In 3.2, we rigorously establish the FSS behaviour of the Green's function of a random-length random walk on both tori and on the infinite-lattice \mathbb{Z}^d . Our theorem shows that the mean walk length of the random-length random walk controls the scaling behaviour of its Green's function.
 - In 3.3, we numerically study the critical PBC behaviour of the two-point function and susceptibility of the self-avoiding walk and the Ising model. We establish the geometric reason for anomalous FSS behaviour on tori, and show that anomalous effects can be removed by defining an alternative two-point function on the torus.
 - In 3.4, we numerically study the FSS behaviour of the two-point function and susceptibility of the self-avoiding walk and the Ising model at pseudo-critical points. In particular, we establish a pseudo-critical point where the

two-point functions and susceptibility exhibit standard mean-field scaling.

- In Chapter 4, we investigate finite-size effects on hypercubic lattices with *reflective* (RBC), *holding* (HBC) and *free* boundaries (FBC). Chapter 4 consists of the following sections:
 - In 4.1, we rigorously study the Green’s function behaviour of a random-length random walk model on hypercubic lattices with reflective and holding boundary conditions.
 - In 4.2, we numerically investigate the critical FBC behaviour of the two-point functions and susceptibility of the self-avoiding walk and Ising model.
 - In 4.3, we numerically study the two-point function and susceptibility of the SAW and Ising model at a specific pseudo-critical point. At this pseudo-critical point, we numerically verify the anomalous FSS behaviour of the two-point functions, as observed with periodic boundaries at criticality.
- Finally, in Chapter 5, we discuss our results, and give an outlook for future work.

CHAPTER 2

Models

In this Chapter, we define the investigated models and observables. We study the FSS behaviour of the investigated models on the following graphs:

- on the hypercubic lattice with periodic boundary conditions (PBC), i.e. $\mathbb{G}_{\text{PBC}} = C_L \square C_L \square \dots$, see Chap. 3
- on the hypercubic lattice $\mathbb{G}_{\text{Box}} = P_L \square P_L \square \dots$ with free (FBC), reflective (RBC) and holding (HBC) boundary conditions, see Chap. 4

where the corresponding vertex sets are subsets of \mathbb{Z}^d (Details will be presented in the following sections). \square denotes the graph cartesian product, and C_L (P_L) is the cycle graph (path graph) with size L .

2.1 Random-length Models

2.1.1 Why study Random-length Models?

The long-standing debate regarding the correct FSS behaviour on periodic and free boundaries above d_c is caused by two key problems. One problem is the computational difficulty of simulating large systems in high dimensions, the other is the general lack of theory which explains the FSS behaviour of high-dimensional Ising models. Therefore, it is of significant interest to investigate models in the appropriate universality class,

which can be studied rigorously.

On an infinite hypercubic lattice for sufficiently high dimensions, it is well-known [36, 37] that the two-point functions of the Self-avoiding Walk (SAW) and Ising model exhibit the same scaling behaviour as the Green's function of the Simple Random Walk (SRW). On finite lattices this connection breaks down, since SRW is recurrent implying that the corresponding Green's function does not exist.

In Chap. 3 and 4, we repair this broken connection, and rigorously establish the FSS behaviour of the Green's function for an appropriate random walk model on finite lattices; the *Random-length* Random Walk. We argue that if one considers random walks with an appropriately distributed random (finite) length, then the Green's function displays the same asymptotics as the two-point functions of the Ising and SAW models.

2.1.2 Random-length Random Walk (RLRW)

Consider a simple random walk $(S_t)_{t \in \mathbb{N}}$ on a finite box, and define its corresponding vertex set by either

$$\mathbb{B}_l := [-l, l]^d \cap \mathbb{Z}^d, \quad L = 2l + 1 \quad (2.1)$$

or

$$\tilde{\mathbb{B}}_l := (-l, l]^d \cap \mathbb{Z}^d, \quad L = 2l \quad (2.2)$$

where $l \in \mathbb{N}$, and L is the side length. We fix the starting point S_0 of the walk to be at the origin 0 of the corresponding box. For each $\mathbf{x} \in \mathbb{B}_l$ or $\mathbf{x} \in \tilde{\mathbb{B}}_l$, we denote the Euclidean norm by $\|\mathbf{x}\| := \sqrt{\mathbf{x} \cdot \mathbf{x}}$. Specifically, we consider the SRW on \mathbb{B}_l or $\tilde{\mathbb{B}}_l$ with reflective, holding and periodic boundary conditions. Let $(C_t)_{t \in \mathbb{N}}$ be an i.i.d. sequence of uniform random variables on $\{\pm \mathbf{e}_1, \dots, \pm \mathbf{e}_d\}$ where \mathbf{e}_i is the (cartesian) unit vector in the i th dimension. Define

- *reflective boundary conditions* (RBC) by

$$S_{t+1} := \begin{cases} S_t + C_{t+1} & \text{if } S_t + C_{t+1} \in \mathbb{B}_l \text{ (or } \tilde{\mathbb{B}}_l) \\ S_t - C_{t+1} & \text{if } S_t + C_{t+1} \notin \mathbb{B}_l \text{ (or } \tilde{\mathbb{B}}_l) \end{cases} \quad (2.3)$$

- *holding boundary conditions* (HBC) by

$$S_{t+1} := \begin{cases} S_t + C_{t+1} & \text{if } S_t + C_{t+1} \in \mathbb{B}_l \text{ (or } \tilde{\mathbb{B}}_l) \\ S_t & \text{if } S_t + C_{t+1} \notin \mathbb{B}_l \text{ (or } \tilde{\mathbb{B}}_l) \end{cases} \quad (2.4)$$

- *periodic boundary conditions* (PBC) by

$$S_{t+1} := \begin{cases} S_t + C_{t+1} & \text{if } S_t + C_{t+1} \in \mathbb{B}_l \text{ (or } \tilde{\mathbb{B}}_l) \\ S_t + C_{t+1}(1 - L) & \text{if } S_t + C_{t+1} \notin \mathbb{B}_l \text{ (or } \tilde{\mathbb{B}}_l) \end{cases} \quad (2.5)$$

Note that \mathbb{B}_l and $\tilde{\mathbb{B}}_l$ with periodic boundary conditions can be naturally viewed as tori. We illustrate a SRW on a two-dimensional box with reflective and holding boundaries in Fig. 2.1 and with periodic boundaries in Fig. 2.2.

Let \mathcal{N} be an \mathbb{N} -valued random variable. We study $(S_t)_{t=0}^{\mathcal{N}}$ where the choice of each step is independent of \mathcal{N} . In words, we stop the SRW process after \mathcal{N} (random) steps. We call this model the *Random-length Random Walk* (RLRW). We study the *Green's function*

$$G_{\text{RLRW}}(\mathbf{x}) := \mathbb{E} \left(\sum_{t=0}^{\mathcal{N}} \mathbb{P}(S_t = \mathbf{x}) \right) \quad (2.6)$$

which is the expected number of visits to $\mathbf{x} \in \mathbb{B}_l$ or $\mathbf{x} \in \tilde{\mathbb{B}}_l$. Here, $\mathbb{P}(S_t = \mathbf{x})$ denotes the probability that the RLRW ends at \mathbf{x} after t steps. If \mathcal{N} is chosen to be (almost surely) infinite, then Eq. (2.6) is simply the usual definition of the Green's function of the random walk. Note that $\sum_{\mathbf{x}} G_{\text{RLRW}}(\mathbf{x}) = \langle \mathcal{N} \rangle$.

Intuitively, the mean walk length $\langle \mathcal{N} \rangle$ of a RLRW can be viewed as a surrogate of temperature of the Ising model and the fugacity for SAWs, respectively. For small fugacities, for instance, SAWs are short, in agreement with small mean walk lengths of a RLRW, while for large fugacities long SAWs are apparent, in agreement with large mean walk lengths.

2.1.3 Random-length Loop-erased Random Walk (RLLERW)

Let ω be a simple random walk on \mathbb{B}_l . The corresponding Loop-erased Random Walk $\text{LERW}(\omega)$ can be obtained by erasing the loops of ω in chronological order. Let \mathcal{N} be an \mathbb{N} -valued random variable. Consider the loop-erased random walk $(\tilde{S}_t)_{t=0}^{\mathcal{N}}$ with $\tilde{S}_0 = 0$ on \mathbb{B}_l with periodic and free boundaries where the choice of each step of the underlying random walk ω is uniform in the number of adjacent vertices and independent of \mathcal{N} .

In analogy with the definition in the RLRW model, we study the RLLERW Green's function

$$g_{\text{RLLERW}}(\mathbf{x}) := \mathbb{E} \left(\sum_{t=0}^{\mathcal{N}} \mathbb{P}(\tilde{S}_t = \mathbf{x}) \right) \quad (2.7)$$

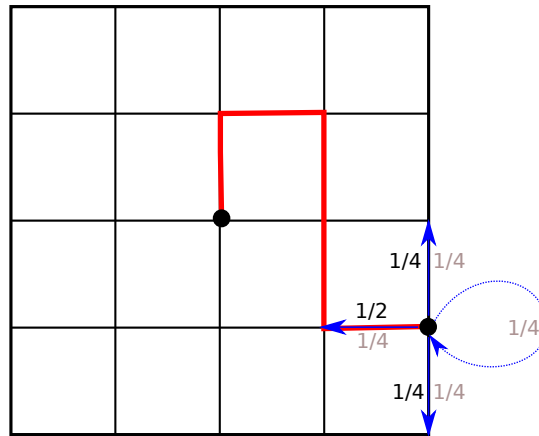


Figure 2.1: Illustration of a simple random walk, and the corresponding transition probabilities on reflective and holding boundary conditions on a square lattice. The blue arrows illustrate the possible transitions for the random walker. The numbers in grey correspond to the transition probabilities for holding boundaries, while the black numbers are the transition probabilities for reflective boundaries.

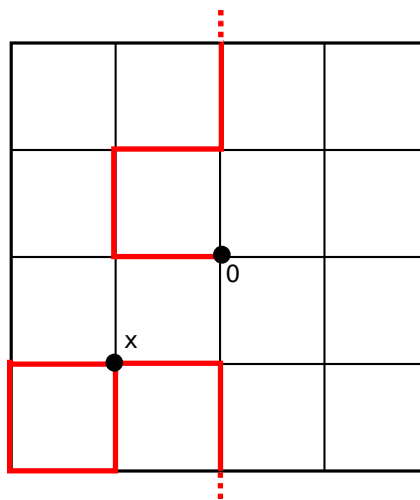


Figure 2.2: Illustration of a simple random walk on a two-dimensional box with periodic boundaries. The red lines illustrate the edges the walker visited (The dashed line illustrates the boundary edge). The walker started at the origin 0 of the box, and ended at the vertex \mathbf{x} . Each move is uniform among the four neighbours.

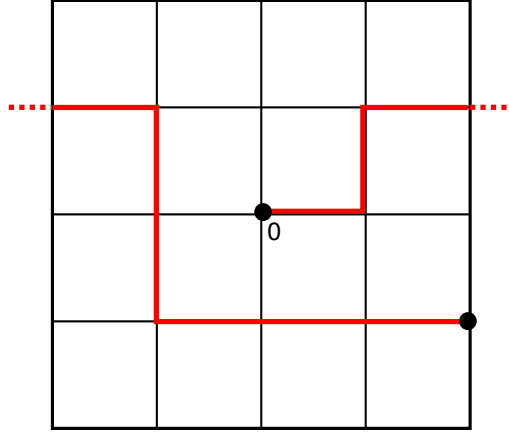


Figure 2.3: Illustration of a RLLERW with walk length $\mathcal{N} = 10$ on a two-dimensional box with periodic boundaries. The dashed line illustrates the boundary edge. The unwrapped length is $\mathcal{U} = (\mathcal{U}_1, \mathcal{U}_2) = (7, -1)$.

where $\tilde{\mathbb{P}}(\tilde{S}_t = \mathbf{x})$ is the probability that the RLLERW ends at \mathbf{x} after t steps.

2.2 n-vector models

We study two special cases of the n -vector model; the Ising model corresponding to $n = 1$ and the SAW corresponding to $n \rightarrow 0$.

2.2.1 Ising model in a loop representation

We study the zero-field ferromagnetic Ising model with Hamiltonian

$$\mathcal{H} = - \sum_{ij \in E} \mathbf{s}_i \mathbf{s}_j \quad (2.8)$$

on \mathbb{B}_l where $\mathbf{s}_i \in \{-1, +1\}$ denotes the spin at position $i \in \mathbb{B}_l$, and E is the edge set of \mathbb{B}_l with either FBC or PBC (see [44] for a detailed definition). We investigate the two-point function ¹

$$g_{\text{Ising}}(\mathbf{x}) := \langle \mathbf{s}_0 \mathbf{s}_{\mathbf{x}} \rangle \quad (2.9)$$

where $\langle \cdot \rangle$ denotes the expectation value with respect to the Gibbs measure.

Let $\mathcal{C}_0 \subset 2^E$ be the subset where all vertices in the spanning subgraph have even degree, and define $\mathcal{C}_{0\mathbf{x}} \subset 2^E$ as the subset in the spanning subgraph where all vertices except the origin $0 \in \mathbb{B}_l$ and $\mathbf{x} \in \mathbb{B}_L$ have even degree. As is well-known, the

¹For the ease of notation, we write $g_{\text{Ising}}(\mathbf{x})$ instead of $g_{\text{Ising}}(0, \mathbf{x})$.

high-temperature expansion [38] provides a natural graphical representation of the two-point function, i.e.

$$g_{\text{Ising}}(\mathbf{x}) = \frac{\sum_{A \in \mathcal{C}_{0\mathbf{x}}} z^{|A|}}{\sum_{A \in \mathcal{C}_0} z^{|A|}} \quad (2.10)$$

where $z := \tanh(1/T)$, T is the Ising temperature. We numerically studied this loop representation via the worm algorithm introduced in [39]².

2.2.2 Self-avoiding Walk in the variable length ensemble

We study the Self-avoiding Walk (SAW) on \mathbb{B}_l in the grand canonical ensemble where walks can have various lengths. The two-point function is given by

$$g_{\text{SAW}}(\mathbf{x}) := \sum_{\omega: 0 \rightarrow \mathbf{x}} z^{|\omega|} \quad (2.11)$$

where z is the fugacity, and the sum is over all SAWs starting at the origin 0 and ending at \mathbf{x} . We simulated this ensemble using a recently introduced irreversible version of the Beretti-Sokal algorithm [40, 41].

2.3 Observables

In addition to the Green's functions of the RLRW/RLLERW, and the two-point functions of the SAW and Ising models, we investigate the following observables:

- The *walk length* \mathcal{N} for the SAW and its mean value $\langle \mathcal{N} \rangle$.
- The *susceptibility* $\chi := |V|^{-1} \sum_{\mathbf{x}, \mathbf{y}} g(\mathbf{x}, \mathbf{y})$ of the SAW and the Ising model, estimated via $\chi = 1/\langle D_0 \rangle$ in the worm and B-S algorithm. Here, D_0 is the indicator function for the event that the actual configuration is an element of \mathcal{C}_0 in the Ising model, and is the empty walk ($\mathcal{N} = 0$) for the SAW, respectively.
- On \mathbb{B}_l with periodic boundaries, we study the *unwrapped SAW two-point function* $\tilde{g}_{\text{SAW}} : [0, \infty) \rightarrow [0, \infty)$ defined by

$$\tilde{g}_{\text{SAW}}(u) := \sum_{\omega: \|\mathcal{U}(\omega)\|=u} z^{|\omega|}. \quad (2.12)$$

The unwrapped length $\mathcal{U}(\omega) := (\mathcal{U}_1, \mathcal{U}_2, \dots, \mathcal{U}_d) \in \mathbb{Z}^d$ is defined algorithmically as follows. For each walk ω , traverse ω from the origin to its endpoint, adding +1

²In Sec. 2.1 of Part 2, we present details of the worm algorithm

(-1) to \mathcal{U}_i for each step of the walk along \mathbf{e}_i ($-\mathbf{e}_i$). The unwrapped length $\mathcal{U}(\omega)$ simply corresponds to the length the walk would have in the infinite lattice, if the torus was unwrapped, so that periodic images are considered distinct.

Moreover, we study the *unwrapped RLLERW Green's function* $\tilde{g}_{\text{RLLERW}} : [0, \infty) \rightarrow [0, \infty)$ defined by

$$\tilde{g}_{\text{RLLERW}}(u) := \frac{\mathbb{P}(\|\mathcal{U}\| = u)}{\mathbb{P}(\|\mathcal{U}\| = 0)} \quad (2.13)$$

where $\mathbb{P}(\cdot)$ is the probability to generate a RLLERW. Note that the unwrapped SAW two-point function from Eq. (2.12) can be defined analogously. We illustrate a RLLERW on a two-dimensional square lattice with periodic boundaries in Fig. 2.3.

- On \mathbb{B}_l with periodic boundaries, we study the *winding number* \mathcal{W} along the first coordinate axis, defined by $\mathcal{W} := \lfloor \frac{\mathcal{U}_1}{L} \rfloor$ where $\lfloor \cdot \rfloor$ denotes the floor function and L is the side-length of the lattice. In the Ising model, we define \mathcal{U}_1 as the unwrapped length of the largest incontractible loop where measurements were taken in \mathcal{C}_0 ³. We emphasize that \mathcal{W} does not distinguish between windings in the positive or negative directions, so that $\mathcal{W} > 0$.

2.4 Numerical details

Our simulations for the Ising model were performed at the exact infinite-volume critical point in two dimensions [43], and at the estimated location of the infinite-volume critical point $z_{c,\text{Ising},5\text{d}} = 0.113\,424\,8(5)$ [33] in five dimensions. The SAW model was simulated at the estimated location of the infinite-volume critical points, $z_{c,\text{SAW},2\text{d}} = 0.379\,052\,277\,758(4)$ [45], $z_{c,\text{SAW},5\text{d}} = 0.113\,140\,84(1)$ [41] and $z_{c,\text{SAW},6\text{d}} = 0.091\,927\,86(4)$ [46]. The simulations for the RLLERW were performed by sampling from the half-normal walk length distribution

$$P(\mathcal{N}) = \frac{2\theta}{\pi} \exp\left(-\frac{\theta^2 \mathcal{N}^2}{\pi}\right) \quad (2.14)$$

with $\theta := 1/\langle \mathcal{N} \rangle$. In line with general expectations, our numerical simulations suggest that the walk length distribution of SAWs on high-dimensional tori is ‘similar’ to the corresponding distribution on the complete graph K_n . One can rigorously

³Finding Hamiltonian circuits in an undirected graph is NP complete [42]. Instead, we perform a Depth-First search to estimate the winding number of the largest cluster. This approach leads only to a lower bound of the winding number. Regardless, as presented in Sec. 3.3, we still observe the expected scaling behaviour in five dimensions.

establish [47] that the walk length distribution of SAWs on K_n is a conditional Poisson distribution. In practice, for large n , this distribution can be approximated by the half-normal distribution from Eq. (2.14). This motivates using the half-normal distribution for generating RLLERWs.

For the Ising model, we simulated linear system sizes up to $L = 71$ in five dimensions. For SAW, we simulated linear system sizes up to $L = 221$ in five dimensions, and $L = 57$ in six dimensions. Finally, we simulated linear system sizes up to $L = 301$ for the RLLERW. A detailed analysis of integrated autocorrelation times is presented in [48] for the worm algorithm and in [41] for the irreversible B-S algorithm. Our fitting methodology and corresponding error estimation follow standard procedures, see for instance [49, 50]. To estimate the exponent value for a generic observable Y we performed least-squares fits to the ansatz $Y = a_Y L^{b_Y} + c_Y$.

FSS on hypercubic lattices with periodic boundaries

3.1 Random-length Random Walk

In this Section, we rigorously establish the FSS behaviour of the RLRW Green's function on the infinite-lattice \mathbb{Z}^d , and on boxes with periodic boundaries $d \geq 3$; see Sec. 2.1 for precise definitions.

On $d \geq 3$ dimensional boxes with periodic boundaries, Theorem 3.2.2 implies the following result. Consider a RLRW with mean walk length scaling as $\langle \mathcal{N} \rangle \asymp L^\mu$ with $\mu > 0$. Then, under certain conditions regarding the distribution of \mathcal{N} , the RLRW Green's function displays the following piecewise asymptotic behaviour

$$G_{\text{RLRW}}(\mathbf{x}) \asymp \begin{cases} \|\mathbf{x}\|^{2-d}, & \|\mathbf{x}\| \leq cL^{(d-\mu)/(d-2)} \\ L^{\mu-d}, & \|\mathbf{x}\| \geq cL^{(d-\mu)/(d-2)}. \end{cases} \quad (3.1)$$

where $c \in \mathbb{R}^+$. In words, $G_{\text{RLRW}}(\mathbf{x})$ exhibits the standard infinite-lattice asymptotic decay $\|\mathbf{x}\|^{2-d}$ at moderate values of \mathbf{x} , but then enters, if $\mu > 2$, a plateau of order $L^{\mu-d}$ which persists to the boundary. For $\mu < 2$, it follows from Eq. (3.1) that this plateau is absent, while the case $\mu = 2$ is marginal. Since a typical RLRW will explore distances of order $\sqrt{\langle \mathcal{N} \rangle}$ from the origin, the absence of a plateau for $\mu < 2$ is simply

because typical walks will be too short to feel the boundary. As a direct consequence of Eq. (3.1), the susceptibility scales as

$$\chi_{\text{RLRW}} \asymp L^\mu. \quad (3.2)$$

In Secs. 3.3 and 3.4 we explain the connection of our theorem to the FSS behaviour of the two-point functions of the SAW and Ising model.

The behaviour of RLRWs on tori and \mathbb{Z}^d can be related in the following way. For each $L \in \mathbb{N}$, we can define an equivalence relation on \mathbb{Z}^d such that, for each $\mathbf{x} \in \mathbb{Z}^d$,

$$[\mathbf{x}]_L := \{\mathbf{x} + L\mathbf{z} : \mathbf{z} \in \mathbb{Z}^d\}. \quad (3.3)$$

Let $(S_t)_{t=0}^{\mathcal{N}}$ be a RLRW on \mathbb{Z}^d . Then, for any $l \in \mathbb{N}$, $([S_t]_{2l+1} \cap \mathbb{B}_l)_{t=0}^{\mathcal{N}}$ is a RLRW on \mathbb{B}_l with periodic boundary conditions, and its Green's function satisfies:

$$\begin{aligned} G_{\text{PBC}, \mathbb{B}_l}(\mathbf{x}) &= \mathbb{E} \left(\sum_{j=0}^{\mathcal{N}} \mathbb{P}([S_j]_{2l+1} \cap \mathbb{B}_l = \mathbf{x}) \right) \\ &= \mathbb{E} \left(\sum_{j=0}^{\mathcal{N}} \mathbb{P}(S_j \in [\mathbf{x}]_{2l+1}) \right) \\ &= \mathbb{E} \left(\sum_{j=0}^{\mathcal{N}} \sum_{\mathbf{x}' \in [\mathbf{x}]_{2l+1}} \mathbb{P}(S_j = \mathbf{x}') \right) \\ &= \sum_{\mathbf{x}' \in [\mathbf{x}]_{2l+1}} G_{\mathbb{Z}^d}(\mathbf{x}') \\ &= \sum_{\mathbf{z} \in \mathbb{Z}^d} G_{\mathbb{Z}^d}(\mathbf{x} + L\mathbf{z}) \end{aligned}$$

for all $\mathbf{x} \in \mathbb{B}_l$, and where $L = 2l + 1$. Similarly, $([S_t]_{2l} \cap \tilde{\mathbb{B}}_l)_{t=0}^{\mathcal{N}}$ is a RLRW on $\tilde{\mathbb{B}}_l$ with periodic boundary conditions, and its Green's function satisfies:

$$\begin{aligned} G_{\text{PBC}, \tilde{\mathbb{B}}_l}(\mathbf{x}) &= \mathbb{E} \left(\sum_{j=0}^{\mathcal{N}} \mathbb{P}([S_j]_{2l} \cap \tilde{\mathbb{B}}_l = \mathbf{x}) \right) \\ &= \sum_{\mathbf{z} \in \mathbb{Z}^d} G_{\mathbb{Z}^d}(\mathbf{x} + L\mathbf{z}) \end{aligned}$$

for all $\mathbf{x} \in \tilde{\mathbb{B}}_l$, and where $L = 2l$. Therefore, defining

$$G_{\text{PBC}, L}(\mathbf{x}) := \sum_{\mathbf{z} \in \mathbb{Z}^d} G_{\mathbb{Z}^d}(\mathbf{x} + L\mathbf{z}), \quad (3.4)$$

we have

$$G_{\text{PBC},L}(\mathbf{x}) = \begin{cases} G_{\text{PBC},\tilde{\mathbb{B}}_{L/2}}(\mathbf{x}), & \text{for } L \text{ even and } \mathbf{x} \in \tilde{\mathbb{B}}_{L/2} \\ G_{\text{PBC},\mathbb{B}_{(L-1)/2}}(\mathbf{x}), & \text{for } L \text{ odd and } \mathbf{x} \in \mathbb{B}_{(L-1)/2} \end{cases} \quad (3.5)$$

To reduce notational clutter, we will generally omit the subscript L on $G_{\text{PBC},L}(\cdot)$ and $[\cdot]_L$ in what follows.

In Theorem 3.2.1, we prove, for distances $\|\mathbf{x}\| \leq c\sqrt{\langle \mathcal{N} \rangle}$ with fixed $c \in \mathbb{R}^+$, that the Green's function of a RLRW on \mathbb{Z}^d scales as

$$G_{\text{RLRW}}(\mathbf{x}) \asymp \|\mathbf{x}\|^{2-d}. \quad (3.6)$$

In Subsec. 3.3.2 we numerically establish the same FSS behaviour for the *unwrapped* two-point functions of the SAW and Ising model on high-dimensional tori, defined in Eq. (2.12). In the case of a SRW, we note that one immediately recovers the SRW behaviour on \mathbb{Z}^d when unwrapping the walk from the torus.

3.1.1 Preliminaries

Consider a RLRW $(S_t)_{t=0}^{\mathcal{N}}$ starting from the origin 0. Define

$$p_n(\mathbf{x}) := \mathbb{P}(S_n = \mathbf{x}). \quad (3.7)$$

We say n has the same parity as \mathbf{x} (denoted by $n \leftrightarrow \mathbf{x}$) if $n + \sum_{i=1}^d x_i$ is even. It follows immediately that $p_n(\mathbf{x}) = 0$ if $n \not\leftrightarrow \mathbf{x}$. Moreover, define

$$\bar{p}_n(\mathbf{x}) := \left[\frac{d}{2\pi n} \right]^{d/2} \exp\left(-\frac{d\|\mathbf{x}\|^2}{2n} \right). \quad (3.8)$$

3.2 Random-length Random Walk

3.2.1 Preliminaries

Consider a RLRW $(S_t)_{t=0}^{\mathcal{N}}$ starting from the origin 0. Define

$$p_n(\mathbf{x}) := \mathbb{P}(S_n = \mathbf{x}). \quad (3.9)$$

We say n has the same parity as \mathbf{x} (denoted by $n \leftrightarrow \mathbf{x}$) if $n + \sum_{i=1}^d x_i$ is even. It follows immediately that $p_n(\mathbf{x}) = 0$ if $n \not\leftrightarrow \mathbf{x}$. Moreover, define

$$\bar{p}_n(\mathbf{x}) := \left[\frac{d}{2\pi n} \right]^{d/2} \exp\left(-\frac{d\|\mathbf{x}\|^2}{2n}\right). \quad (3.10)$$

3.2.2 RLRW Green's function on \mathbb{Z}^d

Theorem 3.2.1. (*RLRW Green's function on \mathbb{Z}^d*) Let $d \geq 3$. For any $c \in \mathbb{R}^+$, if $0 < \|\mathbf{x}\| \leq c\sqrt{\langle \mathcal{N} \rangle}$, then there exists $\alpha_1(c) > 0$ and $\alpha_2 > 0$ such that

$$\alpha_1(c)\mathbb{P}(\mathcal{N} \geq \lceil \langle \mathcal{N} \rceil \rceil)\|\mathbf{x}\|^{2-d} \leq G_{\mathbb{Z}^d}(\mathbf{x}) \leq \alpha_2\|\mathbf{x}\|^{2-d} \quad (3.11)$$

with $\lim_{c \rightarrow \infty} \alpha_1(c) = 0$.

Remark. If $\|\mathbf{x}\| \leq c\sqrt{\langle \mathcal{N} \rangle}$, Eq. (3.11) shows that the Green's function exhibits the scaling behaviour $G_{\mathbb{Z}^d} \asymp \|\mathbf{x}\|^{2-d}$, in agreement with the FSS behaviour of the two-point functions of the Ising and SAW models on \mathbb{Z}^d .

Proof. Setting $\alpha = 2 - 2\epsilon_1/d$ with $\epsilon_1 \in (0, d)$ in Lemma 3.2.11 implies that

$$\sum_{n=1}^{\infty} [p_n(\mathbf{x}) - \bar{p}_n(\mathbf{x})] \mathbb{P}(\mathcal{N} \geq n) \mathbb{1}(n \leftrightarrow \mathbf{x}) = O(\|\mathbf{x}\|^{\epsilon_1-d}).$$

So

$$\begin{aligned} G_{\mathbb{Z}^d}(\mathbf{x}) &= p_0(\mathbf{x}) + \sum_{n=1}^{\infty} p_n(\mathbf{x}) \mathbb{P}(\mathcal{N} \geq n) \mathbb{1}(n \leftrightarrow \mathbf{x}) \\ &= p_0(\mathbf{x}) + \sum_{n=1}^{\infty} \bar{p}_n(\mathbf{x}) \mathbb{P}(\mathcal{N} \geq n) \mathbb{1}(n \leftrightarrow \mathbf{x}) + \sum_{n=1}^{\infty} [p_n(\mathbf{x}) - \bar{p}_n(\mathbf{x})] \mathbb{P}(\mathcal{N} \geq n) \mathbb{1}(n \leftrightarrow \mathbf{x}) \\ &= p_0(\mathbf{x}) + \sum_{n=1}^{\infty} \bar{p}_n(\mathbf{x}) \mathbb{P}(\mathcal{N} \geq n) \mathbb{1}(n \leftrightarrow \mathbf{x}) + O(\|\mathbf{x}\|^{\epsilon_1-d}). \end{aligned} \quad (3.12)$$

where $\mathbb{1}(\cdot)$ is the indicator function.

3.2. RANDOM-LENGTH RANDOM WALK

Let $F(n, \mathbf{x}) := \bar{p}_n(\mathbf{x})\mathbb{P}(\mathcal{N} \geq n)$. Then,

$$\begin{aligned}
& \sum_{n=1}^{\infty} \bar{p}_n(\mathbf{x})\mathbb{P}(\mathcal{N} \geq n)\mathbb{1}(n \leftrightarrow \mathbf{x}) \\
= & \sum_{n=1}^{\infty} F(n, \mathbf{x})\mathbb{1}(n \leftrightarrow \mathbf{x}) \\
= & \frac{1}{2} \sum_{n=1}^{\infty} [F(n, \mathbf{x})\mathbb{1}(n \leftrightarrow \mathbf{x}) + F(n, \mathbf{x})\mathbb{1}(n \nleftrightarrow \mathbf{x}) + F(n, \mathbf{x})\mathbb{1}(n \leftrightarrow \mathbf{x}) - F(n, \mathbf{x})\mathbb{1}(n \nleftrightarrow \mathbf{x})] \\
= & \frac{1}{2} \sum_{n=1}^{\infty} F(n, \mathbf{x}) + E(\mathbf{x}), \tag{3.13}
\end{aligned}$$

where

$$E(\mathbf{x}) = \frac{1}{2} \sum_{n=1}^{\infty} [F(n, \mathbf{x})\mathbb{1}(n \leftrightarrow \mathbf{x}) - F(n, \mathbf{x})\mathbb{1}(n \nleftrightarrow \mathbf{x})]. \tag{3.14}$$

We will see that $E(\mathbf{x})$ is a sub-leading term, and will be bounded in Eqs. (3.18)-(3.21).

The term $\sum_{n=1}^{\infty} F(n, \mathbf{x})$ in (3.13) can be rewritten as

$$\sum_{n=1}^{\infty} F(n, \mathbf{x}) = B(\mathbf{x}) + A(\mathbf{x}), \tag{3.15}$$

where

$$B(\mathbf{x}) := \int_0^{\infty} \left(\frac{d}{2\pi t} \right)^{d/2} e^{-\|\mathbf{x}\|^2 d/(2t)} \mathbb{P}(\mathcal{N} \geq \lfloor t + 1/2 \rfloor) dt$$

and

$$A(\mathbf{x}) = A_1(\mathbf{x}) - A_2(\mathbf{x}).$$

with

$$A_1(\mathbf{x}) := \left(\frac{d}{2\pi} \right)^{d/2} \sum_{n=1}^{\infty} \left[n^{-d/2} e^{-\|\mathbf{x}\|^2 d/(2n)} \mathbb{P}(\mathcal{N} \geq n) - \int_{n-1/2}^{n+1/2} t^{-d/2} e^{-\|\mathbf{x}\|^2 d/(2t)} \mathbb{P}(\mathcal{N} \geq \lfloor t + 1/2 \rfloor) dt \right]$$

and

$$A_2(\mathbf{x}) := \left(\frac{d}{2\pi} \right)^{d/2} \int_0^{1/2} t^{-d/2} e^{-\|\mathbf{x}\|^2 d/(2t)} \mathbb{P}(\mathcal{N} \geq \lfloor t + 1/2 \rfloor) dt.$$

We now establish lower and upper bounds for $B(\mathbf{x})$, while the sub-leading term $A(\mathbf{x})$

is discussed later. For the upper bound, since $\mathbb{P}(\mathcal{N} \geq \lfloor t + 1/2 \rfloor) \leq 1$, we find

$$\begin{aligned}
 B(\mathbf{x}) &= \|\mathbf{x}\|^{2-d} \left(\frac{1}{\pi}\right)^{d/2} \frac{d}{2} \int_0^\infty s^{d/2-2} e^{-s} \mathbb{P}\left(\mathcal{N} \geq \left\lfloor \frac{\|\mathbf{x}\|^2 d}{2s} + \frac{1}{2} \right\rfloor\right) ds \\
 &\leq \|\mathbf{x}\|^{2-d} \left(\frac{1}{\pi}\right)^{d/2} \frac{d}{2} \int_0^\infty e^{-s} s^{d/2-2} ds \\
 &= \|\mathbf{x}\|^{2-d} \left(\frac{1}{\pi}\right)^{d/2} \frac{d}{2} \Gamma(d/2 - 1), \tag{3.16}
 \end{aligned}$$

where we let $s = \|\mathbf{x}\|^2 d / (2t)$ in the first step, and $\Gamma(b) = \int_0^\infty s^{b-1} e^{-s} ds$ is the Gamma function.

For the lower bound, we have

$$\begin{aligned}
 B(\mathbf{x}) &= \|\mathbf{x}\|^{2-d} \left(\frac{1}{\pi}\right)^{d/2} \frac{d}{2} \int_0^\infty s^{d/2-2} e^{-s} \mathbb{P}\left(\mathcal{N} \geq \left\lfloor \frac{\|\mathbf{x}\|^2 d}{2s} + 1/2 \right\rfloor\right) ds \\
 &\geq \|\mathbf{x}\|^{2-d} \left(\frac{1}{\pi}\right)^{d/2} \frac{d}{2} \int_0^\infty s^{d/2-2} e^{-s} \mathbb{P}\left(\mathcal{N} \geq \left\lfloor \frac{c\langle \mathcal{N} \rangle d}{2s} + 1/2 \right\rfloor\right) ds \\
 &\geq \|\mathbf{x}\|^{2-d} \left(\frac{1}{\pi}\right)^{d/2} \frac{d}{2} \mathbb{P}\left(\mathcal{N} \geq \lfloor \langle \mathcal{N} \rangle + 1/2 \rfloor\right) \int_{\frac{cd}{2}}^\infty s^{d/2-2} e^{-s} ds \\
 &\geq \|\mathbf{x}\|^{2-d} \left(\frac{1}{\pi}\right)^{d/2} \frac{d}{2} \mathbb{P}(\mathcal{N} \geq \lceil \langle \mathcal{N} \rangle \rceil) \int_{\frac{cd}{2}}^\infty s^{d/2-2} e^{-s} ds \tag{3.17}
 \end{aligned}$$

We now bound the term $E(\mathbf{x})$ in Eq. (3.14).

$$\begin{aligned}
 |E(\mathbf{x})| &= \frac{1}{2} \left| \sum_{n=1}^\infty \left(F(n, \mathbf{x}) \mathbb{1}(n \leftrightarrow \mathbf{x}) - F(n, \mathbf{x}) \mathbb{1}(n \nleftrightarrow \mathbf{x}) \right) \right| \\
 &= \frac{1}{2} \left| \sum_{k=1}^\infty \left(F(2k, \mathbf{x}) - F(2k-1, \mathbf{x}) \right) \right| \\
 &\leq \frac{1}{2} \sum_{k=1}^\infty |F(2k, \mathbf{x}) - F(2k-1, \mathbf{x})| \\
 &\leq \frac{1}{2} \sum_{n=1}^\infty |F(n, \mathbf{x}) - F(n+1, \mathbf{x})|. \tag{3.18}
 \end{aligned}$$

3.2. RANDOM-LENGTH RANDOM WALK

We then split the sum $\sum_{n=1}^{\infty}$ into $\sum_{n=1}^{\lfloor \|\mathbf{x}\|^{2-\epsilon_2} \rfloor}$ and $\sum_{n=\lfloor \|\mathbf{x}\|^{2-\epsilon_2} \rfloor + 1}^{\infty}$ with $\epsilon_2 \in (0, 2)$. Then,

$$\begin{aligned}
\sum_{n=1}^{\lfloor \|\mathbf{x}\|^{2-\epsilon_2} \rfloor} |F(n, \mathbf{x}) - F(n+1, \mathbf{x})| &\leq \sum_{n=1}^{\lfloor \|\mathbf{x}\|^{2-\epsilon_2} \rfloor} [|F(n, \mathbf{x})| + |F(n+1, \mathbf{x})|] \\
&\leq \sum_{n=1}^{\lfloor \|\mathbf{x}\|^{2-\epsilon_2} \rfloor} \left(\frac{d}{2\pi n} \right)^{d/2} \exp\left(-\frac{\|\mathbf{x}\|^2 d}{2n}\right) \mathbb{P}(\mathcal{N} \geq n) + \\
&\quad \sum_{n=1}^{\lfloor \|\mathbf{x}\|^{2-\epsilon_2} \rfloor} \left[\frac{d}{2\pi(n+1)} \right]^{d/2} \exp\left[-\frac{\|\mathbf{x}\|^2 d}{2(n+1)}\right] \mathbb{P}(\mathcal{N} \geq n+1) \\
&\leq 2 \sum_{n=1}^{\lfloor \|\mathbf{x}\|^{2-\epsilon_2} \rfloor} \left(\frac{d}{2\pi n} \right)^{d/2} \exp\left[-\frac{\|\mathbf{x}\|^2 d}{2(n+1)}\right] \\
&\leq 2 \left(\frac{d}{2\pi} \right)^{d/2} \exp\left[-\frac{\|\mathbf{x}\|^2 d}{2(\|\mathbf{x}\|^{2-\epsilon_2} + 1)}\right] \sum_{n=1}^{\infty} n^{-d/2} \\
&= 2 \left(\frac{d}{2\pi} \right)^{d/2} \exp\left[-\frac{\|\mathbf{x}\|^2 d}{2(\|\mathbf{x}\|^{2-\epsilon_2} + 1)}\right] \zeta(d/2) \tag{3.19}
\end{aligned}$$

where $\zeta(\cdot)$ is the Riemann-Zeta function, and since $\mathbb{P}(\mathcal{N} \geq n) = \mathbb{P}(\mathcal{N} \geq n+1) + \mathbb{P}(\mathcal{N} = n)$,

$$\begin{aligned}
&\sum_{n=\lfloor \|\mathbf{x}\|^{2-\epsilon_2} \rfloor + 1}^{\infty} |F(n, \mathbf{x}) - F(n+1, \mathbf{x})| \\
&\leq \sum_{n=\lfloor \|\mathbf{x}\|^{2-\epsilon_2} \rfloor + 1}^{\infty} \left| \left(\frac{d}{2\pi n} \right)^{d/2} \exp\left(-\frac{\|\mathbf{x}\|^2 d}{2n}\right) - \left[\frac{d}{2\pi(n+1)} \right]^{d/2} \exp\left[-\frac{\|\mathbf{x}\|^2 d}{2(n+1)}\right] \right| \mathbb{P}(\mathcal{N} \geq n) \\
&\quad + \sum_{n=\lfloor \|\mathbf{x}\|^{2-\epsilon_2} \rfloor + 1}^{\infty} \left[\frac{d}{2\pi(n+1)} \right]^{d/2} \exp\left[-\frac{\|\mathbf{x}\|^2 d}{2(n+1)}\right] \mathbb{P}(\mathcal{N} = n) \\
&\leq \sum_{n=\lfloor \|\mathbf{x}\|^{2-\epsilon_2} \rfloor + 1}^{\infty} c_1 n^{-1-d/2} + c_2 \|\mathbf{x}\|^{-d+\epsilon_2 d/2} \\
&\leq c_3 \|\mathbf{x}\|^{-d+\epsilon_2 d/2}. \tag{3.20}
\end{aligned}$$

for $c_1, c_2, c_3 \in (0, \infty)$, where in the penultimate step we used Lemma 3.2.13, and the last steps uses Lemma 3.2.15. These observations lead to

$$E(\mathbf{x}) = O(\|\mathbf{x}\|^{\epsilon'_2 - d}) \tag{3.21}$$

with $\epsilon'_2 = \epsilon_2 d/2 \in (0, d)$.

Finally, we bound the term $A(\mathbf{x})$ which turns out to be sub-leading. Observe that, for fixed \mathbf{x} , $p_n(\mathbf{x})$ is a monotonically increasing function of n on the interval $(0, \|\mathbf{x}\|^2)$. So since $(0, 1/2) \subset (0, \|\mathbf{x}\|^2)$ for $\mathbf{x} \in \mathbb{Z}^d \setminus \{0\}$, we have

$$|A_2(\mathbf{x})| \leq c_4 e^{-d\|\mathbf{x}\|^2}$$

for some $c_4 \in \mathbb{R}^+$. And since $\lfloor t + 1/2 \rfloor = n$ for all $t \in (n - 1/2, n + 1/2)$, we have

$$\begin{aligned} |A_1(\mathbf{x})| &\leq \left(\frac{d}{2\pi} \right)^{d/2} \sum_{n=1}^{\infty} \left| n^{-d/2} e^{-\|\mathbf{x}\|^2 d/(2n)} - \int_{n-1/2}^{n+1/2} t^{-d/2} e^{-\|\mathbf{x}\|^2 d/(2t)} dt \right| \mathbb{P}(\mathcal{N} \geq n) \\ &\leq \left(\frac{d}{2\pi} \right)^{d/2} \sum_{n=1}^{\infty} \left| n^{-d/2} e^{-\|\mathbf{x}\|^2 d/(2n)} - \int_{n-1/2}^{n+1/2} t^{-d/2} e^{-\|\mathbf{x}\|^2 d/(2t)} dt \right| \\ &= O(\|\mathbf{x}\|^{-(2+d)}). \end{aligned}$$

where the last step follows from Lemma 3.2.5. ■

3.2.3 RLRW Green's function on a box with PBC

Theorem 3.2.2. *(RLRW Green's function on a box with periodic boundaries) Let $d \geq 3$. Then there exist $\alpha_1, \alpha_2, \alpha_3, \alpha_4, \alpha_5 \in (0, \infty)$ such that for any $\epsilon > 0$, and all $\mathbf{x} \in [-L/2, L/2]^d \cap \mathbb{Z}^d \setminus \{0\}$*

$$G_{\text{PBC}}(\mathbf{x}) \leq \alpha_1 \|\mathbf{x}\|^{2-d} + \alpha_2 \sum_{n=L^2 d+1}^{\infty} \mathbb{P}(\mathcal{N} \geq n) L^{-d} \quad (3.22)$$

$$G_{\text{PBC}}(\mathbf{x}) \geq \alpha_3 \mathbb{P}(\mathcal{N} \geq L^2 d) \|\mathbf{x}\|^{2-d} + \alpha_4 \sum_{n=L^2 d+1}^{\infty} \mathbb{P}(\mathcal{N} \geq n) L^{-d} - \alpha_5 \langle \mathcal{N} \rangle L^{-d-2+\epsilon} \quad (3.23)$$

Corollary 3.2.3. *If $\langle \mathcal{N} \rangle \asymp L^\mu$ with $\mu > 2$, then $G_{\text{PBC}}(\mathbf{x})$ satisfies Eq. (3.1), i.e.*

$$c_1 \|\mathbf{x}\|^{2-d} + c_2 L^{\mu-d} \leq G_{\text{PBC}}(\mathbf{x}) \leq c_3 \|\mathbf{x}\|^{2-d} + c_4 L^{\mu-d} \quad (3.24)$$

for $c_1, c_2, c_3, c_4 \in (0, \infty)$.

Proof. Let $m \in \mathbb{N}$. Since $\mathbb{P}(\mathcal{N} \geq n) \leq 1$, we have $\sum_{n=1}^m \mathbb{P}(\mathcal{N} \geq n) \leq m$. Thus

$$\begin{aligned} \sum_{n=dL^2}^{\infty} \mathbb{P}(\mathcal{N} \geq n) &= \sum_{n=1}^{\infty} \mathbb{P}(\mathcal{N} \geq n) - \sum_{n=1}^{dL^2-1} \mathbb{P}(\mathcal{N} \geq n) \\ &= \langle \mathcal{N} \rangle - \sum_{n=1}^{dL^2-1} \mathbb{P}(\mathcal{N} \geq n) \\ &\geq \langle \mathcal{N} \rangle - dL^2 \end{aligned} \quad (3.25)$$

It follows that if $\langle \mathcal{N} \rangle \asymp L^\mu$ with $\mu > 2$, then

$$\sum_{n=dL^2}^{\infty} \mathbb{P}(\mathcal{N} \geq n) \asymp L^\mu$$

Since $-\alpha_5 \langle \mathcal{N} \rangle L^{-d-2+\epsilon} = O(L^{\mu-d-(2-\epsilon)})$, Eq. (3.24) follows. ■

We now prove Theorem 3.2.2.

Proof. Let $\mathbf{x} \in [-L/2, L/2]^d \cap \mathbb{Z}^d \setminus \{0\}$. We have

$$\begin{aligned}
 G_{\text{PBC}}(\mathbf{x}) &= \sum_{\mathbf{z} \in \mathbb{Z}^d} \sum_{n=0}^{\infty} p_n(\mathbf{x} + \mathbf{z}L) \mathbb{P}(\mathcal{N} \geq n) \\
 &= \sum_{\mathbf{z} \in \mathbb{Z}^d} p_0(\mathbf{x} + \mathbf{z}L) + \sum_{\mathbf{z} \in \mathbb{Z}^d} \sum_{n=1}^{\infty} p_n(\mathbf{x} + \mathbf{z}L) \mathbb{P}(\mathcal{N} \geq n) \mathbb{1}(n \leftrightarrow \mathbf{x} + \mathbf{z}L) \\
 &=: p_0(\mathbf{x}) + A(\mathbf{x}, L) + B(\mathbf{x}, L). \tag{3.26}
 \end{aligned}$$

where

$$A(\mathbf{x}, L) := \sum_{\mathbf{z} \in \mathbb{Z}^d} \sum_{n=1}^{\infty} [p_n(\mathbf{x} + \mathbf{z}L) - \bar{p}_n(\mathbf{x} + \mathbf{z}L)] \mathbb{P}(\mathcal{N} \geq n) \mathbb{1}(n \leftrightarrow \mathbf{x} + \mathbf{z}L)$$

and

$$B(\mathbf{x}, L) := \sum_{\mathbf{z} \in \mathbb{Z}^d} \sum_{n=1}^{\infty} \bar{p}_n(\mathbf{x} + \mathbf{z}L) \mathbb{P}(\mathcal{N} \geq n) \mathbb{1}(n \leftrightarrow \mathbf{x} + \mathbf{z}L).$$

We now consider the leading term $B(\mathbf{x}, L)$, while $A(\mathbf{x}, L)$, which turns out to be a sub-leading term, is discussed later. We first consider an upper bound for $B(\mathbf{x}, L)$

$$\begin{aligned}
 B(\mathbf{x}, L) &\leq \sum_{\mathbf{z} \in \mathbb{Z}^d} \sum_{n=1}^{\infty} \bar{p}_n(\mathbf{x} + \mathbf{z}L) \mathbb{P}(\mathcal{N} \geq n) \\
 &= \sum_{\mathbf{z} \in \mathbb{Z}^d} \sum_{n=1}^{\infty} \left(\frac{d}{2\pi n} \right)^{d/2} \exp\left(-\frac{\|\mathbf{x} + \mathbf{z}L\|^2 d}{2n} \right) \mathbb{P}(\mathcal{N} \geq n) \tag{3.27}
 \end{aligned}$$

We split the sum $\sum_{n=1}^{\infty}$ into $\sum_{n=1}^M$ and $\sum_{n=M+1}^{\infty}$, where $M \in \mathbb{N}$ will be chosen later. For the sum $\sum_{n=1}^M$, Lemma 3.2.8 leads to

$$\begin{aligned}
 &\sum_{\mathbf{z} \in \mathbb{Z}^d} \sum_{n=1}^M \left(\frac{d}{2\pi n} \right)^{d/2} \exp\left(-\frac{\|\mathbf{x} + \mathbf{z}L\|^2 d}{2n} \right) \mathbb{P}(\mathcal{N} \geq n) \\
 &= \sum_{n=1}^M \left(\frac{d}{2\pi n} \right)^{d/2} \mathbb{P}(\mathcal{N} \geq n) \prod_{i=1}^d \left[\sum_{z_i \in \mathbb{Z}} \exp\left(-\frac{(x_i + z_i L)^2 d}{2n} \right) \right] \\
 &\leq \sum_{n=1}^M e^{-\|\mathbf{x}\|^2 d / (2n)} \left[1 + \sum_{z \in \mathbb{Z}} e^{-z^2 L^2 d / (4n)} \right]^d \left(\frac{d}{2\pi n} \right)^{d/2} \mathbb{P}(\mathcal{N} \geq n). \tag{3.28}
 \end{aligned}$$

3.2. RANDOM-LENGTH RANDOM WALK

Lemma 3.2.7 implies that $\sum_{z \in \mathbb{Z}} e^{-z^2 L^2 d / (4n)} \leq \sqrt{4\pi n / (dL^2)} - 1$, which tends to ∞ as $L \rightarrow \infty$ whenever $n = \omega(L^2)$. Therefore, to obtain a non-trivial upper bound as $L \rightarrow \infty$, we demand $M = O(L^2)$.

For the sum $\sum_{n=M+1}^{\infty}$, using Lemma 3.2.7 and Lemma 3.2.9, we obtain

$$\begin{aligned}
& \sum_{z \in \mathbb{Z}^d} \sum_{n=M+1}^{\infty} \left(\frac{d}{2\pi n} \right)^{d/2} \exp\left(-\frac{\|\mathbf{x} + \mathbf{z}L\|^2 d}{2n}\right) \mathbb{P}(\mathcal{N} \geq n) \\
&= \sum_{n=M+1}^{\infty} \prod_{i=1}^d \left[\sum_{z_i \in \mathbb{Z}} \exp\left(-\frac{(x_i + z_i L)^2 d}{2n}\right) \right] \left(\frac{d}{2\pi n} \right)^{d/2} \mathbb{P}(\mathcal{N} \geq n) \\
&\leq \sum_{n=M+1}^{\infty} \left(1 + \sum_{z \in \mathbb{Z}} e^{-z^2 L^2 d / (2n)} \right)^d \left(\frac{d}{2\pi n} \right)^{d/2} \mathbb{P}(\mathcal{N} \geq n) \\
&\leq \sum_{n=M+1}^{\infty} \left(2 + \sqrt{2\pi n / (dL^2)} \right)^d \left(\frac{d}{2\pi n} \right)^{d/2} \mathbb{P}(\mathcal{N} \geq n) \\
&= L^{-d} \sum_{n=M+1}^{\infty} \left(\sqrt{\frac{2d}{\pi}} \frac{L}{\sqrt{n}} + 1 \right)^d \mathbb{P}(\mathcal{N} \geq n). \tag{3.29}
\end{aligned}$$

Since the ratio $L^2/n \rightarrow +\infty$ as $L \rightarrow \infty$ whenever $n = o(L^2)$, in order to obtain a non-trivial upper bound as $L \rightarrow \infty$, we choose $M = \Omega(L^2)$. Combining this with the requirement $O(L^2)$ from above, then motivates setting $M = \lfloor cL^2 \rfloor$ with $c \in \mathbb{R}^+$.

Substituting $M = \lfloor cL^2 \rfloor$ into (3.28), and applying Lemma 3.2.10 leads to

$$\begin{aligned}
& \sum_{n=1}^{\lfloor cL^2 \rfloor} \prod_{i=1}^d \left[\sum_{z_i \in \mathbb{Z}} \exp\left(-\frac{(x_i + z_i L)^2 d}{2n}\right) \right] \left(\frac{d}{2\pi n} \right)^{d/2} \mathbb{P}(\mathcal{N} \geq n) \\
&\leq \left[1 + \sum_{z \in \mathbb{Z}} e^{-z^2 d / (4c)} \right]^d \sum_{n=1}^{\lfloor cL^2 \rfloor} e^{-\mathbf{x}^2 d / (2n)} \left(\frac{d}{2\pi n} \right)^{d/2} \\
&\leq \frac{d}{2} \left(\frac{1}{\pi} \right)^{d/2} \left[1 + \sum_{z \in \mathbb{Z}} e^{-z^2 d / (4c)} \right]^d \|\mathbf{x}\|^{2-d} \int_{\mathbf{x}^2 d / [(2\lfloor cL^2 \rfloor + 1)]}^{\infty} s^{d/2-2} e^{-s} ds + O(\|\mathbf{x}\|^{-2-d}) \\
&\leq \|\mathbf{x}\|^{2-d} \frac{d}{2} \left(\frac{1}{\pi} \right)^{d/2} [1 + \theta_3(0, e^{-d/(4c)})]^d \Gamma(d/2 - 1) + O(\|\mathbf{x}\|^{-2-d}) \tag{3.30}
\end{aligned}$$

where $\theta_3(u, q) := 1 + 2 \sum_{n=1}^{\infty} q^{n^2} \cos(2nu)$ is an elliptic theta function. Substituting

$M = \lfloor cL^2 \rfloor + 1$ into (3.29) leads to

$$\begin{aligned} & \sum_{n=\lfloor cL^2 \rfloor + 1}^{\infty} \prod_{i=1}^d \left[\sum_{z_i \in \mathbb{Z}} \exp \left(-\frac{(x_i + z_i L)^2 d}{2n} \right) \right] \left(\frac{d}{2\pi n} \right)^{d/2} \mathbb{P}(\mathcal{N} \geq n) \\ & \leq L^{-d} \left(\sqrt{\frac{2d}{\pi c}} + 1 \right)^d \sum_{n=\lfloor cL^2 \rfloor + 1}^{\infty} \mathbb{P}(\mathcal{N} \geq n) \end{aligned} \quad (3.31)$$

Thus, Eqs. (3.30) and (3.31) leads to an upper bound for $B(\mathbf{x})$.

We next consider a lower bound for $B(\mathbf{x}, L)$. Let

$$\begin{aligned} B(\mathbf{x}, L) &= \sum_{\mathbf{z} \in \mathbb{Z}^d} \sum_{n=1}^{\infty} \bar{p}_n(\mathbf{x} + \mathbf{z}L) \mathbb{P}(\mathcal{N} \geq n) \mathbb{1}(n \leftrightarrow \mathbf{x} + \mathbf{z}L) \\ &= B_1(\mathbf{x}, L) + E(\mathbf{x}, L) \end{aligned}$$

where

$$\begin{aligned} B_1(\mathbf{x}, L) &:= \frac{1}{2} \sum_{\mathbf{z} \in \mathbb{Z}^d} \left[\sum_{n=1}^{\infty} \bar{p}_n(\mathbf{x} + \mathbf{z}L) \mathbb{P}(\mathcal{N} \geq n) \mathbb{1}(n \leftrightarrow \mathbf{x} + \mathbf{z}L) \right. \\ & \quad \left. + \sum_{n=1}^{\infty} \bar{p}_n(\mathbf{x} + \mathbf{z}L) \mathbb{P}(\mathcal{N} \geq n-1) \mathbb{1}(n \leftrightarrow \mathbf{x} + \mathbf{z}L) \right] \end{aligned}$$

and

$$\begin{aligned} E(\mathbf{x}, L) &:= \frac{1}{2} \sum_{\mathbf{z} \in \mathbb{Z}^d} \left[\sum_{n=1}^{\infty} \bar{p}_n(\mathbf{x} + \mathbf{z}L) \mathbb{P}(\mathcal{N} \geq n) \mathbb{1}(n \leftrightarrow \mathbf{x} + \mathbf{z}L) \right. \\ & \quad \left. - \sum_{n=1}^{\infty} \bar{p}_n(\mathbf{x} + \mathbf{z}L) \mathbb{P}(\mathcal{N} \geq n-1) \mathbb{1}(n \leftrightarrow \mathbf{x} + \mathbf{z}L) \right] \end{aligned} \quad (3.32)$$

Since $\mathbb{P}(\mathcal{N} \geq n) \leq \mathbb{P}(\mathcal{N} \geq n-1)$, it follows that

$$\begin{aligned} B_1(\mathbf{x}, L) &\geq \frac{1}{2} \sum_{\mathbf{z} \in \mathbb{Z}^d} \left[\sum_{n=1}^{\infty} \bar{p}_n(\mathbf{x} + \mathbf{z}L) \mathbb{P}(\mathcal{N} \geq n) \mathbb{1}(n \leftrightarrow \mathbf{x} + \mathbf{z}L) \right. \\ & \quad \left. + \sum_{n=1}^{\infty} \bar{p}_n(\mathbf{x} + \mathbf{z}L) \mathbb{P}(\mathcal{N} \geq n) \mathbb{1}(n \leftrightarrow \mathbf{x} + \mathbf{z}L) \right] \\ &= \frac{1}{2} \sum_{\mathbf{z} \in \mathbb{Z}^d} \sum_{n=1}^{\infty} \bar{p}_n(\mathbf{x} + \mathbf{z}L) \mathbb{P}(\mathcal{N} \geq n) \end{aligned} \quad (3.33)$$

3.2. RANDOM-LENGTH RANDOM WALK

We again split the $\sum_{n=1}^{\infty}$ into $\sum_{n=1}^{\lfloor cL^2 \rfloor}$ and $\sum_{n=\lfloor cL^2 \rfloor+1}^{\infty}$. For the sum $\sum_{n=1}^{\lfloor cL^2 \rfloor}$, it follows from Lemma 3.2.8 and Lemma 3.2.10 that

$$\begin{aligned}
& \sum_{n=1}^{\lfloor cL^2 \rfloor} \left(\prod_{i=1}^d \sum_{z_i \in \mathbb{Z}} e^{-(x_i+z_i L)^2 d/(2n)} \right) \left(\frac{d}{2\pi n} \right)^{d/2} \mathbb{P}(\mathcal{N} \geq n) \\
& \geq \sum_{n=1}^{\lfloor cL^2 \rfloor} e^{-\|\mathbf{x}\|^2 d/(2n)} \left(\frac{d}{2\pi n} \right)^{d/2} \mathbb{P}(\mathcal{N} \geq n) \\
& \geq \mathbb{P}(\mathcal{N} \geq cL^2) \sum_{n=1}^{\lfloor cL^2 \rfloor} e^{-\|\mathbf{x}\|^2 d/(2n)} \left(\frac{d}{2\pi n} \right)^{d/2} \\
& \geq \mathbb{P}(\mathcal{N} \geq cL^2) \frac{d}{2} \left(\frac{1}{\pi} \right)^{d/2} \left(\|\mathbf{x}\|^{2-d} \int_{\mathbf{x}^2 d/([2\lfloor cL^2 \rfloor+1])}^{\infty} s^{d/2-2} e^{-s} ds + O(\|\mathbf{x}\|^{-2-d}) \right) \\
& \geq \|\mathbf{x}\|^{2-d} \mathbb{P}(\mathcal{N} \geq cL^2) \frac{d}{2} \left(\frac{1}{\pi} \right)^{d/2} \int_{d^2 L^2/([2\lfloor cL^2 \rfloor+1])}^{\infty} s^{d/2-2} e^{-s} ds + O(\|\mathbf{x}\|^{-2-d}) \\
& \geq \|\mathbf{x}\|^{2-d} \mathbb{P}(\mathcal{N} \geq cL^2) \frac{d}{2} \left(\frac{1}{\pi} \right)^{d/2} \int_{d^2/(2c-1)}^{\infty} s^{d/2-2} e^{-s} ds + O(\|\mathbf{x}\|^{-2-d}) \quad (3.34)
\end{aligned}$$

The penultimate step uses $\|\mathbf{x}\|^2 \leq dL^2$, and the last step assumed $c > 1/2$.

For the sum $\sum_{n=\lfloor cL^2 \rfloor+1}^{\infty}$, using Lemma 3.2.9 and 3.2.7, we have

$$\begin{aligned}
& \sum_{n=\lfloor cL^2 \rfloor+1}^{\infty} \left(\prod_{i=1}^d \sum_{z_i \in \mathbb{Z}} e^{-(x_i+z_i L)^2 d/(2n)} \right) \left(\frac{d}{2\pi n} \right)^{d/2} \mathbb{P}(\mathcal{N} \geq n) \\
& \geq \sum_{n=\lfloor cL^2 \rfloor+1}^{\infty} \left(\sum_{z \in \mathbb{Z}} e^{-z^2 L^2 d/(2n)} - 1 \right)^d \left(\frac{d}{2\pi n} \right)^{d/2} \mathbb{P}(\mathcal{N} \geq n) \\
& \geq \sum_{n=\lfloor cL^2 \rfloor+1}^{\infty} \left(\sqrt{\frac{2\pi n}{dL^2}} - 2 \right)^d \left(\frac{d}{2\pi n} \right)^{d/2} \mathbb{P}(\mathcal{N} \geq n) \\
& = L^{-d} \sum_{n=\lfloor cL^2 \rfloor+1}^{\infty} \left(1 - \sqrt{\frac{2d}{\pi}} \frac{L}{\sqrt{n}} \right)^d \mathbb{P}(\mathcal{N} \geq n) \\
& \geq L^{-d} \left(1 - \sqrt{\frac{2d}{\pi c}} \right)^d \sum_{n=\lfloor cL^2 \rfloor+1}^{\infty} \mathbb{P}(\mathcal{N} \geq n) \\
& = L^{-d} \left(1 - \sqrt{2/\pi} \right)^d \sum_{n=dL^2+1}^{\infty} \mathbb{P}(\mathcal{N} \geq n). \quad (3.35)
\end{aligned}$$

In the last step, to guarantee a non-negative lower bound, we set $c = d$. The lower

bound for $B_1(\mathbf{x}, L)$ follows by combining Eqs. (3.34) and (3.35). It remains to bound $|E(\mathbf{x}, L)|$ and $|A(\mathbf{x}, L)|$.

We first consider $E(\mathbf{x}, L)$. A change of variables in the second term of the RHS of Eq. (3.32) shows that

$$\begin{aligned} E(\mathbf{x}, L) &= \frac{1}{2} \sum_{\mathbf{z} \in \mathbb{Z}^d} \sum_{n=1}^{\infty} (\bar{p}_n(\mathbf{x} + \mathbf{z}L) - \bar{p}_{n+1}(\mathbf{x} + \mathbf{z}L)) \mathbb{P}(\mathcal{N} \geq n) \mathbb{1}(n \leftrightarrow \mathbf{x} + \mathbf{z}L) \\ &\quad - \frac{1}{2} \sum_{\mathbf{z} \in \mathbb{Z}^d} \bar{p}_1(\mathbf{x} + \mathbf{z}L) \mathbb{1}(n \leftrightarrow \mathbf{x} + \mathbf{z}L). \end{aligned} \quad (3.36)$$

We therefore have

$$\begin{aligned} |E(\mathbf{x}, L)| &\leq \frac{1}{2} \sum_{\mathbf{z} \in \mathbb{Z}^d} \sum_{n=1}^{\infty} |\bar{p}_n(\mathbf{x} + \mathbf{z}L) - \bar{p}_{n+1}(\mathbf{x} + \mathbf{z}L)| \mathbb{P}(\mathcal{N} \geq n) \\ &\quad + \sum_{\mathbf{z} \in \mathbb{Z}^d} \bar{p}_1(\mathbf{x} + \mathbf{z}L). \end{aligned} \quad (3.37)$$

where

$$\begin{aligned} \sum_{\mathbf{z} \in \mathbb{Z}^d} \bar{p}_1(\mathbf{x} + \mathbf{z}L) &= \bar{p}_1(\mathbf{x}) + \sum_{\mathbf{z} \in \mathbb{Z}^d \setminus \{0\}} \bar{p}_1(\mathbf{x} + \mathbf{z}L) \\ &= \left(\frac{d}{2\pi}\right)^{d/2} \left[e^{-d\|\mathbf{x}\|^2/2} + \sum_{\mathbf{z} \in \mathbb{Z}^d \setminus \{0\}} e^{-d\|\mathbf{x} + \mathbf{z}L\|^2/2} \right]. \end{aligned} \quad (3.38)$$

Since $-1/2 \leq x_i/L \leq 1/2$, we have $(x_i/L + z_i)^2 \geq z_i^2/4$, for all $i \in \{1, \dots, d\}$. Therefore

$$\|\mathbf{x}/L + \mathbf{z}\| \geq \|\mathbf{z}\|/2 \quad (3.39)$$

Combining Eqs. (3.38) and (3.39), and using Lemma 3.2.20 gives

$$\begin{aligned} \sum_{\mathbf{z} \in \mathbb{Z}^d} \bar{p}_1(\mathbf{x} + \mathbf{z}L) &\leq \left(\frac{d}{2\pi}\right)^{d/2} \left[e^{-d\|\mathbf{x}\|^2/2} + \sum_{\mathbf{z} \in \mathbb{Z}^d \setminus \{0\}} e^{-dL^2\|\mathbf{z}\|^2/8} \right] \\ &\leq \left(\frac{d}{2\pi}\right)^{d/2} \left(e^{-d\|\mathbf{x}\|^2/2} + c_1 e^{-dL^2/8} \right) \end{aligned} \quad (3.40)$$

with $c_1 \in (0, \infty)$ where the last step follows from Lemma 3.2.20.

We now split the sum from Eq. (3.37) into $\sum_{n=1}^{\lfloor \|\mathbf{x} + \mathbf{z}L\|^{2-\epsilon_1} \rfloor}$ and $\sum_{n=\lfloor \|\mathbf{x} + \mathbf{z}L\|^{2-\epsilon_1} \rfloor + 1}^{\infty}$. Using Lemma 3.2.19 leads to

$$\begin{aligned}
 & \sum_{\mathbf{z} \in \mathbb{Z}^d} \sum_{n=1}^{\lfloor \|\mathbf{x}+\mathbf{z}\|^{2-\epsilon} \rfloor} |\bar{p}_n(\mathbf{x} + \mathbf{z}L) - \bar{p}_{n+1}(\mathbf{x} + \mathbf{z}L)| \\
 & \leq c_2 \sum_{\mathbf{z} \in \mathbb{Z}^d} e^{-\frac{d}{8}\|\mathbf{x}+\mathbf{z}L\|^\epsilon} \\
 & = c_2 e^{-\frac{d}{8}\|\mathbf{x}\|^\epsilon} + c_2 \sum_{\mathbf{z} \in \mathbb{Z}^d \setminus \{0\}} e^{-\frac{d}{8}\|\mathbf{x}+\mathbf{z}L\|^\epsilon} \\
 & \leq c_2 e^{-\frac{d}{8}\|\mathbf{x}\|^\epsilon} + c_2 \sum_{\mathbf{z} \in \mathbb{Z}^d \setminus \{0\}} e^{-\frac{d}{23+\epsilon}\|\mathbf{z}\|^\epsilon L^\epsilon} \\
 & \leq c_2 e^{-\frac{d}{8}\|\mathbf{x}\|^\epsilon} + c_3 e^{-\frac{d}{23+\epsilon}L^\epsilon}
 \end{aligned} \tag{3.41}$$

where $c_2, c_3 \in (0, \infty)$, and the penultimate step uses Eq. (3.39) and the last step follows by Lemma 3.2.20.

Now by Lemma 3.2.13

$$\begin{aligned}
 & \sum_{\mathbf{z} \in \mathbb{Z}^d} \sum_{n=\lfloor \|\mathbf{x}+\mathbf{z}\|^{2-\epsilon} \rfloor + 1}^{\infty} |\bar{p}_n(\mathbf{x} + \mathbf{z}L) - \bar{p}_{n+1}(\mathbf{x} + \mathbf{z}L)| \mathbb{P}(\mathcal{N} \geq n) \\
 & \leq c_4 \sum_{\mathbf{z} \in \mathbb{Z}^d} \sum_{n=\lfloor \|\mathbf{x}+\mathbf{z}\|^{2-\epsilon} \rfloor + 1}^{\infty} n^{-d/2-1} \mathbb{P}(\mathcal{N} \geq n) \\
 & \leq c_4 \sum_{n=\lfloor \|\mathbf{x}+\mathbf{z}\|^{2-\epsilon} \rfloor + 1}^{\infty} n^{-d/2-1} + c_4 \langle \mathcal{N} \rangle \sum_{\mathbf{z} \in \mathbb{Z}^d \setminus \{0\}} \sum_{n=\lfloor \|\mathbf{x}+\mathbf{z}\|^{2-\epsilon} \rfloor + 1}^{\infty} n^{-d/2-1}
 \end{aligned}$$

by using Markov's inequality in the last step, and $c_4 \in (0, \infty)$. Lemma 3.2.15 then implies

$$\begin{aligned}
 & \sum_{\mathbf{z} \in \mathbb{Z}^d} \sum_{n=\lfloor \|\mathbf{x}+\mathbf{z}\|^{2-\epsilon} \rfloor + 1}^{\infty} |\bar{p}_n(\mathbf{x} + \mathbf{z}L) - \bar{p}_{n+1}(\mathbf{x} + \mathbf{z}L)| \mathbb{P}(\mathcal{N} \geq n) \\
 & \leq c_5 \lfloor \|\mathbf{x}\|^{2-\epsilon} \rfloor^{-d/2} + c_6 \langle \mathcal{N} \rangle \sum_{\mathbf{z} \in \mathbb{Z}^d \setminus \{0\}} \left(\lfloor \|\mathbf{x} + \mathbf{z}L\|^{2-\epsilon} \rfloor \right)^{-d/2-1} \\
 & \leq c_5 \|\mathbf{x}\|^{-d+d\epsilon/2} + c_6 \langle \mathcal{N} \rangle \sum_{\mathbf{z} \in \mathbb{Z}^d \setminus \{0\}} \left(\lfloor \|\mathbf{x} + \mathbf{z}L\|^{2-\epsilon} \rfloor \right)^{-d/2-1}
 \end{aligned}$$

where $c_5, c_6 \in (0, \infty)$.

From Eq. (3.39), it follows that $\|\mathbf{x} + \mathbf{z}L\|^{2-\epsilon} \geq (L/2)^{2-\epsilon} \|\mathbf{z}\|^{2-\epsilon}$ whenever $\epsilon \in (0, 2)$. Thus

$$\lfloor \|\mathbf{x} + \mathbf{z}L\|^{2-\epsilon} \rfloor \geq \lfloor (L/2)^{2-\epsilon} \|\mathbf{z}\|^{2-\epsilon} \rfloor \geq (L/2)^{2-\epsilon} \|\mathbf{z}\|^{2-\epsilon} \left[1 - (L/2)^{-(2-\epsilon)} \|\mathbf{z}\|^{-(2-\epsilon)} \right]$$

Since $\|\mathbf{z}\| \geq 1$ when $\mathbf{z} \neq 0$, under the assumption $L \geq 3$, we have

$$\begin{aligned} & L\|\mathbf{z}\|/2 \geq 3/2 \\ \Rightarrow & (L\|\mathbf{z}\|/2)^{-(2-\epsilon)} \leq (2/3)^{2-\epsilon} \\ \Rightarrow & \left[1 - (L\|\mathbf{z}\|/2)^{-(2-\epsilon)} \right] \geq 1 - (2/\epsilon)^{2-\epsilon} > 0 \quad \forall \epsilon \in (0, 2) \\ \Rightarrow & \lfloor \|\mathbf{x} + \mathbf{z}L\|^{2-\epsilon} \rfloor \geq L^{2-\epsilon} \|\mathbf{z}\|^{2-\epsilon} \left[(1/2)^{2-\epsilon} - (2/3)^{2-\epsilon} \right] \\ \Rightarrow & \lfloor \|\mathbf{x} + \mathbf{z}L\|^{2-\epsilon} \rfloor^{-d/2-1} \leq L^{-d-2+\epsilon(1+d/2)} \left[(1/2)^{3-\epsilon} - (2/3)^{2-\epsilon} \right]^{-d/2-1} \|\mathbf{z}\|^{-d-2+\epsilon(1+d/2)} \end{aligned}$$

It follows that

$$\begin{aligned} & \sum_{\mathbf{z} \in \mathbb{Z}^d} \sum_{n=\lfloor \|\mathbf{x} + \mathbf{z}\|^{2-\epsilon} \rfloor + 1}^{\infty} |\bar{p}_n(\mathbf{x} + \mathbf{z}L) - \bar{p}_{n+1}(\mathbf{x} + \mathbf{z}L)| \mathbb{P}(\mathcal{N} \geq n) \\ & \leq c_5 \|\mathbf{x}\|^{-d+d\epsilon/2} + c_7 \langle \mathcal{N} \rangle L^{-d-2+\epsilon(1+d/2)} \sum_{\mathbf{z} \in \mathbb{Z}^d \setminus \{0\}} \|\mathbf{z}\|^{-d-2+\epsilon(1+d/2)} \end{aligned}$$

Lemma 3.2.12 implies that the series converges provided

$$2 - \epsilon(1 + d/2) > 0 \Rightarrow 2 > \epsilon(1 + d/2) \Rightarrow \epsilon < \frac{2}{1 + d/2}$$

So taking $\epsilon \in (0, \frac{2}{1+d/2})$ we have

$$\begin{aligned} & \sum_{\mathbf{z} \in \mathbb{Z}^d} \sum_{n=\lfloor \|\mathbf{x} + \mathbf{z}\|^{2-\epsilon} \rfloor + 1}^{\infty} |\bar{p}_n(\mathbf{x} + \mathbf{z}L) - \bar{p}_{n+1}(\mathbf{x} + \mathbf{z}L)| \mathbb{P}(\mathcal{N} \geq n) \\ & \leq c_5 \|\mathbf{x}\|^{-d+d\epsilon/2} + c_8 \langle \mathcal{N} \rangle L^{-d-2+\epsilon(1+d/2)} \end{aligned} \tag{3.42}$$

3.2. RANDOM-LENGTH RANDOM WALK

Combining Eq. (3.40) with Eqs. (3.41) and (3.42) and using Lemma 3.2.18, then shows

$$|E(\mathbf{x}, L)| \leq a_1 \|\mathbf{x}\|^{-d+d\epsilon/2} + a_2 \frac{\langle \mathcal{N} \rangle}{L^{d+2-\epsilon(1+d/2)}}$$

for any $\epsilon \in (0, \frac{2}{1+d/2})$, where $a_1, a_2 \in (0, \infty)$ may depend on ϵ and d . Fixing a choice of $\epsilon \in (0, \frac{2}{1+d/2})$, it then follows that for any $\epsilon_1 \geq \frac{d\epsilon}{2}$ and $\epsilon_2 \geq \epsilon(1 + \frac{d}{2})$

$$|E(\mathbf{x}, L)| \leq \frac{c_1}{\|\mathbf{x}\|^{d-\epsilon}} + c_2 \frac{\langle \mathcal{N} \rangle}{L^{d+2-\epsilon_2}}$$

Finally, we consider the term $A(\mathbf{x}, L)$, which satisfies

$$\begin{aligned} |A(\mathbf{x}, L)| &\leq \sum_{\mathbf{z} \in \mathbb{Z}^d} \sum_{n=1}^{\infty} |p_n(\mathbf{x} + \mathbf{z}L) - \bar{p}_n(\mathbf{x} + \mathbf{z}L)| \mathbb{P}(\mathcal{N} \geq n) \mathbb{1}(n \leftrightarrow \mathbf{x} + \mathbf{z}L) \\ &= \sum_{n=1}^{\infty} |p_n(\mathbf{x}) - \bar{p}_n(\mathbf{x})| \mathbb{P}(\mathcal{N} \geq n) \mathbb{1}(n \leftrightarrow \mathbf{x}) \\ &\quad + \sum_{\mathbf{z} \in \mathbb{Z}^d \setminus \{0\}} \sum_{n=1}^{\infty} |p_n(\mathbf{x} + \mathbf{z}L) - \bar{p}_n(\mathbf{x} + \mathbf{z}L)| \mathbb{P}(\mathcal{N} \geq n) \mathbb{1}(n \leftrightarrow \mathbf{x} + \mathbf{z}L). \end{aligned} \quad (3.43)$$

We bound the two terms in the RHS of (3.43) separately. For the first term, using Lemma 3.2.11 with $\alpha = 2 - 2\epsilon_2/d$ and $\epsilon_2 \in (0, d)$ leads to

$$\sum_{n=1}^{\infty} |p_n(\mathbf{x}) - \bar{p}_n(\mathbf{x})| \mathbb{P}(\mathcal{N} \geq n) \mathbb{1}(n \leftrightarrow \mathbf{x}) \leq c \|\mathbf{x}\|^{-d+\epsilon_2}. \quad (3.44)$$

with $c \in (0, \infty)$.

For the second term, we split the n sum into two parts. If $n \leq \|\mathbf{x} + \mathbf{z}L\|^{2-\epsilon_1}$ with $\epsilon_1 \in (0, 2)$, then Lemma 3.2.6 implies that there exist $\beta, c_1 \in (0, \infty)$ such that

$$p_n(\mathbf{x} + \mathbf{z}L) \leq \mathbb{P}\left(\max_{0 \leq i \leq n} |S_i| \geq \|\mathbf{x} + \mathbf{z}L\|\right) \leq c_1 e^{-\beta(\|\mathbf{x} + \mathbf{z}L\|/\sqrt{n})^2} \leq c_1 e^{-\beta \|\mathbf{x} + \mathbf{z}L\|^{\epsilon_1}}. \quad (3.45)$$

Furthermore, we have $\bar{p}_n(\mathbf{x} + \mathbf{z}L) \leq c_2 e^{-\|\mathbf{x} + \mathbf{z}L\|^{\epsilon_1 d/2}}$ from Eq. (3.10) where $c_2 \in (0, \infty)$.

So,

$$\begin{aligned}
 & \sum_{\mathbf{z} \in \mathbb{Z}^d \setminus \{0\}} \sum_{n=1}^{\lfloor \|\mathbf{x} + \mathbf{z}L\|^{2-\epsilon_1} \rfloor} |p_n(\mathbf{x} + \mathbf{z}L) - \bar{p}_n(\mathbf{x} + \mathbf{z}L)| \mathbb{P}(\mathcal{N} \geq n) \\
 & \leq \sum_{\mathbf{z} \in \mathbb{Z}^d \setminus \{0\}} \sum_{n=1}^{\lfloor \|\mathbf{x} + \mathbf{z}L\|^{2-\epsilon_1} \rfloor} [p_n(\mathbf{x} + \mathbf{z}L) + \bar{p}_n(\mathbf{x} + \mathbf{z}L)] \\
 & \leq \sum_{\mathbf{z} \in \mathbb{Z}^d \setminus \{0\}} \sum_{n=1}^{\lfloor \|\mathbf{x} + \mathbf{z}L\|^{2-\epsilon_1} \rfloor} c_3 e^{-\beta' \|\mathbf{x} + \mathbf{z}L\|^{\epsilon_1}} \\
 & \leq \sum_{\mathbf{z} \in \mathbb{Z}^d \setminus \{0\}} c_3 \|\mathbf{x} + \mathbf{z}L\|^{2-\epsilon_1} e^{-\beta' \|\mathbf{x} + \mathbf{z}L\|^{\epsilon_1}} \\
 & = \sum_{\mathbf{z} \in \mathbb{Z}^d \setminus \{0\}} c_3 \left(\|\mathbf{x} + \mathbf{z}L\|^{2-\epsilon_1} e^{-\frac{\beta'}{2} \|\mathbf{x} + \mathbf{z}L\|^{\epsilon_1}} \right) e^{-\frac{\beta'}{2} \|\mathbf{x} + \mathbf{z}L\|^{\epsilon_1}} \\
 & \leq \sum_{\mathbf{z} \in \mathbb{Z}^d \setminus \{0\}} c_4 e^{-\frac{\beta'}{2} \|\mathbf{x} + \mathbf{z}L\|^{\epsilon_1}} \\
 & \leq \sum_{\mathbf{z} \in \mathbb{Z}^d \setminus \{0\}} c_5 e^{-\frac{\beta'}{2} \|L\mathbf{z}/2\|^{\epsilon_1}} \\
 & \leq c_6 \exp\left(\frac{-\beta' L^{\epsilon_1}}{2^{\epsilon_1+1}}\right) \tag{3.46}
 \end{aligned}$$

where $c_3, c_4, c_5, c_6 \in (0, \infty)$, and $\beta' = \min\{\beta, d/2\}$. The third last inequality follows by Lemma 3.2.18, while the last inequality follows by Lemma 3.2.20.

We now consider the region $n > \|\mathbf{x} + \mathbf{z}L\|^{2-\epsilon_1}$. Using the Markov inequality leads to

$$\begin{aligned}
 & \sum_{\mathbf{z} \in \mathbb{Z}^d \setminus \{0\}} \sum_{n=\lfloor \|\mathbf{x} + \mathbf{z}L\|^{2-\epsilon_1} \rfloor + 1}^{\infty} |p_n(\mathbf{x} + \mathbf{z}L) - \bar{p}_n(\mathbf{x} + \mathbf{z}L)| \mathbb{P}(\mathcal{N} \geq n) \mathbb{1}(n \leftrightarrow \mathbf{x} + \mathbf{z}L) \\
 & \leq \sum_{\mathbf{z} \in \mathbb{Z}^d \setminus \{0\}} \sum_{n=\lfloor \|\mathbf{x} + \mathbf{z}L\|^{2-\epsilon_1} \rfloor + 1}^{\infty} |p_n(\mathbf{x} + \mathbf{z}L) - \bar{p}_n(\mathbf{x} + \mathbf{z}L)| \frac{\langle \mathcal{N} \rangle}{n} \mathbb{1}(n \leftrightarrow \mathbf{x} + \mathbf{z}L) \\
 & \leq \langle \mathcal{N} \rangle \sum_{\mathbf{z} \in \mathbb{Z}^d \setminus \{0\}} \sum_{n=\lfloor \|\mathbf{x} + \mathbf{z}L\|^{2-\epsilon_1} \rfloor + 1}^{\infty} \frac{c_7}{n^{d/2+1}} \frac{1}{n} \\
 & \leq \langle \mathcal{N} \rangle \sum_{\mathbf{z} \in \mathbb{Z}^d \setminus \{0\}} c_8 \|\mathbf{x} + \mathbf{z}L\|^{-d-2+\epsilon_1(1+d/2)} \\
 & = \frac{\langle \mathcal{N} \rangle}{L^{d+2-\epsilon_1(1+d/2)}} \sum_{\mathbf{z} \in \mathbb{Z}^d \setminus \{0\}} \frac{c_9}{\|\mathbf{x}/L + \mathbf{z}\|^{d+2-\epsilon_1(1+d/2)}} \tag{3.47}
 \end{aligned}$$

3.2. RANDOM-LENGTH RANDOM WALK

where the second inequality uses Lemma 3.2.4, the penultimate step uses Lemma 3.2.15, and $c_7, c_8, c_9 \in (0, \infty)$. Using Eq. (3.39) and Lemma 3.2.12 leads to

$$\begin{aligned}
& \sum_{\mathbf{z} \in \mathbb{Z}^d \setminus \{0\}} \sum_{n=\|\mathbf{x}+\mathbf{z}L\|^{2-\epsilon_1}}^{\infty} |p_n(\mathbf{x} + \mathbf{z}L) - \bar{p}_n(\mathbf{x} + \mathbf{z}L)| \mathbb{P}(\mathcal{N} \geq n) \mathbb{1}(n \leftrightarrow \mathbf{x} + \mathbf{z}L) \\
& \leq \frac{c_9 \langle \mathcal{N} \rangle}{L^{d+2-\epsilon_1(1+d/2)}} \sum_{\mathbf{z} \in \mathbb{Z}^d \setminus \{0\}} \frac{1}{\|\mathbf{z}\|^{d+2-\epsilon_1(1+d/2)}} \\
& \leq \frac{c_{10} \langle \mathcal{N} \rangle}{L^{d+2-\epsilon_1(1+d/2)}} \tag{3.48}
\end{aligned}$$

where $c_9, c_{10} \in (0, \infty)$.

Combining Eqs. (3.44), (3.46) and (3.48) leads to

$$|A(\mathbf{x}, L)| \leq a_1 \|\mathbf{x}\|^{-d+\epsilon_2} + a_2 \frac{\langle \mathcal{N} \rangle}{L^{d+2-\epsilon_1(1+d/2)}} \tag{3.49}$$

with $a_1, a_2 \in (0, \infty)$. ■

3.2.4 Lemmas

Lemma 3.2.4. *Consider a simple random walk $(S_t)_{t \in \mathbb{N}}$ on \mathbb{Z}^d starting at the origin. For $d \geq 3$, there exists $c \in \mathbb{R}^+$ such that for all $n \in \mathbb{N} \setminus \{0\}$ and $\mathbf{x} \in \mathbb{Z}^d$,*

$$|p_n(\mathbf{x}) - \bar{p}_n(\mathbf{x})| \mathbb{1}(n \leftrightarrow \mathbf{x}) \leq \frac{c}{n^{(d+2)/2}}.$$

Proof. See [51, Theorem 1.2.1]. ■

Lemma 3.2.5. *Let $b > 0$. Then as $r \rightarrow \infty$,*

$$\sum_{n=1}^{\infty} \left| n^{-b} e^{-r/n} - \int_{n-1/2}^{n+1/2} t^{-b} e^{-r/t} dt \right| = O(r^{-1-b}).$$

Proof. This lemma was extracted from the proof in [52, Lemma 4.3.2]. ■

Lemma 3.2.6. *Consider a simple random walk $(S_t)_{t \in \mathbb{N}}$ on \mathbb{Z}^d starting at the origin. There exist $\beta, c \in \mathbb{R}^+$ such that for all $s, n \in \mathbb{R}^+$,*

$$\mathbb{P}\left(\max_{0 \leq j \leq n} |S_j| \geq s\sqrt{n}\right) \leq ce^{-\beta s^2} \tag{3.50}$$

Proof. See [52, Proposition 2.1.2]. ■

Lemma 3.2.7. *If $c > 0$ then*

$$\sqrt{\pi/c} - 1 \leq \sum_{z \in \mathbb{Z}} e^{-cz^2} \leq \sqrt{\pi/c} + 1$$

Proof. Since $e^{-cz^2} \leq e^{-c(t-1/2)^2}$ for $t \in [z - 1/2, z + 1/2]$ and $z \in \mathbb{N} \setminus \{0\}$, we have

$$e^{-cz^2} = \int_{z-1/2}^{z+1/2} e^{-cz^2} dt \leq \int_{z-1/2}^{z+1/2} e^{-c(t-1/2)^2} dt .$$

Similarly, for all $z \in \mathbb{N}$,

$$e^{-cz^2} \geq \int_{z-1/2}^{z+1/2} e^{-c(t+1/2)^2} dt .$$

For the upper bound, we have

$$\sum_{z=1}^{\infty} e^{-cz^2} \leq \sum_{z=1}^{\infty} \int_{z-1/2}^{z+1/2} e^{-c(t-1/2)^2} dt = \int_{1/2}^{\infty} e^{-c(t-1/2)^2} dt = \frac{1}{\sqrt{c}} \int_0^{\infty} e^{-s^2} ds = \frac{1}{2} \sqrt{\pi/c}$$

Thus, the upper bound of this lemma follows since

$$\sum_{z \in \mathbb{Z}} e^{-cz^2} = 2 \sum_{z=1}^{\infty} e^{-cz^2} + 1 \leq \sqrt{\pi/c} + 1$$

Similarly, for the lower bound, we first have

$$\sum_{z=0}^{\infty} e^{-cz^2} \geq \sum_{z=0}^{\infty} \int_{z-1/2}^{z+1/2} e^{-c(t+1/2)^2} dt = \frac{1}{\sqrt{c}} \int_0^{\infty} e^{-s^2} ds = \frac{1}{2} \sqrt{\pi/c}$$

Then,

$$\sum_{z \in \mathbb{Z}} e^{-cz^2} = 2 \sum_{z=0}^{\infty} e^{-cz^2} - 1 \geq \sqrt{\pi/c} - 1$$

■

Lemma 3.2.8. *Let $c, L \in \mathbb{R}^+$, and $-L/2 \leq x \leq L/2$. Then*

$$e^{-cx^2} \leq \sum_{z \in \mathbb{Z}} e^{-c(x+zL)^2} \leq e^{-cx^2} \left(1 + \sum_{z \in \mathbb{Z}} e^{-cz^2 L^2/2} \right)$$

Proof. Since $\sum_{z \in \mathbb{Z}} e^{-c(x+zL)^2}$ is an even function of x , it suffices to consider $0 \leq x \leq$

$L/2$. We have

$$\sum_{z \in \mathbb{Z}} e^{-c(x+zL)^2} = e^{-cx^2} + \sum_{z \in \mathbb{Z} \setminus \{0\}} e^{-c(x+zL)^2} = e^{-cx^2} \left[1 + \sum_{z \in \mathbb{Z} \setminus \{0\}} e^{-c(2zxL+z^2L^2)} \right]$$

The lower bound then follows. For the upper bound, since

$$\begin{aligned} & \sum_{z \in \mathbb{Z} \setminus \{0\}} e^{-c(2zxL+z^2L^2)} \\ = & \sum_{z \in \mathbb{Z}^+} e^{-c(2zxL+z^2L^2)} + \sum_{z \in \mathbb{Z}^-} e^{-c(2zxL+z^2L^2)} \\ \leq & \sum_{z \in \mathbb{Z}^+} e^{-cz^2L^2} + \sum_{z \in \mathbb{Z}^-} e^{-c(z^2+z)L^2} \\ = & \sum_{z \in \mathbb{Z}^+} e^{-cz^2L^2} + 1 + \sum_{z \in \mathbb{Z}^- \setminus \{-1\}} e^{-c(z^2+z)L^2} \\ \leq & \sum_{z \in \mathbb{Z}^+} e^{-cz^2L^2/2} + 1 + \sum_{z \in \mathbb{Z}^- \setminus \{-1\}} e^{-cz^2L^2/2} \\ \leq & \sum_{z \in \mathbb{Z}} e^{-cz^2L^2/2} \end{aligned}$$

the upper bound then follows. ■

Lemma 3.2.9. *Let $c, L \in \mathbb{R}^+$, and $-L \leq x \leq L$. Then,*

$$-1 + \sum_{z \in \mathbb{Z}} e^{-cz^2L^2} \leq \sum_{z \in \mathbb{Z}} e^{-c(x+zL)^2} \leq 1 + \sum_{z \in \mathbb{Z}} e^{-cz^2L^2}$$

Proof. Since $\sum_{z \in \mathbb{Z}} e^{-c(x+zL)^2}$ is an even function of x , it suffices to consider $0 \leq x \leq L$. For the upper bound,

$$\begin{aligned} \sum_{z \in \mathbb{Z}} e^{-c(x+zL)^2} & \leq \sum_{z \in \mathbb{Z}^+} e^{-cz^2L^2} + e^{-cx^2} + \sum_{z \in \mathbb{Z}^-} e^{-c(z+1)^2L^2} \\ & \leq \sum_{z \in \mathbb{Z}^+} e^{-cz^2L^2} + 1 + \sum_{z \in \mathbb{Z}^-} e^{-cz^2L^2} + 1 \\ & = 1 + \sum_{z \in \mathbb{Z}} e^{-cz^2L^2} \end{aligned}$$

For the lower bound,

$$\begin{aligned}
 \sum_{z \in \mathbb{Z}} e^{-c(x+zL)^2} &\geq \sum_{z \in \mathbb{Z}^+} e^{-c(z+1)^2 L^2} + e^{-cL^2} + \sum_{z \in \mathbb{Z}^-} e^{-cz^2 L^2} \\
 &= \sum_{z \in \mathbb{Z}^+} e^{-cz^2 L^2} + \sum_{z \in \mathbb{Z}^-} e^{-cz^2 L^2} \\
 &= -1 + \sum_{z \in \mathbb{Z}} e^{-cz^2 L^2}
 \end{aligned}$$

■

Lemma 3.2.10. *Let $b > 1$, $\beta > 0$ and $a \in \mathbb{N} \setminus \{0\}$. As $r \rightarrow \infty$,*

$$\sum_{n=1}^a n^{-b} e^{-\beta r/n} = \beta^{1-b} r^{1-b} \int_{2\beta r/(2a+1)}^{\infty} s^{b-2} e^{-s} ds + O(r^{-1-b}),$$

Proof. We note that

$$\begin{aligned}
 \sum_{n=1}^a n^{-b} e^{-\beta r/n} &= \int_0^{a+1/2} t^{-b} e^{-\beta r/t} dt - \int_0^{1/2} t^{-b} e^{-\beta r/t} dt + \\
 &\quad \sum_{n=1}^a \left[n^{-b} e^{-\beta r/n} - \int_{n-1/2}^{n+1/2} t^{-b} e^{-\beta r/t} dt \right]. \tag{3.51}
 \end{aligned}$$

The second term in the RHS of (3.51) is $O(e^{-2r\beta})$ as $r \rightarrow \infty$. The third term is $O(r^{-1-b})$, from Lemma 3.2.5. But a simple change of variables shows the first term satisfies

$$\int_0^{a+1/2} t^{-b} e^{-\beta r/t} dt = \beta^{1-b} r^{1-b} \int_{2\beta r/(2a+1)}^{\infty} s^{b-2} e^{-s} ds. \tag{3.52}$$

■

Lemma 3.2.11. *Consider a simple random walk $(S_t)_{t \in \mathbb{N}}$ on \mathbb{Z}^d starting at the origin. For any $\alpha \in (0, 2)$ and $d \geq 3$,*

$$\sum_{n=1}^{\infty} |p_n(\mathbf{x}) - \bar{p}_n(\mathbf{x})| \mathbb{1}(n \leftrightarrow \mathbf{x}) \leq c \|\mathbf{x}\|^{-\alpha d/2}, \tag{3.53}$$

with $c \in (0, \infty)$.

Proof. If $n \leq \|\mathbf{x}\|^\alpha$ with $0 < \alpha < 2$, it is immediate that $\bar{p}_n(\mathbf{x}) \leq \left(\frac{d}{2\pi}\right)^{d/2} e^{-\frac{d}{2}\|\mathbf{x}\|^{2-\alpha}}$,

3.2. RANDOM-LENGTH RANDOM WALK

and moreover we have

$$p_n(\mathbf{x}) \leq \mathbb{P}\left(\max_{0 \leq i \leq n} |S_i| \geq \|\mathbf{x}\|\right) \leq c_1 e^{-\beta(\|\mathbf{x}\|/\sqrt{n})^2} \leq c_1 e^{-\beta\|\mathbf{x}\|^{2-\alpha}},$$

where $c_1 \in (0, \infty)$, and the last inequality follows from Lemma 3.2.6 with $\beta \in (0, \infty)$.

So, if $n \leq \|\mathbf{x}\|^\alpha$, then by Lemma 3.2.18

$$\sum_{n=1}^{\lfloor \|\mathbf{x}\|^\alpha \rfloor} |p_n(\mathbf{x}) - \bar{p}_n(\mathbf{x})| \leq c_2 e^{-\beta'\|\mathbf{x}\|^\alpha}. \quad (3.54)$$

with $c_2 \in (0, \infty)$, and $\beta' < \beta$.

If $n > \|\mathbf{x}\|^\alpha$, then applying Lemma 3.2.4 leads to

$$\sum_{n > \|\mathbf{x}\|^\alpha} |p_n(\mathbf{x}) - \bar{p}_n(\mathbf{x})| \mathbb{1}(n \leftrightarrow \mathbf{x}) \leq \sum_{n > \|\mathbf{x}\|^\alpha} \frac{c_3}{n^{(d+2)/2}} \leq c_4 \|\mathbf{x}\|^{-\alpha d/2}. \quad (3.55)$$

with $c_3, c_4 \in (0, \infty)$. The Lemma follows by combining Eqs. (3.54) and (3.55). \blacksquare

Lemma 3.2.12. *If $\delta > 0$, then*

$$\sum_{\mathbf{z} \in \mathbb{Z}^d \setminus \{0\}} \frac{1}{\|\mathbf{z}\|^{d+\delta}} < \infty.$$

Proof. Let $\partial\mathbb{B}_x = \mathbb{B}_x \setminus \mathbb{B}_{x-1}$ be the set of vertices on the surface of the d -dimensional box $\mathbb{B}_x = [-x, x]^d \cap \mathbb{Z}^d$. Since $\mathbb{B}_{x-1} \subset \mathbb{B}_x$, we have

$$\begin{aligned} |\partial\mathbb{B}_x| &= |\mathbb{B}_x| - |\mathbb{B}_{x-1}| = (2x+1)^d - (2x-1)^d \leq (2x)^d \left[\left(1 + \frac{1}{2x}\right)^d - \left(1 - \frac{1}{2x}\right)^d \right] \\ &\leq d(2^{d-1} + 1)(2x)^{d-1} \end{aligned} \quad (3.56)$$

The last step uses Lemma 3.2.16 and Lemma 3.2.17. Then,

$$\sum_{\mathbf{z} \in \mathbb{Z}^d \setminus \{0\}} \frac{1}{\|\mathbf{z}\|^{d+\delta}} = \sum_{x=1}^{\infty} \sum_{\mathbf{z} \in \partial\mathbb{B}_x} \frac{1}{\|\mathbf{z}\|^{d+\delta}} \leq \sum_{x=1}^{\infty} d2^{d-1} (2^{d-1} + 1) x^{-1-\delta} < \infty. \quad (3.57)$$

Lemma 3.2.13. *Fix $\gamma, \lambda \in \mathbb{R}^+$ and define $f : \mathbb{R}^+ \rightarrow \mathbb{R}$ via $f(x) = x^{-\gamma} e^{-\lambda/x}$. Then there exists $c_\gamma \in \mathbb{R}^+$ such that for all $x \in \mathbb{R}^+$*

$$|f(x) - f(x+1)| \leq c_\gamma x^{-1-\gamma}.$$

Proof. It follows by the triangle inequality that

$$\begin{aligned}
 |f(x) - f(x+1)| &= |x^{-\gamma}e^{-\lambda/x} - (x+1)^{-\gamma}e^{-\lambda/x} + (x+1)^{-\gamma}e^{-\lambda/x} - (x+1)^{-\gamma}e^{-\lambda/(x+1)}| \\
 &\leq |x^{-\gamma} - (x+1)^{-\gamma}| e^{-\lambda/x} + (x+1)^{-\gamma} |e^{-\lambda/x} - e^{-\lambda/(x+1)}| \\
 &\leq x^{-\gamma} \left| 1 - \left(1 + \frac{1}{x}\right)^{-\gamma} \right| + x^{-\gamma} |e^{-\lambda/x} - e^{-\lambda/(x+1)}|
 \end{aligned}$$

Lemma 3.2.14 implies that $|e^{-\lambda/x} - e^{-\lambda/(x+1)}| \leq \frac{1}{x}$. Lemma 3.2.16 gives $(1 + 1/x)^{-\gamma} \geq 1 - \gamma/x$. So,

$$|f(x) - f(x+1)| \leq (1 + \gamma)x^{-1-\gamma}. \quad (3.58)$$

Setting $c_\gamma = 1 + \gamma$ completes the proof. ■

Lemma 3.2.14. *Let $\lambda \in \mathbb{R}^+$. Then, for all $x \in \mathbb{R}^+$*

$$|e^{-\lambda/x} - e^{-\lambda/(x+1)}| \leq \frac{1}{x}$$

Proof. Define $h : \mathbb{R}^+ \rightarrow \mathbb{R}$ via $h(x) = e^{-\lambda/x}$, and let $x \in \mathbb{R}^+$. Since $h(x)$ is differentiable on $[x, x+1]$, the mean value theorem implies that there exists $\xi \in (x, x+1)$ such that

$$h(x+1) - h(x) = h'(\xi) = \frac{\lambda}{\xi^2} e^{-\lambda/\xi}$$

Therefore,

$$|h(x+1) - h(x)| \leq \frac{1}{x} \frac{\lambda}{\xi} e^{-\lambda/\xi} \leq \frac{1}{x}$$

where the last step uses the fact that $xe^{-x} \leq 1$ for all $x > 0$. ■

Lemma 3.2.15. *Let $a \in \mathbb{N} \setminus \{0\}$. Then, for all $\gamma > 1$,*

$$\sum_{n=a}^{\infty} n^{-\gamma} \leq \frac{(a-1)^{1-\gamma}}{\gamma-1}.$$

Proof. Fix a positive integer n . Since $(t-1/2)^{-\gamma} > n^{-\gamma}$ for all $t \in (n-1/2, n+1/2)$

we have

$$\begin{aligned}
 \sum_{n=a}^{\infty} n^{-\gamma} &= \sum_{n=a}^{\infty} \int_{n-1/2}^{n+1/2} n^{-\gamma} dt \\
 &\leq \sum_{n=a}^{\infty} \int_{n-1/2}^{n+1/2} (t-1/2)^{-\gamma} dt \\
 &\leq \int_{a-1/2}^{\infty} (t-1/2)^{-\gamma} dt \\
 &= \frac{1}{\gamma-1} (a-1)^{1-\gamma}.
 \end{aligned} \tag{3.59}$$

■

Lemma 3.2.16. *Let $\alpha \in \mathbb{R}$. Then, for all $x \in [0, 1]$,*

$$1 + c_2 x \leq (1+x)^\alpha \leq 1 + c_1 x \tag{3.60}$$

where $c_1 = \max\{\alpha, \alpha 2^{\alpha-1}\}$ and $c_2 = \min\{\alpha, \alpha 2^{\alpha-1}\}$.

Proof. Define $f : (-1, 2) \rightarrow \mathbb{R}$ by $f(x) = (1+x)^\alpha$. Since f is differentiable, Taylor's theorem implies that for any $x \in (0, 1]$ there exists $\xi \in (0, x)$ such that

$$f(x) = f(0) + f'(\xi)x = 1 + f'(\xi)x.$$

Since $f'(x) = \alpha(1+x)^{\alpha-1}$ is monotonic, it follows that $c_2 \leq f'(x) \leq c_1$ for all $x \in [0, 1]$ where $c_1 = \max\{f'(0), f'(1)\}$ and $c_2 = \min\{f'(0), f'(1)\}$. The lemma follows by noting that $f'(0) = \alpha$ and $f'(1) = \alpha 2^{\alpha-1}$. ■

Lemma 3.2.17. *Let $\alpha > 1$. Then, for all $x \in [0, 1]$,*

$$(1-x)^\alpha \geq 1 - \alpha x.$$

Proof. Define $f : [0, 1] \rightarrow \mathbb{R}$ by $f(x) = (1-x)^\alpha$. Since f is differentiable, Taylor's theorem implies that for any $x \in (0, 1]$ there exists $\xi \in (0, x)$ such that

$$f(x) = f(0) + f'(\xi)x = 1 - \alpha(1-\xi)^{\alpha-1}x \geq 1 - \alpha x. \tag{3.61}$$

■

Lemma 3.2.18. *Let $\beta > 0$. For any $\alpha, \gamma \in (0, \infty)$, there exists $c = c(\alpha, \beta, \gamma) \in (0, \infty)$ such that*

$$e^{-\beta x^\alpha} \leq c x^{-\gamma}.$$

for all $x \geq 0$.

Proof. The case $x = 0$ is immediate. For $x > 0$, we define $f(x) := x^\gamma e^{-\beta x^\alpha}$ and the first derivative is

$$f'(x) = x^{\gamma-1} e^{-\beta x^\alpha} (\gamma - \alpha \beta x^\alpha). \quad (3.62)$$

So $f'(x) > 0$ if $x \in (0, (\frac{\gamma}{\alpha\beta})^{1/\alpha})$ and $f'(x) < 0$ if $x \in ((\frac{\gamma}{\alpha\beta})^{1/\alpha}, \infty)$. The maximum is at $x = \frac{\gamma}{\alpha\beta}$. Choosing $c = f((\frac{\gamma}{\alpha\beta})^{1/\alpha})$ gives $f(x) \leq c$ which proves the lemma. ■

Lemma 3.2.19. *Let $\mathbf{y} \in \mathbb{Z}^d \setminus \{0\}$. For any $\epsilon > 0$, there exists $c(\epsilon, d) \in (0, \infty)$ such that*

$$\sum_{n=1}^{\lfloor \|\mathbf{y}\|^2 - \epsilon \rfloor} |\bar{p}_n(\mathbf{y}) - \bar{p}_{n+1}(\mathbf{y})| \leq c \exp\left(-\frac{d}{8} \|\mathbf{y}\|^\epsilon\right)$$

Proof. Let $M \in \mathbb{N}$ and $\mathbf{y} \in \mathbb{Z}^d$. Then

$$\begin{aligned} & \sum_{n=1}^M |\bar{p}_n(\mathbf{y}) - \bar{p}_{n+1}(\mathbf{y})| \\ & \leq \sum_{n=1}^M (\bar{p}_n(\mathbf{y}) + \bar{p}_{n+1}(\mathbf{y})) \\ & = \sum_{n=1}^M \left(\frac{d}{2\pi n} \right)^{d/2} e^{-\frac{\|\mathbf{y}\|^2 d}{2n}} + \left(\frac{d}{2\pi(n+1)} \right)^{d/2} e^{-\frac{\|\mathbf{y}\|^2 d}{2(n+1)}} \\ & \leq \left(\frac{d}{2\pi} \right)^{d/2} \sum_{n=1}^M \left(e^{-\frac{\|\mathbf{y}\|^2 d}{2n}} + e^{-\frac{\|\mathbf{y}\|^2 d}{2(n+1)}} \right) \end{aligned}$$

But since $n+1 \leq 2n$ for all $n \in \mathbb{N}$, it follows that

$$\begin{aligned} & \sum_{n=1}^M |\bar{p}_n(\mathbf{y}) - \bar{p}_{n+1}(\mathbf{y})| \\ & \leq 2 \left(\frac{d}{2\pi} \right)^{d/2} \sum_{n=1}^M e^{-\frac{d\|\mathbf{y}\|^2}{4n}} \\ & \leq 2 \left(\frac{d}{2\pi} \right)^{d/2} M e^{-\frac{d\|\mathbf{y}\|^2}{4M}} \\ & = 2 \left(\frac{d}{2\pi} \right)^{d/2} \left(M e^{-\frac{d\|\mathbf{y}\|^2}{8M}} \right) e^{-\frac{d\|\mathbf{y}\|^2}{8M}} \\ & \leq c e^{-\frac{d\|\mathbf{y}\|^2}{8M}} \end{aligned}$$

3.2. RANDOM-LENGTH RANDOM WALK

by Lemma 3.2.18 with $c \in (0, \infty)$.

Now demand $\mathbf{y} \neq 0$ and choose $M = \lfloor \|\mathbf{y}\|^{2-\epsilon} \rfloor$, so that

$$\frac{\|\mathbf{y}\|^2}{M} = \frac{\|\mathbf{y}\|^2}{\lfloor \|\mathbf{y}\|^{2-\epsilon} \rfloor} \geq \frac{\|\mathbf{y}\|^2}{\|\mathbf{y}\|^{2-\epsilon}} = \|\mathbf{y}\|^\epsilon$$

and we obtain

$$\sum_{n=1}^{\lfloor \|\mathbf{y}\|^{2-\epsilon} \rfloor} |\bar{p}_n(\mathbf{y}) - \bar{p}_{n+1}(\mathbf{y})| \leq ce^{-\frac{d\|\mathbf{y}\|^\epsilon}{8M}}$$

■

Lemma 3.2.20. *Let $d \in \mathbb{N}$ and $\beta \geq 1$. For any $\epsilon > 0$, there exists $c(d, \epsilon) \in (0, \infty)$ such that*

$$\sum_{\mathbf{z} \in \mathbb{Z}^d \setminus \{0\}} e^{-\beta \|\mathbf{z}\|^\epsilon} \leq c(d, \epsilon) e^{-\beta}$$

Proof.

$$\begin{aligned} & \sum_{\mathbf{z} \in \mathbb{Z}^d \setminus \{0\}} e^{-\beta \|\mathbf{z}\|^\epsilon} \\ &= 2de^{-\beta} + \sum_{\substack{\mathbf{z} \in \mathbb{Z}^d \\ \|\mathbf{z}\| > 1}} e^{-\beta \|\mathbf{z}\|^\epsilon} \\ &\leq 2de^{-\beta} \left[1 + \frac{1}{2d} \sum_{\substack{\mathbf{z} \in \mathbb{Z}^d \\ \|\mathbf{z}\| > 1}} e^{-\beta(\|\mathbf{z}\|^\epsilon - 1)} \right] \end{aligned}$$

But $\beta(\|\mathbf{z}\|^\epsilon - 1) \geq \|\mathbf{z}\|^\epsilon - 1$ for all $\mathbf{z} \in \mathbb{Z}^d$ with $\|\mathbf{z}\| > 1$, since $\beta \geq 1$ and $\|\mathbf{z}\|^\epsilon - 1 > 0$, so

$$\begin{aligned}
 & \sum_{\mathbf{z} \in \mathbb{Z}^d \setminus \{0\}} e^{-\beta \|\mathbf{z}\|^\epsilon} \\
 & \leq 2d e^{-\beta} \left[1 + \frac{1}{2d} \sum_{\substack{\mathbf{z} \in \mathbb{Z}^d \\ \|\mathbf{z}\| > 1}} e^{-(\|\mathbf{z}\|^\epsilon - 1)} \right] \\
 & \leq 2d \left[1 + \sum_{\substack{\mathbf{z} \in \mathbb{Z}^d \\ \|\mathbf{z}\| > 1}} e^{-\|\mathbf{z}\|^\epsilon} \right] e^{-\beta} \\
 & \leq 2d \left(\sum_{\mathbf{z} \in \mathbb{Z}^d} e^{-\|\mathbf{z}\|^\epsilon} \right) e^{-\beta}
 \end{aligned}$$

since the series $e^{-\|\mathbf{z}\|^\epsilon}$ converges (combining Lemma 3.2.12 and 3.2.18 suffice to establish this), we have

$$\sum_{\substack{\mathbf{z} \in \mathbb{Z}^d \\ \|\mathbf{z}\| > 1}} e^{-\beta \|\mathbf{z}\|^\epsilon} \leq c(d, \epsilon) e^{-\beta} \tag{3.63}$$

with $c(d, \epsilon) \in (0, \infty)$. ■

3.3 SAW and Ising model at criticality

We now focus on the FSS behaviour of the two-point functions and susceptibility of the SAW and Ising models at the infinite-volume critical point z_c . Our main results in this section can be summarized as follows:

- We argue that the two-point functions of the SAW and Ising model exhibit the scaling behaviour in Eq. (3.1) with $\mu = d/2$. We numerically confirm that the Green's function of a RLLERW with mean walk length $L^{d/2}$ exhibits the same FSS behaviour.
- We study unwrapped two-point functions for the RLLERW and SAW, defined in Eq. (2.12). In contrast to the two-point functions on the Euclidean scale, the unwrapped two-point function accounts for windings on the torus. We numerically show that the unwrapped two-point functions for systems with PBC display standard mean-field behaviour, in agreement with the (Euclidean) two-point functions on the infinite-lattice.

3.3.1 Two-point functions and susceptibility

On the complete graph K_n at criticality, it is rigorously established [47] that $\langle \mathcal{N}_{\text{SAW}} \rangle \asymp n^{1/2}$. Therefore, it is natural to expect the critical PBC behaviour $\langle \mathcal{N}_{\text{SAW}} \rangle \asymp L^{d/2}$ for $d > d_c$. Figure 3.1 shows the scaling of $\langle \mathcal{N}_{\text{SAW}} \rangle$ on five-dimensional tori at criticality. Our fit leads to the exponent value 2.50(1) by discarding $L < 41$, in agreement with

$$\langle \mathcal{N} \rangle \asymp L^{d/2}. \quad (3.64)$$

We now numerically verify that Eq. (3.1) with $\mu = d/2$ correctly predicts the behaviour of the two-point functions of the SAW and Ising models. Figure 3.2 (a) shows $g_{\text{SAW,Ising}}(\mathbf{x})$ on five-dimensional toroidal grids. At moderate values of \mathbf{x} , the two-point functions exhibit the standard infinite-lattice asymptotic decay $\|\mathbf{x}\|^{2-d}$, but then enter a plateau of order $L^{\mu-d}$ which persists to the boundary. Figure 3.2 (b) shows an appropriately scaled version of the two-point functions of the Ising and SAW models against the dimensionless variable $y := \|\mathbf{x}\|/L^{(d-\mu)/(d-2)}$ with $\mu = d/2$. For small values of y , one observes a constant region which corresponds to mean-field scaling, while at larger values the two-point functions exhibit a power-law, in agreement with the spatially independent background term $L^{\mu-d}$. The excellent data collapse in both regions provides strong evidence that the two-point functions exhibit the scaling from Eq. (3.1) with $\mu = d/2$. Moreover, Figures 3.2 (a) and 3.2 (b) show that the Green's function of a RLLERW with mean walk length $L^{d/2}$ display the same FSS behaviour as the critical Ising and SAW two-point functions. We note that our conjectured critical PBC behaviour of the Ising two-point function is in contrast to [29], and in agreement with the conjectured scaling in [28, 30].

Finally, we investigated the FSS behaviour of the susceptibility $\chi_{\text{SAW,Ising}}$. Informed by Eq. (3.2), we expect that the susceptibility scales as $\chi_{\text{SAW,Ising}} \asymp L^{d/2}$ since $\langle \mathcal{N}_{\text{SAW}} \rangle \asymp L^{d/2}$. Fig. 3.1 verifies this prediction for both models. Our fits lead to the exponent values 2.50(1) for the SAW by discarding $L < 41$, and 2.51(2) for the Ising model by discarding $L < 21$, in agreement with $\chi_{\text{SAW,Ising}} \asymp L^{d/2}$. This FSS behaviour for the Ising susceptibility is in broad agreement with the numerical observations in [17, 32, 30].

3.3.2 Windings and unwrapped two-point functions

In order to explain the physical mechanism behind the anomalous bulk behaviour of the two-point functions on hypercubic lattices with periodic boundaries above d_c ,

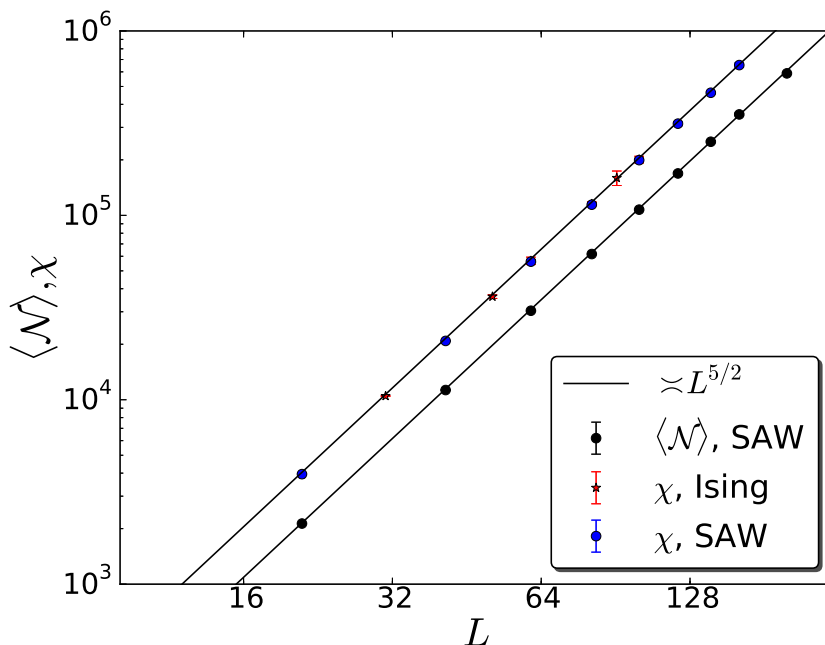


Figure 3.1: Critical PBC scaling of the mean walk length $\langle \mathcal{N}_{\text{SAW}} \rangle$ and susceptibility $\chi_{\text{Ising, SAW}}$ in five dimensions. Our results show that $\langle \mathcal{N}_{\text{SAW}} \rangle \simeq L^{d/2}$. In agreement with the prediction from Eq. (3.2), the susceptibility of the SAW and Ising models displays the scaling $\chi_{\text{SAW, Ising}} \simeq L^{d/2}$. To emphasize the universal scaling, the data for Ising and SAW susceptibility were translated onto a single curve.

it proves useful to investigate geometric quantities such as the average number of windings $\langle \mathcal{W} \rangle$.

We first present a heuristic scaling argument which characterizes the proliferation of windings in the SAW model in terms of the exponent d/d_c . Consider a uniformly random SAW of fixed length N in \mathbb{Z}^d , with $d > d_c$. The second virial coefficient $B_2^{N,N}$ provides a measure of the excluded volume between a pair of such SAWs, and is believed to scale like $B_2^{N,N} \simeq N^2$ (see e.g. [54]). This suggests that in order to wrap such a walk onto a torus \mathbb{Z}_L^d , without introducing intersections, would require $N^2 \lesssim L^d$. Considering now a variable length ensemble at z_c , we expect the mean of \mathcal{N}_{SAW} to be of the order of its maximum, which implies $\langle \mathcal{N}_{\text{SAW}} \rangle \simeq L^{d/2}$. Figure 3.1 verifies this prediction. Furthermore, if one were to take a typical SAW on the torus \mathbb{Z}_L^d , and unwrap it into \mathbb{Z}^d , it would have root-mean-square displacement of order $\langle \mathcal{W}_{\text{SAW}} \rangle L$. But for a uniformly-random fixed-length SAW in \mathbb{Z}^d with $d > d_c$, the mean-square displacement scales like the walk length. Combining this with the above observation shows that $\langle \mathcal{W}_{\text{SAW}} \rangle \simeq L^{d/d_c - 1}$.

We now numerically confirm this predicted FSS behaviour for the average winding number of SAWs in five and six dimensions, and extend our results to the Ising model

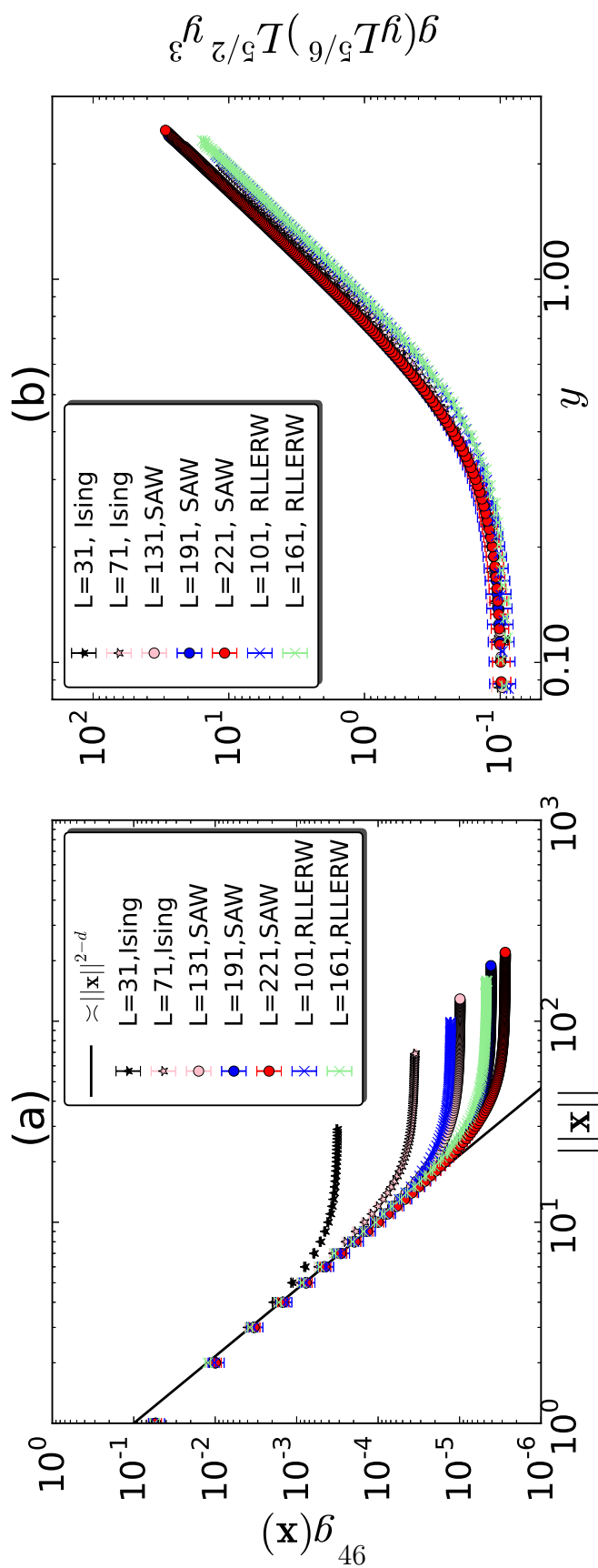


Figure 3.2: (a) Critical two-point functions of the SAW and Ising models, and Green's function of a RLLERW with mean walk length $L^{d/2}$ in five dimensions. (b) Appropriately scaled versions of the critical two-point and Green's functions onto the ansatz in Eq. (3.1) with $y := \|\mathbf{x}\|/L^{(d-\mu)/(d-2)}$ with $\mu = d/2$. The data collapse in each model strongly suggests that the prediction from Eq. (3.1) correctly describes the FSS behaviour of the SAW and Ising models.

and RLLERW. Fig. 3.3 shows the average winding number against L . In dimensions below d_c , we find that $\langle \mathcal{W} \rangle$ is bounded as $L \rightarrow \infty$. In contrast, we observe that windings proliferate for $d > d_c$. For $d = 5$, our fits lead to the exponent value 0.24(3) for $\langle \mathcal{W}_{\text{Ising}} \rangle$ by discarding $L < 9$, and 0.27(4) for $\langle \mathcal{W}_{\text{SAW}} \rangle$ by discarding $L < 81$. We also studied the average winding number of a RLLERW with mean walk length $L^{d/2}$ where our fits lead to the exponent value 0.24(2) by discarding $L < 31$. For $d = 6$, our fits for $\langle \mathcal{W}_{\text{SAW}} \rangle$ lead to the exponent value 0.54(7) by discarding $L < 15$.

We emphasize that the exponent value $d/d_c - 1$ appeared in a recent rigorous study on critical bond percolation on high dimensional tori [53]. It was proved there that, with high probability, large clusters contain long cycles, i.e. cycles with linear extension L , which wind around the torus at least $L^{d/d_c - 1}$ times.

Finally, we show that the anomalous FSS behaviour of the two-point functions in Eq. (3.1) can be removed by considering *unwrapped* two-point functions which correctly account for the proliferation of windings above d_c . Figure 3.4 shows the unwrapped two-point function of the SAW. Moreover, we plot the unwrapped Green's function of a RLLERW with mean walk length $L^{d/2}$. We find that both unwrapped two-point functions display the scaling $g(u) \asymp u^{2-d}$ at distances in the bulk. This observation is consistent with the scaling behaviour for the RLRW Green's function on \mathbb{Z}^d , established in Theorem 3.2.1.

3.4 SAW and Ising model at pseudo-critical points

Recently, there has been debate [32, 30, 34] concerning FSS behaviour of physical observables at pseudo-critical points z_L with $\lim_{L \rightarrow \infty} z_L = z_c$. In particular, we investigate the question of whether it is possible to observe the standard mean-field scaling $\chi \asymp L^2$, as established for FBC at criticality (see Sec. 4.2).

The main results in this section can be summarized as follows:

- We establish the FSS behaviour of the Ising/SAW two-point functions and susceptibility at various pseudo-critical points; see Eqs. (3.66) and (3.67). In particular, by contrast to the critical PBC behaviour, we numerically show that $\chi \asymp L^2$ at an appropriate pseudo-critical point.
- We numerically show that the FSS behaviour of the SAW two-point function is controlled by the corresponding mean walk length. In particular, we numerically verify that Eq. (3.1) correctly describes the FSS behaviour of the SAW and Ising two-point functions.

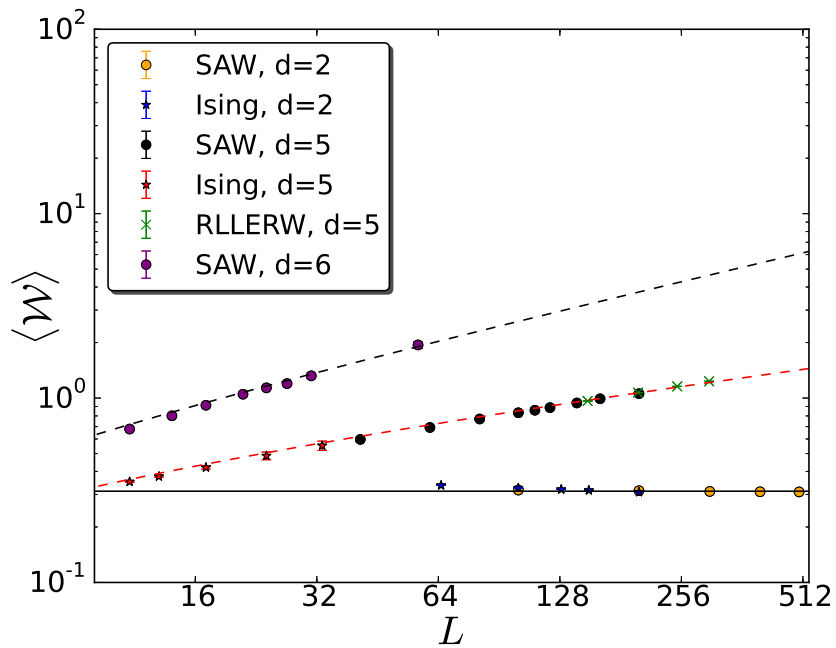


Figure 3.3: Average winding number, $\langle \mathcal{W} \rangle$, for Ising and SAW models, and for a RLLERW with mean walk length $L^{d/2}$ on periodic boundaries at criticality. The number of windings is asymptotically constant in L for $d < d_c$. Above d_c , windings proliferate with increasing L . To emphasize the universal scaling, the data for Ising, SAW and RLLERW were translated onto a single curve for both $d = 2$ and $d = 5$.

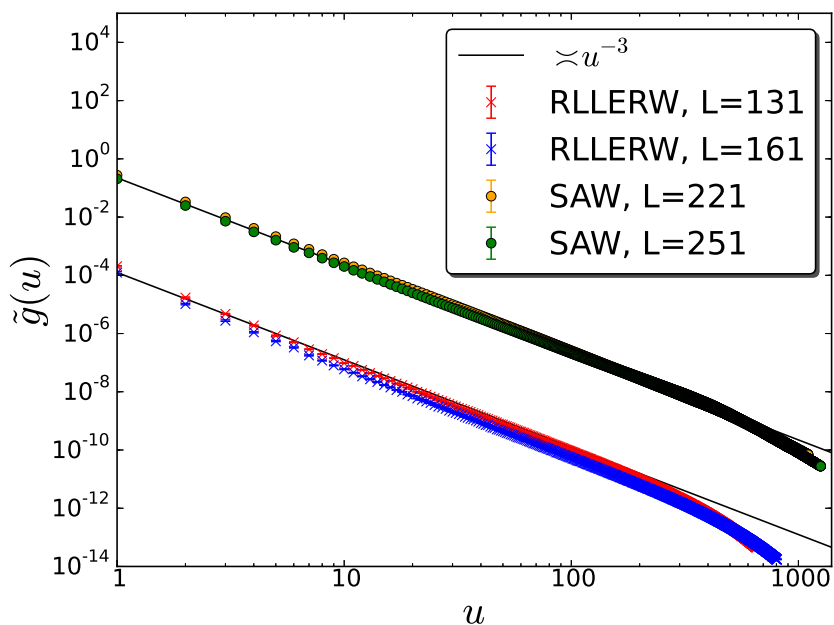


Figure 3.4: *Unwrapped* critical two-point function of SAW, and unwrapped Green's function of a RLLERW with mean walk length $L^{d/2}$ on five-dimensional lattices with periodic boundaries. In agreement with the well-known behaviour of the (standard Euclidean) two-point functions on the infinite-lattice, these unwrapped two-point functions display the standard mean-field scaling $g(u) \asymp u^{2-d}$ on the torus. For clarity, the data for RLLERW were translated downwards.

We first investigate the scaling behaviour of the mean walk length of a SAW at $z_L = z_c - aL^{-\lambda}$ where $a \in \mathbb{R}^+$ is a constant, and $\lambda \in \mathbb{R}^+$ denotes the speed of convergence to z_c . We choose $a > 0$ (i.e. shifting to high temperature), since we aim to establish a pseudo-critical point where we observe $\langle \mathcal{N}_{\text{SAW}} \rangle \asymp L^2$ instead of the larger critical mean walk length scaling $\langle \mathcal{N}_{\text{SAW}} \rangle \asymp L^{d/2}$. Informed by Eq. (3.2), we expect that the susceptibility of a SAW with mean walk length $\langle \mathcal{N}_{\text{SAW}} \rangle \asymp L^2$ scales as $\chi_{\text{SAW}} \asymp L^2$ which we numerically confirm below. We note that our simulations are performed at the fixed value $a = 0.1$. However, as suggested by several numerical tests, our results in this section hold regardless of the specific choice of a .

Figure 3.7 (a) shows the scaling of the mean walk length of a SAW for $\lambda = 1, 3/2, 2, 5/2, 3$. Our fits lead to the exponent values 0.998(2) for $\lambda = 1$ by discarding $L < 81$, 1.499(2) for $\lambda = 3/2$ by discarding $L < 41$, 2.01(1) for $\lambda = 2$ by discarding $L < 31$, 2.46(3) for $\lambda = 5/2$ by discarding $L < 41$, and 2.51(3) for $\lambda = 3$ by discarding $L < 41$. From these observations, we conjecture the FSS behaviour

$$\langle \mathcal{N}_{\text{SAW}} \rangle \asymp \begin{cases} L^{d/2}, & \lambda \geq d/2, \\ L^\lambda, & \lambda < d/2. \end{cases} \quad (3.65)$$

We now investigate the two-point functions and susceptibility of the Ising and SAW models at z_L . Informed by (3.1) and (3.65), we conjecture the following piecewise asymptotics:

- If $\lambda \geq d/2$:

$$g(\mathbf{x}) \asymp \begin{cases} \|\mathbf{x}\|^{2-d}, & \|\mathbf{x}\| \leq c_1 L^{d/[2(d-2)]}, \\ L^{-d/2}, & \|\mathbf{x}\| \geq c_1 L^{d/[2(d-2)]} \end{cases} \quad (3.66)$$

where $c_1 \in \mathbb{R}^+$.

- If $\lambda < d/2$:

$$g(\mathbf{x}) \asymp \begin{cases} \|\mathbf{x}\|^{2-d}, & \|\mathbf{x}\| \leq c_2 L^{(d-\lambda)/(d-2)}, \\ L^{\lambda-d}, & \|\mathbf{x}\| \geq c_2 L^{(d-\lambda)/(d-2)} \end{cases} \quad (3.67)$$

where $c_2 \in \mathbb{R}^+$.

This implies the following scaling for the susceptibility:

- If $\lambda \geq d/2$:

$$\chi \asymp L^{d/2} \quad (3.68)$$

- If $\lambda < d/2$:

$$\chi \asymp L^\lambda \tag{3.69}$$

We now numerically confirm these conjectures. Figures 3.5 and 3.6 show the FSS behaviour of the two-point functions of the Ising and SAW models for $\lambda = 1, 3/2, 2$. The corresponding FSS behaviour of the two-point functions is in excellent agreement with Eq. (3.67). For $\lambda = 1, 3/2$, Fig. 3.5 verifies the predicted absence of a plateau for the SAW and Ising two-point functions. For $\lambda = 2$, the rescaled version of the two-point functions in Fig. 3.6 (b) show an excellent data collapse onto the ansatz in Eq. (3.67) with $\lambda = 2$, corresponding to standard mean-field behaviour. Furthermore, Figs. 3.5 and 3.6 show the RLLERW Green's function with mean walk lengths L^μ where $\mu = 1, 3/2, 2$. Each case displays the same FSS behaviour as the corresponding two-point functions of the Ising and SAW models. We note that our numerical simulations suggest that the Ising and SAW two-point functions display the critical FSS behaviour from Fig. 3.2, when $\lambda \geq d/2$. I.e. the pseudo-critical point z_L lies in the critical scaling window in this case.

We now turn to the FSS behaviour of the susceptibility. Figure 3.7 (b) shows the scaling behaviour of the susceptibility for $\lambda = 1, 3/2, 2, 5/2, 3$. Our fits for the Ising susceptibility lead to exponent estimates 1.00(1) for $\lambda = 1$ by discarding $L < 41$, 1.51(2) for $\lambda = 3/2$ by discarding $L < 31$, 2.05(7) for $\lambda = 2$ by discarding $L < 31$, 2.5(2) for $\lambda = 5/2$ by discarding $L < 31$, and 2.5(2) for $\lambda = 3$ by discarding $L < 31$. For SAW, our fits lead to the exponent value 1.005(6) for $\lambda = 1$ by discarding $L < 61$, 1.503(5) for $\lambda = 3/2$ by discarding $L < 61$, 2.00(1) for $\lambda = 2$ by discarding $L < 31$, 2.46(5) for $\lambda = 5/2$ by discarding $L < 31$, and 2.48(5) for $\lambda = 3$ by discarding $L < 31$. These observations are in agreement with Eqs. (3.69) and (3.68).

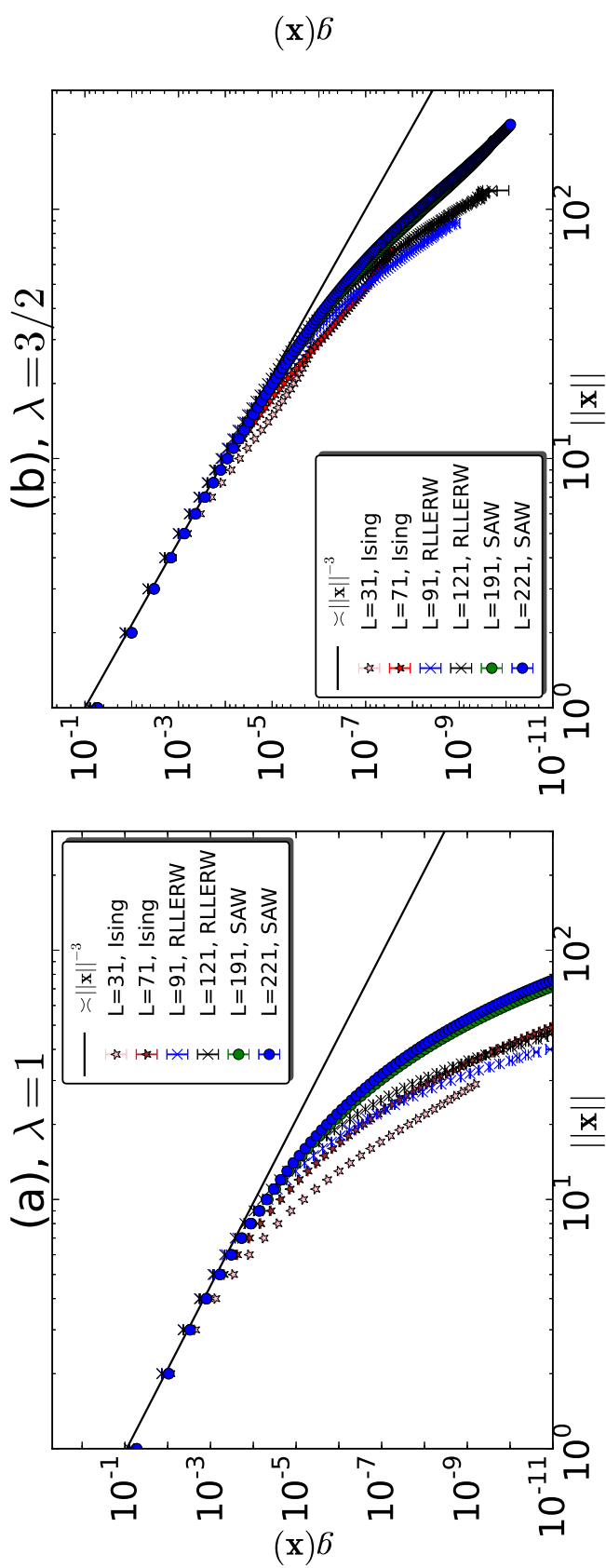


Figure 3.5: (a) Pseudo-critical two-point functions of the SAW and Ising models for $\lambda = 1$, and Green's function of a RLLERW with mean walk length L . (b) Pseudo-critical two-point functions of the SAW and Ising models for $\lambda = 3/2$, and Green's function of a RLLERW with mean walk length $L^{3/2}$.

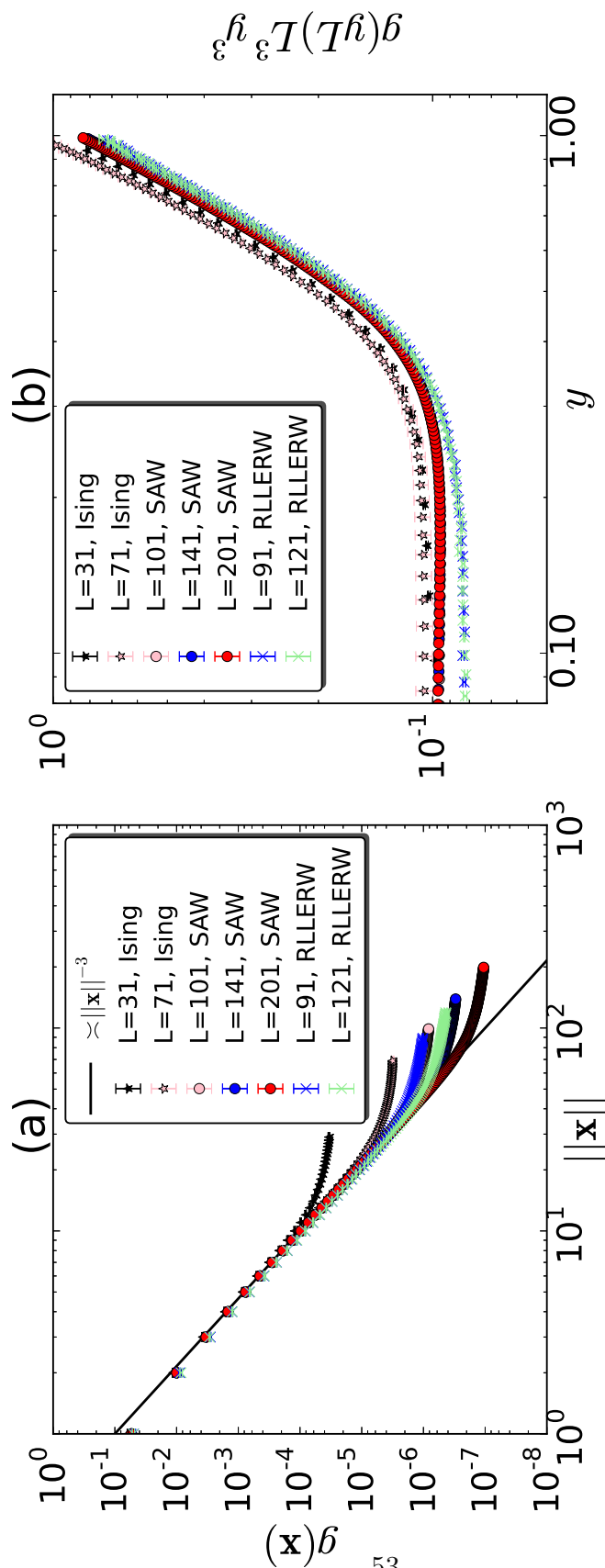


Figure 3.6: (a) Pseudo-critical two-point functions of the SAW and Ising models at $z_L = z_c - aL^{-2}$ and Green's function of a RLLERW with mean walk length L^2 . (b) Appropriately scaled versions of the two-point and Green's functions onto the ansatz in Eq. (3.1) with $y := \|\mathbf{x}\|/L^{(d-\mu)/(d-2)}$ with $\mu = 2$ (Equivalently, onto the ansatz in Eq. (3.67) with $\lambda = 2$). The data collapse in each model strongly suggests that the prediction from Eq. (3.1) correctly describes the FSS behaviour of the SAW and Ising models. Note that the observed scaling $g(\mathbf{x}) \propto \|\mathbf{x}\|^{2-d}$ corresponds to standard-mean field scaling, as observed for free boundaries at criticality (see Sec. 4.2).

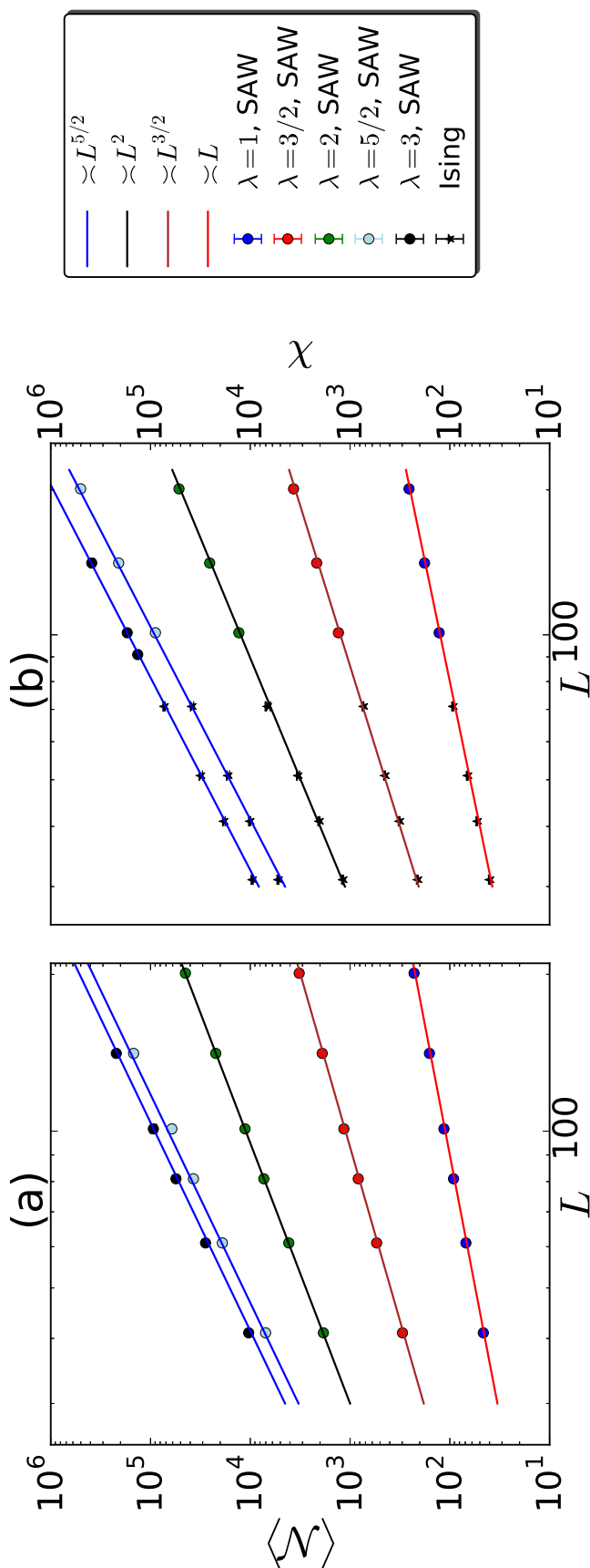


Figure 3.7: FSS behaviour of the mean walk length $\langle N_{\text{SAW}} \rangle$ and the susceptibility $\chi_{\text{Ising,SAW}}$ on periodic and free boundaries in five dimensions. The circles display data points for the SAW, while the stars display Ising data. For clarity, the Ising data was translated onto the same curve as the SAW. The extracted exponents match with the theoretical predictions in Eq. (3.65) for the mean walk length, and Eqs. (3.69), (3.68) for the susceptibility. (a) FSS behaviour of $\langle N_{\text{SAW}} \rangle$ for $\lambda = 1, 3/2, 2, 5/2, 3$. (b) FSS behaviour of $\chi_{\text{Ising,SAW}}$ for the Ising model and SAW for $\lambda = 1, 3/2, 2, 5/2, 3$.

FSS on hypercubic lattices with free, reflective and holding boundaries

With free boundary conditions (FBC), the possible existence of the FSS behaviour $\chi \asymp L^{d/2}$ at appropriate *pseudo-critical* points is the subject of ongoing debate [32, 30, 34]. Specifically, denoting by T_L the temperature which maximizes the (modulus) susceptibility $\bar{\chi}(T, L) := \text{Var}(|\sum_i \mathbf{s}_i|)^{1/2}$ on a box with linear size L , it was observed numerically in [32] that $\bar{\chi}(T_L, L)$ scales as $L^{d/2}$, as observed at criticality for periodic systems. The results in [30] are in agreement with this observation, however, the more recent work [34] refuted this claim, and numerically observed only the standard mean-field scaling L^2 .

Our main results can be summarized as follows:

- We rigorously establish that Eq. (3.1) also correctly describes the FSS behaviour of the Green's function of a RLRW on hypercubic lattices with holding and reflective boundaries.
- Informed by this observation, we argue that one *can* observe $\chi \asymp L^{d/2}$ at a pseudo-critical point where the mean walk length scales as $L^{d/2}$. We support this claim by establishing an appropriate pseudo-critical point for the Ising model where the susceptibility exhibits this FSS behaviour.

¹Both $\bar{\chi}$ and $\chi = \text{Var}(\sum_i \mathbf{s}_i)$ are expected to display the same FSS behaviour, supported by numerical observations in [34]

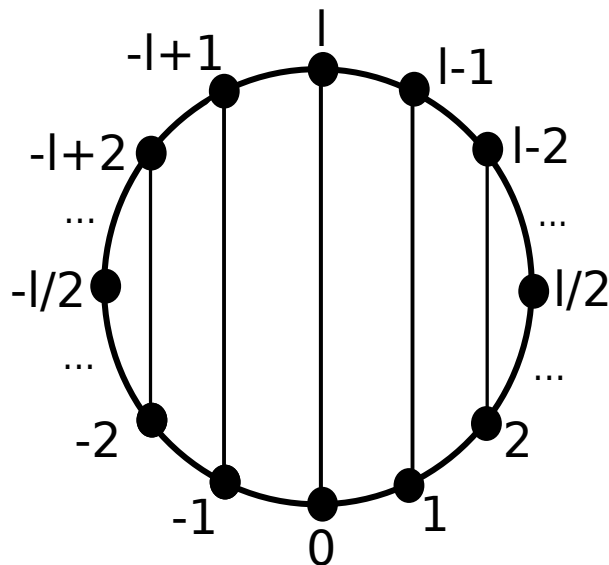


Figure 4.1: Illustration of the mapping from a SRW on a cycle with linear size $2l$ (l is an *even* integer) to a SRW on a path graph with reflective boundary conditions. The lines illustrate the equivalences $0 \equiv l$, $1 \equiv l - 1$ etc.

4.1 RLRW on boxes with reflective and holding boundary conditions

We rigorously study a random-length random walk on a box with reflective and holding boundary conditions, defined in Sec. 2.1. The minor difference compared with *free* boundaries, which we impose for the Ising and SAW models in Secs. 4.2 and 4.3, is that the transition probabilities on the boundary of the box are not uniform in the number of adjacent vertices².

To study RLRW on boxes with reflective or holding boundary conditions, we use the rigorous results on the torus from the last chapter, and define an appropriate mapping between the RLRW behaviour on the torus and the box with reflective and holding boundary conditions. We rigorously establish this mapping in Lemma 4.1.8. As an illustration, we present the main idea of the mapping in Figs. 4.1 and 4.2 for a RLRW on the cycle \mathbb{Z}_{2l} (i.e. for $d = 1$). We emphasize that if l is chosen to be odd, then the torus maps to a box with holding boundary conditions, while if l is chosen to be even, then the torus maps to a box with reflective boundaries.

²A numerical study of a RLRW on hypercubic lattices with reflective and holding boundaries strongly suggests that its Green's function displays the same FSS behaviour as on free boundaries

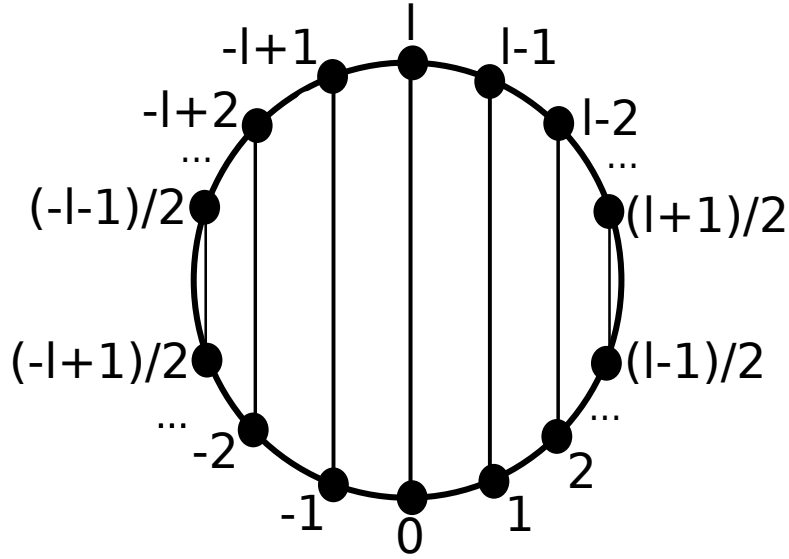


Figure 4.2: Illustration of the mapping from a SRW on a cycle with linear size $2l$ (l is an odd integer) to a SRW on a path graph with holding boundary conditions. The lines illustrate the equivalences $0 \equiv l, 1 \equiv l - 1$ etc.

4.1.1 Preliminaries

Definition 4.1.1. Let $(X_t)_{t \in \mathbb{N}}$ be a Markov chain on a finite set S with transition matrix P . Let \mathcal{N} be an \mathbb{N} -valued random variable with $\langle \mathcal{N} \rangle < \infty$ and tail distribution $F(t)$. The corresponding Green's function is

$$G(x, y) := \sum_{t=0}^{\infty} P^t(x, y) F(t), \quad \forall x, y \in S.$$

Definition 4.1.2. Let $(X_t)_{t \in \mathbb{N}}$ be a Markov chain on a finite set S . Let \equiv denote an equivalence relation on S . For each $x \in S$, define its equivalence class by $[x] := \{x' \in S : x' \equiv x\}$. Moreover, define $S^\# := \{[x] : x \in S\}$.

Lemma 4.1.3. Let $(X_t)_{t \in \mathbb{N}}$ be a Markov chain on a finite set S with transition matrix P . If $P(x, [y]) = P(x', [y])$ for all $x' \equiv x$, then $([X_t])_{t \in \mathbb{N}}$ is a Markov chain on $S^\#$ with transition matrix $P^\#$.

Proof. This is proved in [55, Lemma 2.5]; see also [56]. ■

Lemma 4.1.4. Let $(X_t)_{t \in \mathbb{N}}$ be a Markov Chain on a finite set S with transition matrix P satisfying

$$P(x, [y]) = P(x', [y])$$

for all $x' \equiv x$. Let G and $G^\#$ be the Green's functions of $(X_t)_{t \in \mathbb{N}}$ and $([X_t])_{t \in \mathbb{N}}$,

respectively. Then

$$G^\#([x], [y]) = \sum_{y' \in [y]} G(x', y'), \quad \forall x' \in [x]$$

Proof. The key step is to prove $(P^\#)^t([x], [y]) = P^t(x', [y])$ for all integers $t \geq 0$ and all $x' \in [x]$. The $t = 0$ case is immediate. Assume the statement holds for $t \geq 0$. Then, if $x' \in [x]$

$$\begin{aligned} (P^\#)^{t+1}([x], [y]) &= \sum_{[z] \in S^\#} (P^\#)^t([x], [z]) P^\#([z], [y]) \\ &= \sum_{[z] \in S^\#} P^t(x', [z]) P^\#([z], [y]) \\ &= \sum_{[z] \in S^\#} \sum_{z' \in [z]} P^t(x', z') P^\#([z], [y]) \\ &= \sum_{[z] \in S^\#} \sum_{z' \in [z]} P^t(x', z') P(z', [y]) \\ &= \sum_{y' \in [y]} \sum_{z' \in S} P^t(x', z') P(z', y') \\ &= \sum_{y' \in [y]} P^{t+1}(x', y') \\ &= P^{t+1}(x', [y]). \end{aligned}$$

The initial claim then follows by induction. Therefore if $x' \in [x]$, it follows that

$$G^\#([x], [y]) = \sum_{t=0}^{\infty} P^t(x', [y]) F(t) = \sum_{y' \in [y]} \sum_{t=0}^{\infty} P^t(x', y') F(t) = \sum_{y' \in [y]} G(x', y'). \quad (4.1)$$

■

4.1.2 RLRW Green's function on a box with reflective and holding boundary conditions

Definition 4.1.5. Let $l \in \mathbb{N} \setminus \{0\}$, and define $\mathbb{Z}_{2l} := \{1 - l, 2 - l, \dots, l\}$. For each $x \in \mathbb{Z}_{2l}$, define the equivalence class $[x] := \{x, l - x\}$. For each $\mathbf{x}, \mathbf{y} \in \mathbb{Z}_{2l}^d$, define $\mathbf{x} \equiv \mathbf{y}$ if and only if $y_i \in [x_i]$ for all $i \in \{1, \dots, d\}$.

Remark. Note that the vertex set of \mathbb{Z}_{2l}^d can be taken to be the box $\tilde{\mathbb{B}}_l$, which is endowed with the Euclidean norm $\|\cdot\|$, as defined in Sec. 2.1.

Theorem 4.1.6 (RLRW Green's function on the box with RBC and HBC). *Let $b \in \mathbb{N}$. Consider a RLRW on a $d \geq 3$ dimensional box \mathbb{B}_b with either reflective or holding boundary conditions. If $\langle \mathcal{N} \rangle \asymp b^\mu$ with $\mu > 2$, then there exists $c_1, c_2, c_3, c_4 \in \mathbb{R}^+$ such that the Green's function satisfies:*

$$c_1 \|\mathbf{x}\|^{2-d} + c_2 b^{\mu-d} \leq G_{\text{HBC,RBC}}(\mathbf{x}) \leq c_3 \|\mathbf{x}\|^{2-d} + c_4 b^{\mu-d} \quad (4.2)$$

Remark. This FSS behaviour coincides with Eq. (3.1) which we established on a box with periodic boundaries in Corollary 3.24.

Proof. Let $b \in \mathbb{N}$, and consider \mathbb{B}_b and $\tilde{\mathbb{B}}_b$, defined in Sec. 2.1. Let $P_{\text{HBC},b}$ and $P_{\text{RBC},b}$ denote the transition matrices of a SRW on \mathbb{B}_b with holding and reflecting boundary conditions, respectively. Let $P_{\text{PBC},b}$ denote the transition matrix of a SRW on $\tilde{\mathbb{B}}_b$ with periodic boundary conditions. Let $\mathbf{x}, \mathbf{y} \in \mathbb{B}_b$. Then by Lemma 4.1.8 it follows that

$$P_{\text{HBC},b} = P_{\text{PBC},2b+1}^\#([\mathbf{x}], [\mathbf{y}]) \quad (4.3)$$

$$P_{\text{RBC},b} = P_{\text{PBC},2b}^\#([\mathbf{x}], [\mathbf{y}]) \quad (4.4)$$

But by Lemma 4.1.7 we know that for any $l \in \mathbb{N}$ $P_{\text{PBC},l}$ satisfies the conditions of Lemma 4.1.4. We thus have

$$G^\#([0], [\mathbf{x}]) = \sum_{\mathbf{x}' \in [\mathbf{x}]} G_{\text{PBC}}(0, \mathbf{x}') = G_{\text{PBC}}(0, \mathbf{x}) + \sum_{\mathbf{x}' \in [\mathbf{x}] \setminus \mathbf{x}} G_{\text{PBC}}(0, \mathbf{x}').$$

Let l be $2b$ or $2b + 1$, and let $\mathbf{x} \in \mathbb{B}_b \subset \mathbb{B}_l$. Consider the equivalence relation on \mathbb{B}_l given in Definition 4.1.5. For all $\mathbf{x}' \in [\mathbf{x}] \setminus \mathbf{x}$, there must exist an $i \in \{1, \dots, d\}$ such that $x'_i = l - x_i$. So,

$$\|\mathbf{x}'\| \geq |l - x_i| \geq l/2.$$

But since $\mathbf{x}' \in \tilde{\mathbb{B}}_b$, we also have $\|\mathbf{x}'\| \leq \sqrt{dl}$. From Corollary 3.24 we know that if $\langle \mathcal{N} \rangle \asymp l^\mu$ with $\mu > 2$, then

$$\alpha_1 \|\mathbf{x}'\|^{2-d} + \alpha_2 l^{\mu-d} \leq G_{\text{PBC}}(0, \mathbf{x}') \leq \beta_1 \|\mathbf{x}'\|^{2-d} + \beta_2 l^{\mu-d}, \quad (4.5)$$

where $\alpha_1, \alpha_2, \beta_1, \beta_2 \in \mathbb{R}^+$. Combining these observations, we find

$$\tilde{\alpha}_1 l^{2-d} + \tilde{\alpha}_2 l^{\mu-d} \leq \sum_{\mathbf{x}' \in [\mathbf{x}] \setminus \mathbf{x}} G_{\text{PBC}}(0, \mathbf{x}') \leq \tilde{\beta}_1 l^{2-d} + \tilde{\beta}_2 l^{\mu-d}. \quad (4.6)$$

4.1. RLRW ON A BOX WITH RBC AND HBC

for $\tilde{\alpha}_1, \tilde{\alpha}_2, \tilde{\beta}_1, \tilde{\beta}_2 \in \mathbb{R}^+$. It then follows that

$$c_1 \|\mathbf{x}\|^{2-d} + c_2 l^{\mu-d} \leq G_{\text{PBC},l}^\#([0], [\mathbf{x}]) \leq c_3 \|\mathbf{x}\|^{2-d} + c_4 l^{\mu-d}. \quad (4.7)$$

Combining this with Eqs. (4.3) and (4.4) yields the stated result. \blacksquare

Lemma 4.1.7. *Let P be the transition matrix of the simple random walk on \mathbb{Z}_{2l}^d . If $\mathbf{x}, \mathbf{y} \in \mathbb{Z}_{2l}^d$, then $P(\mathbf{x}, [\mathbf{y}]) = P(\mathbf{x}', [\mathbf{y}])$ for all $\mathbf{x}' \equiv \mathbf{x}$.*

Proof. Let $\mathbf{x}, \mathbf{y} \in \mathbb{Z}_{2l}^d$ and let $\mathbf{x}' \equiv \mathbf{x}$. Then

$$P(\mathbf{x}, [\mathbf{y}]) = \sum_{\mathbf{y}' \in [\mathbf{y}]} P(\mathbf{x}, \mathbf{y}') = \frac{1}{2d} |N(\mathbf{x}) \cap [\mathbf{y}]| \quad (4.8)$$

where $N(\mathbf{x}) := \{\mathbf{y} \in \mathbb{Z}_{2l}^d : \mathbf{x} \sim \mathbf{y}\}$ is the set of neighbours of \mathbf{x} . Define $f : N(\mathbf{x}) \cap [\mathbf{y}] \rightarrow N(\mathbf{x}') \cap [\mathbf{y}]$ via

$$f(\mathbf{x} + \delta \mathbf{e}_k) = \begin{cases} \mathbf{x}' + \delta \mathbf{e}_k, & x'_k = x_k \\ \mathbf{x}' - \delta \mathbf{e}_k, & x'_k \neq x_k \end{cases} \quad (4.9)$$

for all $\mathbf{x} + \delta \mathbf{e}_k \in N(\mathbf{x}) \cap [\mathbf{y}]$.

Let $\mathbf{z}' \in N(\mathbf{x}') \cap [\mathbf{y}]$. Then $\mathbf{z}' = \mathbf{x}' + \delta \mathbf{e}_k$ for some $\delta \in \{-1, 1\}$ and $1 \leq k \leq d$. Consider

$$\mathbf{z} = \begin{cases} \mathbf{x} + \delta \mathbf{e}_k, & x'_k = x_k \\ \mathbf{x} - \delta \mathbf{e}_k, & x'_k \neq x_k \end{cases} \quad (4.10)$$

Clearly, $\mathbf{z} \in N(\mathbf{x})$. Moreover, for all $i \neq k$ we have $z_i = x_i \equiv x'_i = z'_i \equiv y_i$ since $\mathbf{z}' \in [\mathbf{y}]$, so that $z_i \equiv y_i$. Furthermore, if $x_k = x'_k$ then $z_k = x_k + \delta = x'_k + \delta = z'_k \equiv y_k$, while if $x_k \neq x'_k$ then $z_k = x_k - \delta = (l - x'_k) - \delta = l - (x'_k + \delta) \equiv x'_k + \delta = z'_k \equiv y_k$, so that in either case $z_k \equiv y_k$. It then follows that $\mathbf{z} \equiv \mathbf{y}$ and so $\mathbf{z} \in N(\mathbf{x}) \cap [\mathbf{y}]$. But

$$\begin{aligned} f(\mathbf{z}) &= \begin{cases} f(\mathbf{x} + \delta \mathbf{e}_k), & x'_k = x_k \\ f(\mathbf{x} - \delta \mathbf{e}_k), & x'_k \neq x_k \end{cases} \\ &= \mathbf{x}' + \delta \mathbf{e}_k \\ &= \mathbf{z}' \end{aligned} \quad (4.11)$$

Since this holds for all $\mathbf{z}' \in N(\mathbf{x}') \cap [\mathbf{y}]$, f is surjective.

Now suppose $\mathbf{z}, \mathbf{z}' \in N(\mathbf{x}) \cap [\mathbf{y}]$ satisfy $f(\mathbf{z}) = f(\mathbf{z}')$. Suppose $\mathbf{z} = \mathbf{x} + \delta \mathbf{e}_k$, so

that

$$(f(\mathbf{z}))_k = \begin{cases} x'_k + \delta, & x'_k = x_k \\ x'_k - \delta, & x'_k \neq x_k \end{cases} \quad (4.12)$$

If $\mathbf{z}' = \mathbf{x} + \delta' \mathbf{e}_{k'}$ with $k' \neq k$, then $(f(\mathbf{z}'))_k = x'_k \neq x'_k \pm \delta$. So $f(\mathbf{z}) = f(\mathbf{z}') \Rightarrow k' = k$, and it follows that

$$(f(\mathbf{z}'))_k = \begin{cases} x'_k + \delta', & x'_k = x_k \\ x'_k - \delta', & x'_k \neq x_k \end{cases} \quad (4.13)$$

and $(f(\mathbf{z}))_k = (f(\mathbf{z}'))_k$ implies $\delta = \delta'$. Therefore, $\mathbf{z}' = \mathbf{x} + \delta \mathbf{e}_k = \mathbf{z}$, which implies f is injective. We conclude that since f bijective, $|N(\mathbf{x}) \cap [\mathbf{y}]| = |N(\mathbf{x}') \cap [\mathbf{y}]|$. \blacksquare

Lemma 4.1.8. *Let $b \in \mathbb{N}$, and let $P_{HBC,b}$ and $P_{RBC,b}$ denote the transition matrices of a SRW on \mathbb{B}_b with holding and reflective boundary conditions, respectively. Let $P_{PBC,b}$ denote the transition matrix of a SRW on $\tilde{\mathbb{B}}_b = (-b, b] \cap \mathbb{Z}^d$ with periodic boundary conditions. Then*

$$P_{HBC,b} = P_{PBC,2b+1}^\#([\mathbf{x}], [\mathbf{y}])$$

$$P_{RBC,b} = P_{PBC,2b}^\#([\mathbf{x}], [\mathbf{y}])$$

for all $\mathbf{x}, \mathbf{y} \in \mathbb{B}_b$.

Proof. Let $l = 2b$. According to our definitions, \mathbb{Z}_{2l}^d coincides with $\tilde{\mathbb{B}}_l$ with addition in each coordinate interpreted mod $2l$. It follows that $\mathbb{B}_b \subset \tilde{\mathbb{B}}_{2b} = \mathbb{Z}_{2l}^d$. Let $S_{2b}^\#$ denote the set of equivalence classes on \mathbb{Z}_{2l}^d corresponding to Definition 4.1.5. Since, by Lemma 4.1.9, the map $\mathbb{B}_b \rightarrow S_{2b}^\#$ defined by $\mathbf{x} \mapsto [\mathbf{x}]$ is a bijection, and since both $P_{RBC,b}$ and $P_{PBC,2b}^\#$ are stochastic, in order to show that $P_{RBC,b} = P_{PBC,2b}^\#([\mathbf{x}], [\mathbf{y}])$ for all $\mathbf{x}, \mathbf{y} \in \mathbb{B}_b$, it suffices to consider only pairs $(\mathbf{x}, \mathbf{y}) \in \mathbb{B}_b^2$ with $P_{RBC,b}(\mathbf{x}, \mathbf{y}) > 0$. By definition, $P_{RBC,b}(\mathbf{x}, \mathbf{y}) > 0$ only if $\mathbf{y} = \mathbf{x} + \delta \mathbf{e}_k$ for some $\delta \in \{-1, 1\}$ and $k \in \{1, \dots, d\}$.

Let $l = 2b$, and let $\mathbf{x} \in \mathbb{Z}_{2l}^d$ with $-l/2 \leq x_i \leq l/2$ for all $i \in \{1, \dots, d\}$. Suppose $\mathbf{y} = \mathbf{x} + \delta \mathbf{e}_k$ for $\delta \in \{-1, 1\}$ and $k \in \{1, \dots, d\}$. Clearly, $\mathbf{y} \in N(\mathbf{x}) \cap [\mathbf{y}]$. Suppose $\mathbf{y}' \in [\mathbf{y}]$. Then either $y'_k = y_k = x_k + \delta$ or $y'_k = l - y_k = l - (x_k + \delta)$. Clearly $x_k + \delta \neq x_k$, and $l - (x_k + \delta) = x_k$ if and only if $l - \delta = 2x_k$, but the latter cannot hold when l is even (since the LHS is odd and the RHS is even). We therefore see that $y'_k \neq x_k$. In order for \mathbf{y}' to be in $N(\mathbf{x})$, it is therefore necessary that $y'_i = x_i$ for all $i \neq k$. Defining $\tilde{\mathbf{y}}$ via $\tilde{y}_i = x_i$ and $\tilde{y}_k = l - (x_k + \delta)$ we conclude that $\{\mathbf{y}\} \subset N(\mathbf{x}) \cap [\mathbf{y}] \subset \{\mathbf{y}, \tilde{\mathbf{y}}\}$. Since $\tilde{\mathbf{y}} \in [\mathbf{y}]$ by construction we have

$$N(\mathbf{x}) \cap [\mathbf{y}] = \begin{cases} \{\mathbf{y}, \tilde{\mathbf{y}}\}, & \tilde{\mathbf{y}} \in N(\mathbf{x}) \\ \{\mathbf{y}\}, & \tilde{\mathbf{y}} \notin N(\mathbf{x}) \end{cases} \quad (4.14)$$

But $\tilde{\mathbf{y}} \in N(\mathbf{x})$ if and only if $\tilde{y}_k = x_k + \epsilon$ for some $\epsilon \in \{-1, 1\}$. And $\tilde{\mathbf{y}} \neq \mathbf{y}$ if and only if $y'_k \neq y_k$. So $|N(\mathbf{x}) \cap [\mathbf{y}]| = 2$ if and only if $\tilde{y}_k = x_k - \delta \iff l - (x_k + \delta) = x_k - \delta \iff l - x_k = x_k \iff x_k \in \{-l/2, l/2\}$. It follows that if $\mathbf{y} = \mathbf{x} + \delta \mathbf{e}_k$ then

$$P_{\text{PBC}, 2b}^\#([\mathbf{x}], [\mathbf{y}]) = P_{\text{PBC}, 2b}(\mathbf{x}, [\mathbf{y}]) = \frac{1}{2d} |N(\mathbf{x}) \cap [\mathbf{y}]| = \begin{cases} 1/(2d), & x_k \neq \pm l/2 \\ 1/d, & x_k = \pm l/2 \end{cases} = P_{\text{RBC}, b}(\mathbf{x}, \mathbf{y}) \quad (4.15)$$

Now let $l = 2b + 1$, and note that $\mathbb{B}_b \subset \tilde{\mathbb{B}}_{2b+1} = \mathbb{Z}_{2l}^d$. Let $S_{2b+1}^\#$ denote the set of equivalence classes on \mathbb{Z}_{2l}^d corresponding to Definition 4.1.5. Since, by Lemma 4.1.9, the map $\mathbb{B}_b \rightarrow S_{2b+1}^\#$ defined by $\mathbf{x} \mapsto [\mathbf{x}]$ is a bijection, and since both $P_{\text{HBC}, b}$ and $P_{\text{PBC}, 2b+1}^\#$ are stochastic, in order to show that $P_{\text{HBC}, b}(\mathbf{x}, \mathbf{y}) = P_{\text{PBC}, 2b+1}^\#([\mathbf{x}], [\mathbf{y}])$ for all $\mathbf{x}, \mathbf{y} \in \mathbb{B}_b$, it suffices to consider only pairs $(\mathbf{x}, \mathbf{y}) \in \mathbb{B}_b^2$ with $P_{\text{HBC}, b}(\mathbf{x}, \mathbf{y}) > 0$. By definition, $P_{\text{HBC}, b}(\mathbf{x}, \mathbf{y}) > 0$ only if $\mathbf{y} = \mathbf{x} + \delta \mathbf{e}_k$ for some $\delta \in \{-1, 1\}$ and $k \in \{1, \dots, d\}$ or if $\mathbf{y} = \mathbf{x}$.

Let $\mathbf{x} \in \mathbb{B}_b$. It is straightforward to show that $\mathbf{x} + \delta \mathbf{e}_k \equiv \mathbf{x}$ if and only if $x_k = \frac{\delta(l-1)}{2}$ which implies $|N(\mathbf{x}) \cap [\mathbf{x}]| = \sum_{i=1}^d \mathbb{1}(|x_i| = \frac{l-1}{2})$ where $\mathbb{1}(\cdot)$ denotes the indicator function, and so

$$P_{\text{PBC}, 2b+1}^\#([\mathbf{x}], [\mathbf{x}]) = P_{\text{PBC}}(\mathbf{x}, [\mathbf{x}]) = \frac{1}{2d} \sum_{i=1}^d \mathbb{1}\left(|x_i| = \frac{l-1}{2}\right) = P_{\text{HBC}}(\mathbf{x}, \mathbf{x}). \quad (4.16)$$

Suppose instead that $\mathbf{y} = \mathbf{x} + \delta \mathbf{e}_k$ with $x_k \neq \delta(l-1)/2$. Then $\mathbf{y} \not\equiv \mathbf{x}$ and so if $\mathbf{y}' \in [\mathbf{y}]$ then $\mathbf{y}' \neq \mathbf{x}$. If $\mathbf{y}' \in [\mathbf{y}]$ then either $y'_k = y_k = x_k + \delta$ or $y'_k = l - y_k$. But $x_k \in \{-(l-3)/2, \dots, (l-3)/2\} \Rightarrow x_k + \delta \in \{-(l-1)/2, \dots, (l-1)/2\}$ and $l - (x_k + \delta) \in \{-(l+1)/2, \dots, (l+1)/2\}$ so $l - (x_k + \delta) \neq x_k + \delta \iff l - y_k \neq y'_k$. It follows that $y'_k = y_k = x_k + \delta$. Then, since $y'_k = x_k + \delta$, in order for \mathbf{y}' to be in $N(\mathbf{x})$ it is necessary that $y'_i = x_i = y_i$ for all $i \neq k$, so that $\mathbf{y}' = \mathbf{y}$. We have therefore established that $N(\mathbf{x}) \cap [\mathbf{y}] = \{\mathbf{y}\}$ when $\mathbf{y} = \mathbf{x} + \delta \mathbf{e}_k$ with $x_k \neq \delta(l-1)/2$, and it follows that

$$P_{\text{PBC}, 2b+1}^\#([\mathbf{x}], [\mathbf{y}]) = P_{\text{PBC}, 2b+1}(\mathbf{x}, [\mathbf{y}]) = 1/(2d) = P_{\text{HBC}}(\mathbf{x}, \mathbf{y}). \quad (4.17)$$

■

Lemma 4.1.9. *The maps*

$$\phi : \mathbb{B}_b \rightarrow S_{2b}^\# \text{ such that } \phi(\mathbf{x}) = [\mathbf{x}] \quad \forall \mathbf{x} \in \mathbb{B}_b \quad (4.18)$$

$$\psi : \mathbb{B}_b \rightarrow S_{2b+1}^\# \text{ such that } \psi(\mathbf{x}) = [\mathbf{x}] \quad \forall \mathbf{x} \in \mathbb{B}_b \quad (4.19)$$

are bijections.

Proof. Let $[\mathbf{x}'] \in S_{2b}^\#$. Let $l = 2b$. If $\mathbf{x}' \notin \mathbb{B}_b$ then there must be indices i_1, i_2, \dots, i_m such that $x'_{i_j} \notin [-b, b] = [-l/2, l/2]$. But, by definition, $x'_{i_j} \in (-l, l] \cap \mathbb{Z}$ so we must have $x'_{i_j} \in (-l, -l/2 - 1] \cup [l/2 + 1, l]$. If $x'_{i_j} \in \{-l, \dots, -l/2 - 1\}$ then $l - x'_{i_j} \in \{0, -1, \dots, -l/2 + 1\}$. Defining \mathbf{x} so that $x_i = l - x'_i$ for all $i \in \{i_1, \dots, i_m\}$, and $x_i = x'_i$ otherwise, we then have $\mathbf{x} \in \mathbb{B}_b$ and $\mathbf{x} \equiv \mathbf{x}'$. It follows that $[\mathbf{x}] = [\mathbf{x}']$ and so $\phi(\mathbf{x}) = [\mathbf{x}']$. This shows that ϕ is surjective.

Now suppose $\mathbf{x}, \mathbf{x}' \in \mathbb{B}_b$ and $\phi(\mathbf{x}) = \phi(\mathbf{x}') \iff [\mathbf{x}] = [\mathbf{x}'] \iff \mathbf{x} \equiv \mathbf{x}' \iff \forall 1 \leq i \leq d$ we have $x_i = x'_i$ or $x_i = l - x'_i$. If $x'_i = \delta l/2$ then $l - x'_i = \delta l/2 = x'_i$ so $x_i = x'_i$. If $x'_i \in \{-l/2 + 1, \dots, l/2 - 1\}$ then $l - x'_i \in \{-l/2, \dots, l/2\}$ and since $x_i \in \{-l/2, \dots, l/2\}$ it follows that $x_i \neq l - x'_i$, and thus we have $x_i = x'_i$. It follows that $\mathbf{x} = \mathbf{x}'$ and so ϕ is injective, and therefore bijective.

Now let $[\mathbf{x}'] \in S_{2b+1}^\#$, and let $l = 2b + 1$. If $\mathbf{x}' \notin \mathbb{B}_b$ then there must be indices i_1, i_2, \dots, i_m such that $x'_{i_j} \notin [-b, b] = [-(l-1)/2, (l-1)/2]$. But, by definition, $x'_{i_j} \in (-l, l] \cap \mathbb{Z}$ so we must have $x'_{i_j} \in (-l, -l/2 - 1] \cup [l/2 + 1, l]$. If $x'_{i_j} \in \{-l, \dots, -l/2 - 1\}$ then $l - x'_{i_j} \in \{0, -1, \dots, -l/2 + 1\}$. Defining \mathbf{x} so that $x_i = l - x'_i$ for all $i \in \{i_1, \dots, i_m\}$, and $x_i = x'_i$ otherwise, we then have $\mathbf{x} \in \mathbb{B}_b$ and $\mathbf{x} \equiv \mathbf{x}'$. It follows that $[\mathbf{x}] = [\mathbf{x}']$ and so $\psi(\mathbf{x}) = [\mathbf{x}']$. This shows that ψ is surjective.

Now suppose $\mathbf{x}, \mathbf{x}' \in \mathbb{B}_b$ and $\psi(\mathbf{x}) = \psi(\mathbf{x}') \iff [\mathbf{x}] = [\mathbf{x}'] \iff \mathbf{x} \equiv \mathbf{x}' \iff \forall 1 \leq i \leq d$ we have $x_i = x'_i$ or $x_i = l - x'_i$. Since $x'_i \in \{-l/2 + 1, \dots, l/2 - 1\}$ we have $l - x'_i \notin \{-l/2 + 1, \dots, l/2 - 1\}$ and since $x_i \in \{-l/2 + 1, \dots, l/2 - 1\}$ it follows that $x_i \neq l - x'_i$, and thus we have $x_i = x'_i$. It follows that $\mathbf{x} = \mathbf{x}'$ and so ψ is injective, and therefore bijective. ■

4.2 SAW and Ising model at criticality

Figure 4.3 shows the scaling of the mean walk length of a SAW on five-dimensional hypercubic lattices with free boundaries. Our fits lead to the exponent value 2.00(1) by discarding $L < 125$, in agreement with $\langle \mathcal{N}_{\text{SAW}} \rangle \asymp L^2$. Figure 4.4 shows that the

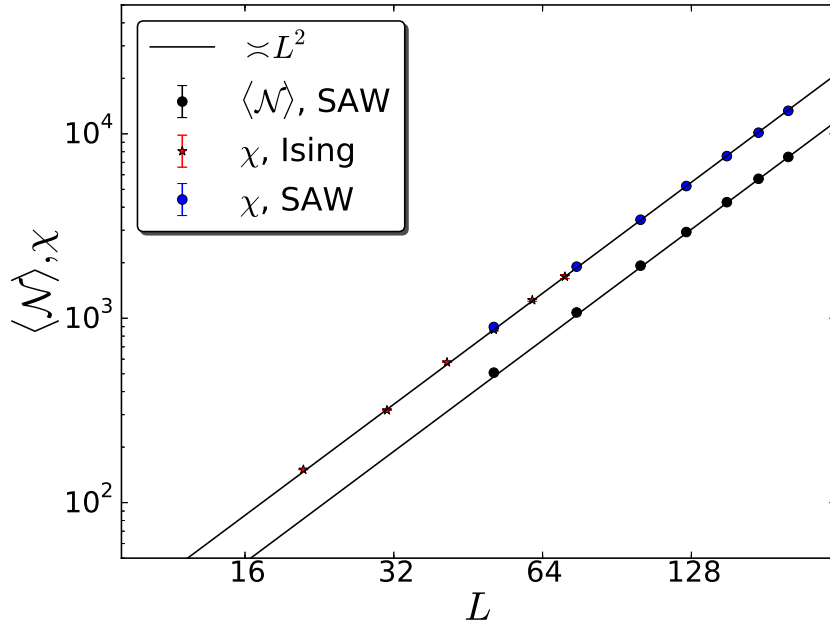


Figure 4.3: Critical FBC scaling of the mean walk length $\langle \mathcal{N}_{\text{SAW}} \rangle$ and susceptibility $\chi_{\text{Ising,SAW}}$ in five dimensions. Our numerics show that $\langle \mathcal{N}_{\text{SAW}} \rangle \simeq L^2$. In agreement with the prediction from Eq. (3.2), the susceptibility of the SAW and Ising models displays the same FSS behaviour. To emphasize the universal scaling, the data for Ising and SAW susceptibility were translated onto a single curve.

two-point function of the Ising and SAW models exhibit the standard mean-field scaling $\|\mathbf{x}\|^{2-d}$, in agreement with the FSS behaviour of the Green's function of a RLLRW with mean walk length $\langle \mathcal{N}_{\text{RLLRW}} \rangle \simeq L^2$.

Furthermore, we investigated the FSS behaviour of the susceptibility for the SAW and the Ising model in Fig 4.3. Our fits lead to the exponent value 1.99(1) for χ_{SAW} by discarding $L < 125$, and 2.01(8) for χ_{Ising} by discarding $L < 31$. These exponent values are in agreement with the standard mean-field expectation $\chi \simeq L^2$ which has been numerically observed in [31, 33] for the Ising model.

4.3 SAW and Ising model at pseudo-criticality

We numerically demonstrate the universality of Eq. (3.1) by showing that the RLLERW Green's function displays the same FSS behaviour as on PBC, if the mean walk length on free boundaries is chosen to scale in the same way as on periodic boundaries. Figures 4.5, 4.6, 4.7 show the (rescaled) Green's function of a RLLERW with mean walk length L^μ for $\mu = 3/2, 2, 5/2$. The simulations for RLLERW were performed with the

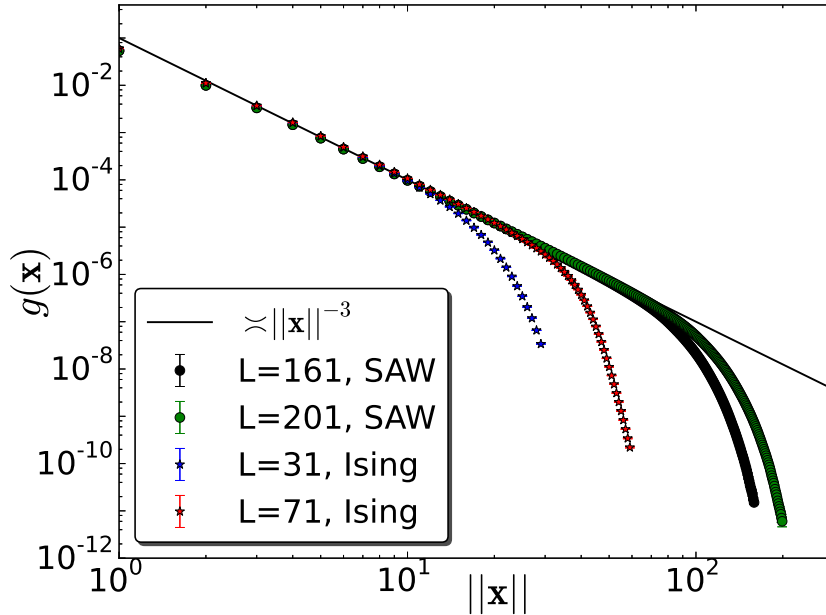


Figure 4.4: Critical FBC scaling of the two-point functions of the SAW and Ising model on five-dimensional lattices. Both cases display the standard mean-field behaviour $g_{\text{Ising,SAW}}(\mathbf{x}) \asymp \|\mathbf{x}\|^{2-d}$.

conjectured asymptotic distribution on tori³, and we tested our claims with various other distributions such as the exponential, uniform and geometric distribution.

We now turn to the SAW and Ising models. There has been considerable debate [32, 30, 34] concerning the FSS behaviour of the susceptibility at the pseudo-critical point z_L , defined to be the location of the maximum of the (modulus) susceptibility in a finite box with side length L . It has been numerically established that this pseudo-critical point has shift exponent $\lambda = 2$ [32, 30, 34]. Our RLRW results predict that we need $\langle \mathcal{N}_{\text{SAW}} \rangle \asymp L^{d/2}$ to observe the critical PBC behaviour of the two-point functions. Since, for FBC, the mean walk length of SAW scales as $\langle \mathcal{N}_{\text{SAW}} \rangle \asymp L^2$ at criticality, we consider the pseudo-critical point $z_L = z_c - aL^{-2}$ with $a < 0$ where the average walk length of SAW is larger than at z_c .

A simple methodology to determine if it is possible to have $\chi \asymp L^{d/2}$ at z_L is to first determine a sequence $a(L)$ such that $\chi_{\text{PBC},z_c} = \chi_{\text{FBC},z_c - a(L)L^{-2}}$, and then show that $a(L)$ converges. If such a convergent sequence exists with $\lim_{a \rightarrow \infty} a(L) = a_\infty$, this approach forces $\chi_{z_c - a(L)L^{-2}}$ to scale as $L^{d/2}$. The inset of Fig. 4.9 shows the sequence $a(L)$ in the Ising and SAW models. Even though the system sizes are too small to extract a decent estimator in the Ising case, we observe that both sequences converge.

³A numerical study suggests that this is the half-normal distribution from Eq. (2.14)

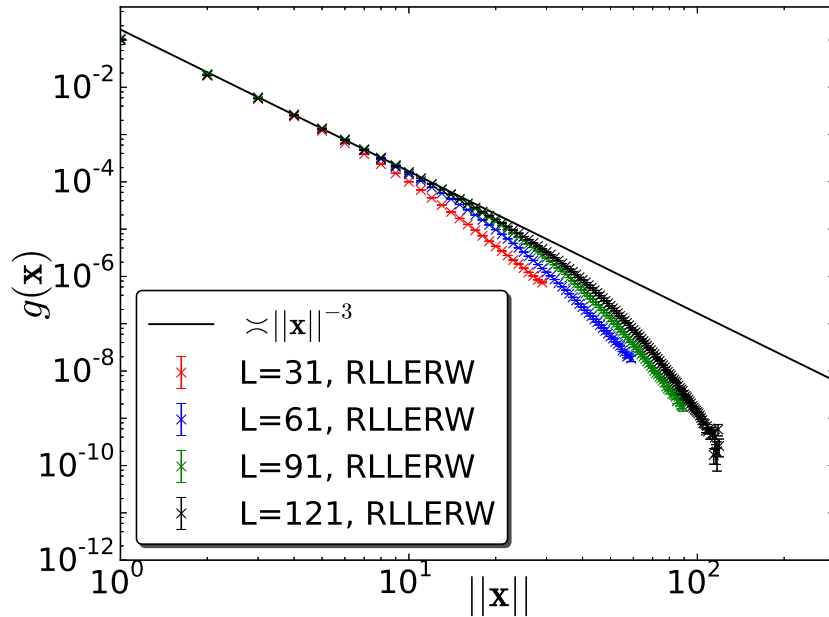


Figure 4.5: Green's function of a RLLERW with mean walk length $L^{1.5}$ on five-dimensional hypercubic lattices with free boundaries. As predicted by Eq. (3.1), the plateau region is absent.

For SAW, our fits lead to $a_{\text{SAW},\infty} = 0.824(2)$.

Figure 4.8 (a) shows the two-point functions of the Ising and SAW models at z_L . Moreover, Figure 4.8 (b) shows an appropriately scaled version onto the ansatz from Eq. (3.1) with $\mu = d/2$. We identify three regions. At moderate values of \mathbf{x} , the two-point functions exhibit the standard mean-field scaling $\|\mathbf{x}\|^{2-d}$, and then enter a plateau for longer distances in the bulk. At distances close to the boundary, we observe that the two-point functions decay faster than $\|\mathbf{x}\|^{2-d}$. Figure 4.8 (b) shows an excellent data collapse except at distances close to the boundary. This strong boundary effect may explain the apparent discrepancies [32, 30, 34] in determining the correct scaling behaviour for free boundaries. Regardless, we conclude from Fig. 4.8 (b) that the anomalous FSS behaviour, observed on periodic boundaries at criticality, *can* be observed on free boundaries. We also numerically extracted the exponent value 2.48(6) for $\langle \mathcal{N}_{\text{SAW}} \rangle$ in Fig. 4.9 by discarding $L < 101$, in agreement with the critical PBC behaviour.

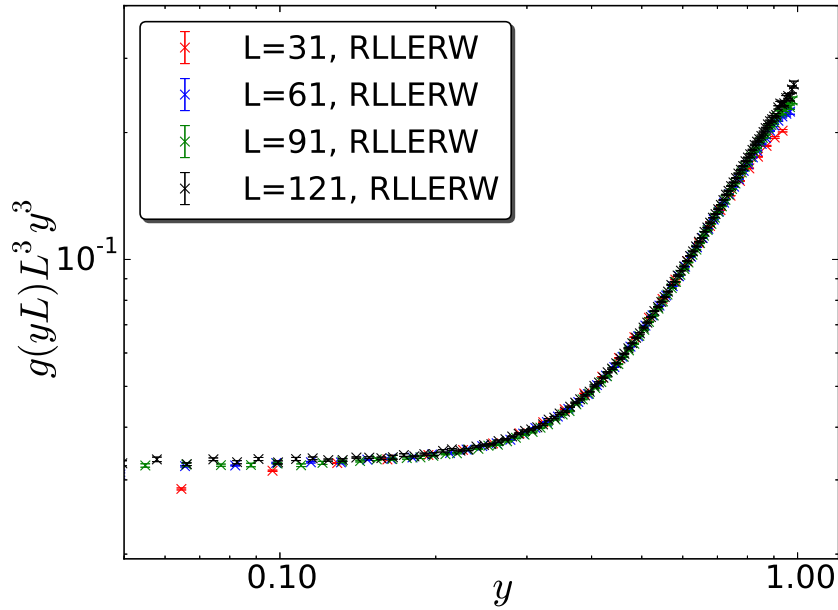


Figure 4.6: Appropriately scaled Green's function of a RLLERW with mean walk length L^2 on five-dimensional hypercubic lattices with free boundaries. The Green's function displays the FSS behaviour of Eq. (3.1) with $\mu = 2$.

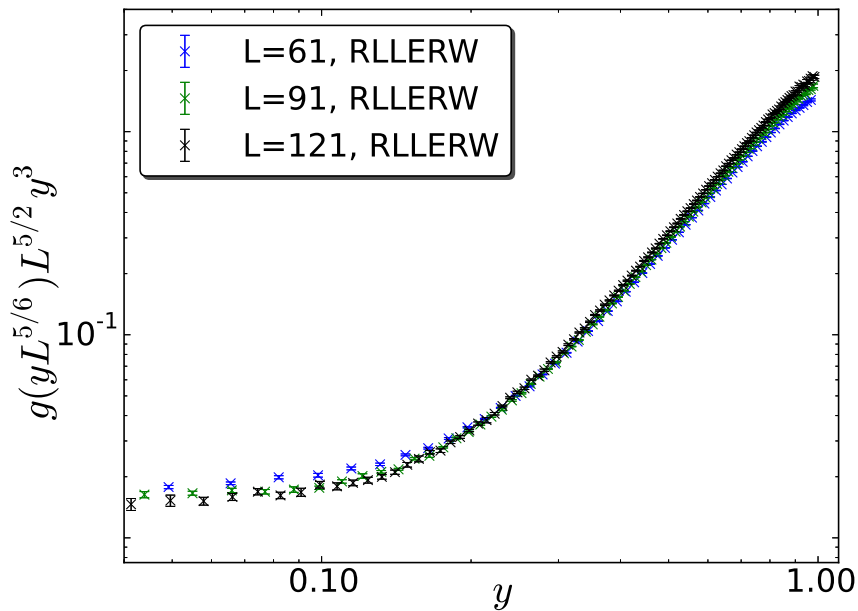


Figure 4.7: Appropriately scaled Green's function of a RLLERW with mean walk length $L^{5/2}$ on five-dimensional hypercubic lattices with free boundaries. The Green's function displays the FSS behaviour of Eq. (3.1) with $\mu = d/2$.

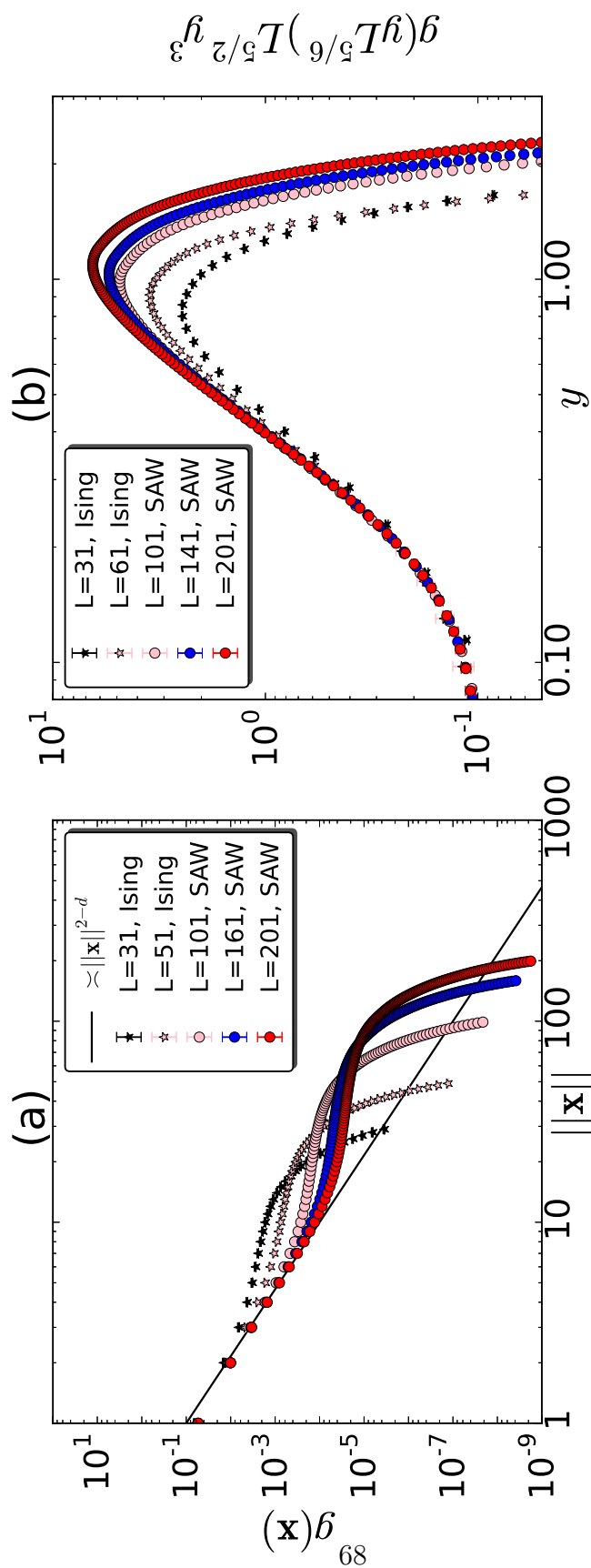


Figure 4.8: (a) Two-point functions of the Ising model and SAW on five-dimensional hypercubic lattices with free boundaries at $z_L = z_c + a(L)L^{-2}$. (b) Appropriately scaled versions of the two-point functions onto the ansatz in Eq. (3.1) with $\mu = d/2$. In agreement with the critical PBC behaviour, the two-point functions collapse except at distances close to the boundary.

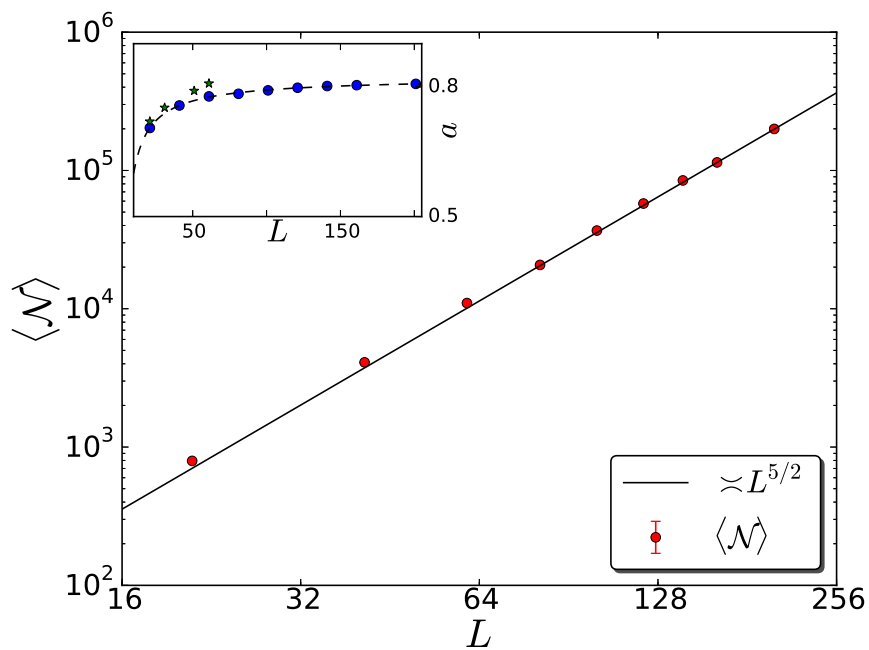


Figure 4.9: FBC behaviour of the mean walk length $\langle \mathcal{N}_{\text{SAW}} \rangle$ at $z_L = z_c + a(L)L^{-2}$ where we observe $\langle \mathcal{N}_{\text{SAW}} \rangle \approx L^{d/2}$. The inset shows the convergent sequence $a(L)$ for the SAW (circles) and the Ising model (stars).

Discussion

In this part, we have introduced a random-length random walk model which we rigorously studied on hypercubic lattices with periodic (see Theorem 3.2.2), and reflective/holding boundary conditions (see Theorem 4.1.6). We established that the FSS behaviour of the RLRW Green's function is controlled by the mean walk length $\langle \mathcal{N}_{\text{RLRW}} \rangle$. This result holds independently of the boundary conditions imposed. Informed by this observation, we numerically established the FSS behaviour of $\langle \mathcal{N}_{\text{SAW}} \rangle$ at both critical and pseudo-critical points, and investigated the corresponding FSS behaviour of the SAW two-point function. Our central result is that if $\langle \mathcal{N}_{\text{RLRW}} \rangle$ is chosen to scale as $\langle \mathcal{N}_{\text{SAW}} \rangle$, then the FSS behaviour of the SAW two-point function displays the scaling behaviour from Eq. (3.1). We numerically verified the universality of our observations by computing the two-point function of the Ising model.

More precisely, these results shed light on the following questions regarding the FSS behaviour of the Ising model above d_c .

- On the complete graph K_n at criticality, it is rigorously established [47] that $\langle \mathcal{N}_{\text{SAW}} \rangle \asymp n^{1/2}$. We numerically verified that this scaling behaviour correctly predicts the FSS behaviour on high dimensional tori. Informed by Eq. (3.1), we numerically confirmed that the critical PBC behaviour of the Ising two-point function is naturally embedded in Eq. (3.1) for $\mu = d/2$, in agreement with the conjectures in [28, 30], and in contrast to [29]. Moreover, we established the PBC behaviour at various pseudo-critical points $z_L(\lambda) = z_c - aL^{-\lambda}$. In particular, at

$z_L(2)$, we argued that the Ising two-point function displays standard mean-field behaviour, in contrast to the anomalous PBC behaviour at criticality.

- On five-dimensional boxes with free boundaries, we numerically established that $\langle \mathcal{N}_{\text{SAW}} \rangle \asymp L^2$. Informed by Theorem 3.2.2, we argued that the critical Ising two-point function displays the predicted scaling behaviour from Eq. (3.1) with $\mu = 2$. This result implies that the susceptibility scales as L^2 , in agreement with the numerical observation in [33]. We also studied the actively debated FSS behaviour at the pseudo-critical point $z_L = z_c + aL^{-2}$. We established that there exists an $a > 0$ such that the Ising two-point function displays the same FSS behaviour as on periodic boundaries at criticality. This result is consistent with the numerical observations in [32, 30].

Finally, we present some open points for discussion and possible future work.

- We established that the essential reason for anomalous finite-size scaling on tori above d_c is manifested in the proliferation of windings, absent for dimensions below d_c . We investigated an alternative two-point function, the unwrapped two-point function, which accounts for these windings. We numerically verified for the SAW and RLLERW that these unwrapped versions display the same scaling limit as the corresponding two-point functions on the infinite-lattice. It would be interesting to define an appropriate candidate for the unwrapped length in the Ising model.
- For the Ising and SAW models with periodic boundaries, we studied the FSS behaviour of physical observables at pseudo-critical fugacities $z(L) = z_c - aL^{-\lambda}$. For free boundaries, we investigated the FSS behaviour at $z(L) = z_c + aL^{-2}$. In both cases we chose $a \in \mathbb{R}^+$. It would be of interest to study the FSS behaviour at $z(L) = z_c + aL^{-\lambda}$ for PBC. For FBC, it would be interesting to investigate both the FSS behaviour at $z(L) = z_c + aL^{-\lambda}$ and $z(L) = z_c - aL^{-\lambda}$ for various λ . We note that a recent study [34] investigated the FBC behaviour of χ and $\bar{\chi}$ at various pseudo-critical points in the Ising model.

Bibliography

- [1] M. E. Fisher, *Critical Phenomena*, in Proceedings of the 51st Enrico Fermi Summer School, Varenna, Italy, edited by M. S. Green, Academic Press, New York (1971).
- [2] M. E. Fisher and M. N. Barber, *Scaling theory for finite-size effects in the critical region*, Phys. Rev. Lett. 28, 1516 (1972).
- [3] J. Cardy, *Finite-size scaling*, Elsevier Science Publishers B.V., New York : Elsevier Science Pub. Co., (1980).
- [4] R. Fernández, J. Fröhlich, and A. D. Sokal, *Random Walks, Critical Phenomena, and Triviality in Quantum Field Theory*, Springer, Heidelberg (1992).
- [5] M. E. Fisher, *The renormalization group in the theory of critical behavior*, Rev. Mod. Phys. 46, no. 4, 597—616 (1974).
- [6] A. D. Sokal, *A rigorous inequality for the specific heat of an Ising or ϕ^4 ferromagnet*, Phys. Lett. A 71, no. 5–6, 451–453 (1979).
- [7] M. Aizenman, *Geometric analysis of ϕ^4 fields and Ising models. parts I and II*, Commun. Math. Phys. 86, no. 1, 1–48 (1982).
- [8] M. Aizenman, *Rigorous studies of critical behavior II. In: Statistical Physics and Dynamical Systems: Rigorous Results (edited by J. Fritz, A. Jaffe, and D. Szász)*, vol. 10 of Progress in Physics, p. 481. Birkhäuser (1985).
- [9] M. Aizenman, *Rigorous studies of critical behavior*, Physica A 140, no. 1–2, 225–231 (1986).
- [10] D. Brydges and T. Spencer, *Self-avoiding walk in 5 or more dimensions*, Commun. Math. Phys. 97, no. 1, 125–148 (1985).
- [11] T. Hara and G. Slade, *Self-avoiding walk in five or more dimensions. I. The*

- critical behaviour*, Commun. Math. Phys. 147, no. 1, 101–136 (1992).
- [12] G. F. Lawler, *Intersections of Random Walk*, Probability and its Applications, Birkhäuser (1996).
- [13] E. Brézin, *An investigation of finite size scaling*, J. Phys. 43, 15–22 (1982).
- [14] M.E. Fisher, *Scaling, universality and renormalization group theory*, F.J.W. Hahne (Ed.), Critical Phenomena, in: Lecture Notes in Physics, vol. 186, Springer, Berlin, pp. 1–139, (1983).
- [15] V. Privman and M. E. Fisher, *Finite-Size Effects at First-Order Transitions*, J. Stat. Phys. 33, 385 (1983).
- [16] K. Binder, M. Nauenberg, V. Privman, A. P. Young, *Finite size tests of hyperscaling*, Phys. Rev. B 31, 1498–1502, (1985).
- [17] K. Binder, *Critical properties and finite-size effects of the five-dimensional Ising model*, Z. Phys. B 61, 13–23 (1985).
- [18] E. Brézin, J. Zinn-Justin, *Finite size effects in phase transitions*, Nucl. Phys. B 257, 867–893 (1985).
- [19] Ch. Rickwardt, P. Nielaba, K. Binder, *A finite-size scaling study of the five-dimensional Ising model*, Ann. Phys. 3, 483–493 (1994).
- [20] E. Luijten, H.W.J. Blöte, *Finite-size scaling and universality above the upper critical dimension*, Phys. Rev. Lett. 76, 1557–1561 (1996); E. Luijten, H.W.J. Blöte, *Finite-size scaling and universality above the upper critical dimension*, Phys. Rev. Lett. 76, 3662 (Erratum) (1996).
- [21] M. Aizenman and R. Fernández, *Critical exponents for long-range interactions*, Letters in Mathematical Physics, Volume 16, Issue 1, pp 39–49, (1988).
- [22] X. S. Chen and V. Dohm, *Failure of universal finite-size scaling above the upper critical dimension*, Physica A 251, no. 3–4, 439–451 (1998).
- [23] X. S. Chen and V. Dohm, *Finite-size effects in the ϕ^4 field and lattice theory above the upper critical dimension*, Int. J. Mod. Phys. C 9, no. 7, 1007–1019 (1998).
- [24] X. S. Chen and V. Dohm, *Lattice ϕ^4 theory of finite-size effects above the upper critical dimension*, Int. J. Mod. Phys. C 9, no. 7, 1073–1105 (1998).
- [25] J. Shapiro and J. Rudnick, *The fully finite spherical model*, J. Stat. Phys. 43, 51 (1986); J. Rudnick, in Finite Size Scaling and Numerical Simulation of Statistical Systems, edited by V. Privman (World Scientific, Singapore, 1990), p.142.
- [26] G. Parisi, J.J. Ruiz-Lorenzo, *Scaling above the upper critical dimension in Ising*

- models*, Phys. Rev. B 54, R3698–R3702 (1996).
- [27] K. Binder, E. Luijten, M. Müller, N.B. Wilding, H.W.J. Blöte, Monte Carlo investigations of phase transitions: status and perspectives, Physica A 281, 112–128, (2000).
- [28] V. Papathanakos, *Finite-Size Effects in High-Dimensional Statistical Mechanical Systems: The Ising Model With Periodic Boundary Conditions*, Ph.D. thesis, Princeton University, Princeton, New Jersey, (2006).
- [29] R. Kenna and B. Berche, *Fisher’s scaling relation above the upper critical dimension*, Europhys. Lett. 105, 26005 (2014).
- [30] M. Wittmann and A. P. Young, *Finite-size scaling above the upper critical dimension*, Phys. Rev. E 90, 062137 (2014).
- [31] P. H. Lundow and K. Markström, *Non-vanishing boundary effects and quasi-first-order phase transitions in high dimensional Ising models*, Nucl. Phys. B845, 120 (2011).
- [32] B. Berche, R. Kenna, and J.-C. Walter, *Hyperscaling above the upper critical dimension*, Nucl. Phys. B865, 115 (2012).
- [33] P. H. Lundow and K. Markström, *Finite size scaling of the 5D Ising model with free boundary conditions*, Nucl. Phys. B889, 249 (2014).
- [34] P. H. Lundow and K. Markström, *The scaling window of the 5D Ising model with free boundary conditions*, Nucl. Phys. B911, 163 (2016).
- [35] E. Flores-Sola, B. Berche, R. Kenna, and M. Weigel, *Role of Fourier Modes in Finite-Size Scaling above the Upper Critical Dimension*, Phys. Rev. Lett. 116, 115701 (2016).
- [36] T. Hara, *Decay of correlations in nearest-neighbor self avoiding walk, percolation, lattice trees, and animals*, Ann. Probab. 36, 530 (2008).
- [37] A. Sakai, *Lace Expansion for the Ising Model Akira Sakai*, Commun. Math. Phys. 272, 283–344 (2007).
- [38] C. J. Thompson, *Mathematical Statistical Mechanics*, Princeton University Press (1979).
- [39] N. Prokof’ev, B. Svistunov, *Worm Algorithms for Classical Statistical Models*, Phys. Rev. Lett. 87, 160601 (2001).
- [40] A. Berretti, A. D. Sokal, *New Monte Carlo method for the self-avoiding walk*, J. Stat. Phys. 40, 483 (1985).
- [41] H. Hu, X. Chen, Y. Deng, *Irreversible Markov chain Monte Carlo algorithm for*

- self-avoiding walk*, *Frontiers of Physics*, 12:120503, (2017).
- [42] Michael R. Garey, D. S. Johnson, *Computers and Intractability. A Guide to the Theory of NP-Completeness*, *Journal of Symbolic Logic* 48 (2):498-500 (1983).
- [43] R. J. Baxter, *Exactly solved models in statistical mechanics*, London: Academic Press Inc. [Harcourt Brace Jovanovich Publishers] (1982).
- [44] S. Friedli, Y. Velenik, *Statistical Mechanics of Lattice Systems: a Concrete Mathematical Introduction*, Cambridge: Cambridge University Press, (2017).
- [45] I. Jensen, *A parallel algorithm for the enumeration of self-avoiding polygons on the square lattice*, *J. Phys. A: Math. Gen.* 36, 5731 (2003).
- [46] A. L. Owczarek, T. Prellberg, *Scaling of self-avoiding walks in high dimensions*, *J. Phys. A: Math. Gen.* 34, 5773 (2001).
- [47] A. Yadin, *Self-avoiding walks on finite graphs of large girth*, *ALEA, Lat. Am. J. Probab. Math. Stat.* 13, 521–544 (2016).
- [48] Y. Deng, T. M. Garoni, A. Sokal, *Dynamic critical behavior of the worm algorithm for the Ising model*, *Phys. Rev. Lett.* 99, 110601 (2007).
- [49] P. Young, *Everything You Wanted to Know About Data Analysis and Fitting but Were Afraid to Ask*, SpringerBriefs (2015).
- [50] A. D. Sokal, *Monte Carlo Methods in Statistical Mechanics: Foundations and New Algorithms*, Lectures at the Cargèse Summer School on ‘Functional Integration: Basics and Applications’ (1996).
- [51] G.F. Lawler, *Intersections of Random Walks. Probability and Its Applications*, Birkhäuser Boston, (2013).
- [52] G.F. Lawler, V. Limic, *Random Walk: A Modern Introduction*, Cambridge Studies in Advanced Mathematics. Cambridge University Press, (2010).
- [53] M. Heydenreich, R. van der Hofstad, *Progress in high-dimensional percolation and random graphs*, Lecture notes for the CRM-PIMS Summer School in Probability 2015. CRM Short Courses Series with Springer Volume 1. ISBN 978-3-319-62473.
- [54] B. Li, N. Madras, A. D. Sokal, *Critical exponents, hyperscaling, and universal amplitude ratios for two- and three-dimensional self-avoiding walks*, *Journal of Statistical Physics* 80.3-4, 661-754 (1995).
- [55] D. A. Levin, Y. Peres, E. L. Wilmer, *Markov Chains and Mixing Times*, American Mathematical Society, (2009).
- [56] P. H. Lundow, *Compression of transfer matrices*, *Discrete Mathematics* 231, 321–329, (2001).

Part II

Lifted worm algorithm for the Ising model

Introduction

Markov-chain Monte Carlo (MCMC) algorithms are a powerful and widely-used tool in various areas of physics and other disciplines, such as in machine learning [1] and statistics [2]. In many practical applications MCMC algorithms are constructed via the Metropolis [3] or heat bath update scheme [4]. Such algorithms are necessarily *reversible*.

One important example of a Metropolis algorithm is the Prokof'ev-Svistunov Worm Algorithm (P-S worm algorithm) which has widespread application for both classical and quantum systems [5, 6]. As opposed to cluster algorithms like the Wolff [7] or Swendsen-Wang algorithm [8], the updates of the worm algorithm are purely *local*. On the simple-cubic lattice with periodic boundaries, it was numerically observed that the P-S worm algorithm for the zero-field ferromagnetic Ising model outperforms the Swendsen-Wang algorithm for simulating both the magnetic susceptibility and the second-moment correlation length [9]. Another numerical work suggested that the spin-spin correlation function can also be simulated efficiently [10]. Recently, it was rigorously established [11] that the P-S worm algorithm for the Ising model is rapidly mixing on any finite graph for the whole temperature range.

In recent years, various *irreversible* MCMC algorithms have also been studied [13, 14, 12, 16, 17, 15, 18, 19, 20, 21, 22]. Many of these algorithms are based on the lifting technique introduced in [23]. The general idea of lifting is to enlarge the original state space and define transition probabilities such that the lifted chain projects down to

the original one. The intuition underlying a potential efficiency improvement is the reduction of diffusive behavior, compared with the original Markov-chain. Rather than exploring states via random walk in the reversible chain one introduces directed flows in the lifted chain to move between relevant states significantly faster.

Even though lifting is considered as a promising method to speed up MCMC algorithms, it is an open question how it affects efficiency in specific examples [24]. For the Ising model on the complete graph, it was numerically observed that the lifted single-spin flip Metropolis algorithm improves the scaling (with volume) of the rate of decay of the autocorrelation function of the magnetization [14]. Another study [13] proved that a lifted MCMC algorithm for uniformly sampling leaves from a given tree reduces the mixing time. In other examples [20, 16, 22] it was numerically observed that lifting speeds up reversible MCMC algorithms by a possibly large constant factor but does not asymptotically affect the scaling with the system size.

In Part 2 of the thesis, we investigate how lifting affects worm algorithms. More precisely, we design a lifted worm algorithm for the zero-field ferromagnetic Ising model, and numerically study the dynamic critical behavior of the number of occupied edges \mathcal{N} , which is related to the energy of the Ising system (see Chap. 3). Our simulations were performed on both the complete graph and toroidal grids in dimensions $2 \leq d \leq 5$ at the (estimated, when $d \geq 3$) infinite-volume critical point.

On the complete graph we find that the lifted worm algorithm significantly improves the dynamic critical exponent z_{int} of \mathcal{N} . In particular, we show that \mathcal{N} exhibits critical speeding-up [26, 27] in the lifted process ($z_{\text{int}} \approx -0.5$), while we observe $z_{\text{int}} \approx 0$ for the corresponding reversible counterpart. On toroidal grids we find that the lifted worm algorithm does not affect the scaling with the system size. We emphasize, however, that the lifted process still reduces the variance of \mathcal{N} by a significant constant. This constant improvement becomes more pronounced for larger dimensions with up to a factor of approximately 141 for $d = 5$.

1.1 Outline

We will now present the outline of Part 2

- In Chapter 2, we introduce the investigated algorithms, and explain how to construct an irreversible worm algorithm for the Ising model.
- In Chapter 3, we present the details of our numerical setup.
- In Chapter 4, we study the dynamic properties of the lifted worm algorithm on

toroidal grids and the complete graph, and compare our findings with reversible worm algorithms.

- Finally, in Chapter 5, we summarize our findings, and give an outlook for future work.

Worm algorithms

2.1 P-S Worm Algorithm

As is well known [28], the zero-field ferromagnetic Ising model can be mapped to an ensemble of high-temperature graphs. Let $G = (V, E)$ be a finite graph with vertex set V and edge set E . Define the closed loop space \mathcal{C}_0 as the set of all configurations $\omega \subseteq E$ such that every vertex has even degree, and \mathcal{C}_2 as the set of all $\omega \subseteq E$ where exactly two vertices have odd degree. We call the subgraph (V, ω) Eulerian whenever $\omega \in \mathcal{C}_0$. In the high-temperature expansion the partition function of the Ising model can be written as the sum over all Eulerian subgraphs [28], i.e.

$$Z = 2^{|V|} \cosh^{|E|}(\beta) \sum_{\omega \in \mathcal{C}_0} \tanh^{|\omega|}(\beta), \quad (2.1)$$

where β denotes the inverse Ising temperature.

The P-S worm algorithm samples these high-temperature graphs via elementary local moves. The main idea is to enlarge the state space \mathcal{C}_0 to $\mathcal{W} := \mathcal{C}_0 \cup \mathcal{C}_2$ by introducing two vertices with odd degree (defects). These defects are moved through \mathcal{W} via random walk. Whenever the two defects meet, the subgraph becomes Eulerian and one reaches a state of the original configuration space \mathcal{C}_0 .

In the original algorithm [5] only one of the defects is mobile and can be moved through \mathcal{W} . In this work, we use a slightly different worm version where we flip a fair

coin to select the mobile defect in \mathcal{C}_2 . The *transition probabilities*

$$q(\omega, \omega') = p(\omega, \omega')a(\omega, \omega') \tag{2.2}$$

from an initial state ω to a target state ω' can be calculated by metropolizing [3] the proposals $p(\omega, \omega')$ with respect to the stationary measure $\pi(\omega) = \frac{1}{\mathcal{Z}} \tanh^{|\omega|}(\beta)\Psi(\omega)$. Here, \mathcal{Z} is an appropriate normalization on \mathcal{W} , $\Psi(\omega) := |V|$ if $\omega \in \mathcal{C}_0$, and $\Psi(\omega) := 2$ if $\omega \in \mathcal{C}_2$, respectively. Furthermore, $p(\omega, \omega')$ denotes the *proposal probability* and $a(\omega, \omega')$ the *acceptance probability*. See [11] for explicit expressions for the transition matrix (2.2).

The algorithm is presented in Alg. 1 with $\omega\Delta xx'$ denoting the symmetric difference of ω and the edge xx' ; i.e. $xx' \in \omega\Delta xx'$ if and only if $xx' \notin \omega$. In words, if $xx' \in \omega$ we propose to delete xx' , while if $xx' \notin \omega$ we propose to add it.

Algorithm 1 P-S Worm Algorithm

```

if  $\omega \in \mathcal{C}_0$  then
    Choose a uniformly random vertex  $x$ 
else
    Choose a uniformly random odd vertex  $x$ 
end if
Choose a uniformly random edge  $xx'$  among the set of edges incident to  $x$ . With
probability  $a_{\text{P-S}}(\omega, \omega\Delta xx')$ , let  $\omega \rightarrow \omega\Delta xx'$ . Otherwise  $\omega \rightarrow \omega$ 

```

2.2 Irreversible Worm Algorithm

We construct the irreversible worm algorithm in two steps. In Sec. 2.2.1 we first define an alternative *reversible* worm algorithm. This worm algorithm will be an appropriate starting point to apply lifting. In Sec. 2.2.2 we use lifting to construct the irreversible counterpart.

2.2.1 B-S type Worm Algorithm

Since it is not obvious how to apply the lifting technique to the P-S process in a natural way, we first construct an alternative reversible worm algorithm with slightly different proposals. This algorithm can be seen as the Ising analogue of the Berretti-Sokal algorithm [29] for simulating self-avoiding walks in the grand canonical ensemble. We thus call it the *B-S type worm algorithm*.

2.2. IRREVERSIBLE WORM ALGORITHM

The proposals are as follows: We first decide to either increase (+) or decrease (−) the number of occupied edges by flipping a fair coin. Then, if the current state belongs to \mathcal{C}_2 , we flip a fair coin to select one of the two defects as the mobile vertex. Otherwise, if the current state is an element of \mathcal{C}_0 , we choose a uniformly random vertex as the mobile vertex. If we decide to add (delete) an edge, we select the next position of the mobile vertex uniformly at random among the set of vacant (occupied) edges incident to the current mobile vertex. We now construct the transition probabilities by metropolizing the proposals with respect to the same measure as in Sec. 2.1.

For $\omega \in \mathcal{W}$, $v \in V$ and $\lambda \in \{-1, 1\}$, define

$$N_\omega(x, \lambda) = \begin{cases} \{uv \notin \omega : u = x \text{ or } v = x\}, & \text{if } \lambda = +1 \\ \{uv \in \omega : u = x \text{ or } v = x\}, & \text{if } \lambda = -1 \end{cases} \quad (2.3)$$

Note that, for any $\omega \in \mathcal{W}$, $|N_\omega(x, +1) + N_\omega(x, -1)|$ equals the degree of x .

Fix $z := \tanh(\beta)$, and let $\omega, \omega\Delta xx' \in \mathcal{W}$. The proposal and acceptance probabilities for the transition $\omega \rightarrow \omega\Delta xx'$ are as follows

(i) If $\omega \in \mathcal{C}_0$:

$$p_{\text{B-S}}(\omega, \omega\Delta xx') = \frac{1}{2} \frac{1}{|V|} \left[\frac{1}{|N_\omega(x, |\omega\Delta xx'| - |\omega|)|} + \frac{1}{|N_\omega(x', |\omega\Delta xx'| - |\omega|)|} \right] \quad (2.4)$$

$$a_{\text{B-S}}(\omega, \omega\Delta xx') = \min \left[1, \frac{z^{|\omega\Delta xx'|} |N_{\omega\Delta xx'}(x, |\omega| - |\omega\Delta xx'|)|^{-1} + |N_{\omega\Delta xx'}(x', |\omega| - |\omega\Delta xx'|)|^{-1}}{z^{|\omega|} |N_\omega(x, |\omega\Delta xx'| - |\omega|)|^{-1} + |N_\omega(x', |\omega\Delta xx'| - |\omega|)|^{-1}} \right] \quad (2.5)$$

(ii) If $\omega \in \mathcal{C}_2$, $\omega\Delta xx' \in \mathcal{C}_2$ and x is a defect in ω :

$$p_{\text{B-S}}(\omega, \omega\Delta xx') = \frac{1}{2} \frac{1}{2} \frac{1}{|N_\omega(x, |\omega\Delta xx'| - |\omega|)|} \quad (2.6)$$

$$a_{\text{B-S}}(\omega, \omega\Delta xx') = \min \left[1, \frac{z^{|\omega\Delta xx'|} |N_\omega(x, |\omega\Delta xx'| - |\omega|)|}{z^{|\omega|} |N_{\omega\Delta xx'}(x', |\omega| - |\omega\Delta xx'|)|} \right] \quad (2.7)$$

(iii) If $\omega \in \mathcal{C}_2$, $\omega\Delta xx' \in \mathcal{C}_0$:

$$p_{\text{B-S}}(\omega, \omega\Delta xx') = \frac{1}{2} \frac{1}{2} \left[\frac{1}{|N_\omega(x, |\omega\Delta xx'| - |\omega|)|} + \frac{1}{|N_\omega(x', |\omega\Delta xx'| - |\omega|)|} \right] \quad (2.8)$$

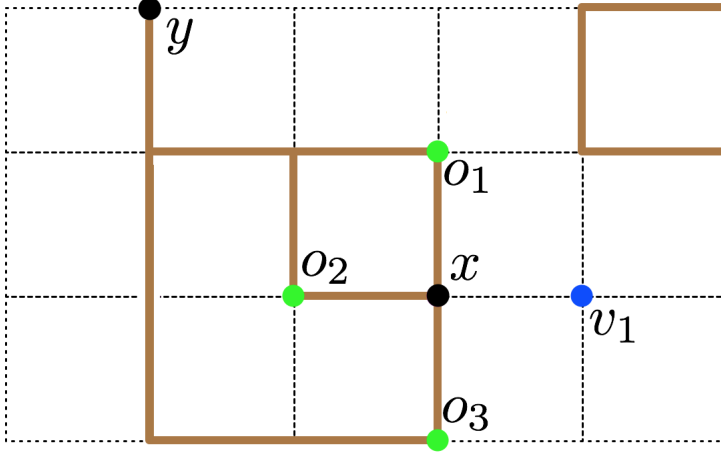


Figure 2.1: Worm configuration $\omega \in \mathcal{C}_2$ where x, y are the vertices with odd degree, $N_\omega(x, -) = \{xo_1, xo_2, xo_3\}$, and $N_\omega(x, +) = \{xv_1\}$. If x is selected as the mobile vertex and one proposes to increase the number of edges in the *B-S type worm algorithm*, the only possible transition is $\omega \rightarrow \omega\Delta xx'$ where $\omega\Delta xx' \in \mathcal{C}_2$. The corresponding proposal and acceptance probabilities are stated in Eq. (2.6) and (2.7).

$$a_{\text{B-S}}(\omega, \omega\Delta xx') = \min \left[1, \frac{z^{|\omega\Delta xx'|} |N_{\omega\Delta xx'}(x, |\omega| - |\omega\Delta xx'|)|^{-1} + |N_{\omega\Delta xx'}(x', |\omega| - |\omega\Delta xx'|)|^{-1}}{z^{|\omega|} |N_\omega(x, |\omega\Delta xx' - |\omega||)|^{-1} + |N_\omega(x', |\omega\Delta xx' - |\omega||)|^{-1}} \right] \quad (2.9)$$

We give an example for case (ii) in Fig. 2.1. All other off-diagonal transition probabilities are zero. The full algorithmic description is presented in Alg. 2. We remark that the choice to allow both defects to move in Alg. 2 is not actually necessary, and one can construct a modification of Alg. 2 in which only one defect is mobile.

Algorithm 2 B-S type Worm Algorithm

Choose $\lambda = \{+, -\}$ uniformly at random

if $\omega \in \mathcal{C}_0$ **then**

 Choose a uniformly random vertex x

else

 Choose a uniformly random odd vertex x

end if

if $N_\omega(x, \lambda) = \emptyset$ **then**

 Set $\omega \rightarrow \omega$ and skip all following steps

else

 Choose a uniformly random edge $xx' \in N_\omega(x, \lambda)$. With probability $a_{\text{B-S}}(\omega, \omega\Delta xx')$, let $\omega \rightarrow \omega\Delta xx'$. Otherwise $\omega \rightarrow \omega$.

end if

2.2.2 Irreversible Worm Algorithm

In the following, we construct the irreversible counterpart of the B-S type worm algorithm. Consider the enlarged state space $\mathcal{W}' := \mathcal{W} \times \{-, +\}$ where $\{-, +\}$ is a set to indicate to either choose to increase (+) or decrease (-) the number of edges. Our aim is to define a Markov-chain on \mathcal{W}' such that we never propose to delete an edge if a state belongs to $\mathcal{W} \times \{+\}$, while we never propose to add edges as long as the chain belongs to $\mathcal{W} \times \{-\}$. If a move $(\omega, \lambda) \rightarrow (\omega \Delta xx', \lambda)$ is rejected, we make the transition $(\omega, \lambda) \rightarrow (\omega, -\lambda)$. Note that this process does not allow diagonal transitions.

For $(\omega, \lambda) \in \mathcal{W}'$, let $\tilde{\pi}(\omega, \lambda) = \frac{1}{2}\pi(\omega)$. For $xx' \in E$, let

$$\tilde{q}((\omega, +), (\omega \cup xx', +)) = q_{\text{B-S}}(\omega, \omega \cup xx') \text{ if } xx' \notin \omega \quad (2.10)$$

$$\tilde{q}((\omega, -), (\omega \setminus xx', -)) = q_{\text{B-S}}(\omega, \omega \setminus xx') \text{ if } xx' \in \omega \quad (2.11)$$

All other entries in row $\tilde{q}((\omega, \lambda), (\cdot, \cdot))$ are zero except $\tilde{q}((\omega, \lambda), (\omega, -\lambda))$ which is fixed by stochasticity. Observe that skew-detailed balance [14, 25] between \tilde{q} and $\tilde{\pi}$ follows immediately from detailed balance between q and π , and so \tilde{q} has stationary distribution $\tilde{\pi}$.

The full algorithmic description of the lifted worm algorithm is given in Alg. 3. From a practical perspective, we emphasize that only minor code changes to the B-S type worm algorithm are needed to construct the irreversible counterpart.

Algorithm 3 Irreversible Worm Algorithm

if $\tilde{\omega} = (\omega, \lambda)$ where $\omega \in \mathcal{C}_0$ **then**

 Choose a uniformly random vertex x

else

 Choose a uniformly random odd vertex x

end if

if $N_\omega(x, \lambda) = \emptyset$ **then**

 Set $(\omega, \lambda) \rightarrow (\omega, -\lambda)$ and skip all following steps

else

 Choose a uniform random edge $xx' \in N_\omega(x, \lambda)$. With probability $a_{\text{B-S}}(\omega, \omega \Delta xx')$, let $(\omega, \lambda) \rightarrow (\omega \Delta xx', \lambda)$. Otherwise $(\omega, \lambda) \rightarrow (\omega, -\lambda)$

end if

Time scales and numerical setup

3.1 Time Scales in MCMC algorithms

To compare the efficiency of competing Markov-chain Monte Carlo algorithms, a number of relevant time scales exist. These fall into two main types; quantities that characterise how long the chain takes to reach stationarity, and quantities that characterise the strength of autocorrelations at stationarity. The main quantities of the latter type are the *integrated autocorrelation times*, as defined in Eq. (3.2). The integrated autocorrelation time for a particular observable provides an important measure of efficiency, since the error bar of the corresponding estimator is controlled by the product of the integrated autocorrelation time and the static variance of the observable; see Eq. (3.1). We emphasize that Eq. (3.1) holds regardless of whether the process is reversible or irreversible.

With regard to quantities describing the approach to stationarity, the most fundamental example is the *mixing time*, which describes the time scale required for the distribution at time t to reach a prescribed distance (e.g. in total variation) from the stationary distribution. For reversible processes, the mixing time is closely related to the *exponential autocorrelation time*. Therefore, in the reversible setting, an understanding of the exponential autocorrelation time gives information on how long a process takes to reach approximate stationarity. For irreversible processes, however, no such relationship exists in general. Consequently, there is no reason to

expect that the exponential autocorrelation time should characterise the time to reach approximate stationarity for the lifted worm process. We therefore focus on studying the integrated autocorrelation time which holds for both lifted and unlifted processes.

3.2 Numerical Setup

Let $\omega \in \mathcal{W}$. We numerically study dynamic properties of the *number of occupied edges* $\mathcal{N} := |\omega|$. We note that the mean energy of the Ising system is given by $\langle \mathcal{E} \rangle = -\tanh(\beta) [|E| + \langle \mathcal{N} | \mathcal{C}_0 \rangle \sinh^2(\beta)]$, where $\langle \mathcal{N} | \mathcal{C}_0 \rangle$ denotes the expectation of \mathcal{N} conditioned on being in \mathcal{C}_0 . The conditional variance of \mathcal{N} is similarly related to the specific heat [5]. We emphasize that in what follows, $\langle \cdot \rangle$ denotes the expectation with respect to the stationary distribution of the worm algorithm on the full space \mathcal{W} (or \mathcal{W}' in the lifted case). Such expectations are then estimated via the sample mean; e.g. $\langle \mathcal{N} \rangle$ is estimated via $\bar{\mathcal{N}} = \frac{1}{M} \sum_{i=1}^M \mathcal{N}_i$ where M is total number of measurements, and \mathcal{N}_i the value of the random variable at the i -th Monte Carlo step after a sufficiently long burn-in sequence has been discarded.

In Chap. 4 we compare the variance of $\bar{\mathcal{N}}$ (in the limit of $M \rightarrow \infty$) by using

$$\text{Var}(\bar{\mathcal{N}}) \sim 2\tau_{\text{int}}^{(\mathcal{N})} \frac{\text{Var}(\mathcal{N}_1)}{M} \quad M \rightarrow \infty \quad (3.1)$$

among the P-S, B-S type and irreversible worm algorithms. Here, $\tau_{\text{int}}^{(\mathcal{N})}$ is the *integrated autocorrelation time*

$$\tau_{\text{int}}^{(\mathcal{N})} := \frac{1}{2} + \sum_{t=1}^{\infty} \rho^{(\mathcal{N})}(t). \quad (3.2)$$

where $\rho^{(\mathcal{N})}(t)$ denotes the *normalized autocorrelation function*

$$\rho^{(\mathcal{N})}(t) := \frac{\langle \mathcal{N}_1 \mathcal{N}_t \rangle - \langle \mathcal{N}_1 \rangle^2}{\text{Var}(\mathcal{N}_1)}. \quad (3.3)$$

Our simulations for the Ising model were performed on the complete graph K_n on n vertices, and on toroidal grids \mathbb{G}_{PBC} in dimensions $2 \leq d \leq 5$. On the complete graph, we simulated at the critical point $\beta_{\text{crit}} = 1/n$. On the torus, our simulations were performed at the exact critical point in two dimensions [30], and at the estimated critical points $\beta_{\text{crit},3d} = 0.22165455(3)$ [31], $\beta_{\text{crit},4d} = 0.1496947(5)$ [32], and $\beta_{\text{crit},5d} = 0.1139150(4)$ [35] for $d \geq 3$.

In each time series, we truncated the summation in Eq. (3.2) self-consistently by using the windowing method [34]. We emphasize that particular care has to be

taken when choosing the windowing parameter c for the irreversible worm algorithm, see Chap. 4 and Appendix A.1. For fitting and error estimations we follow standard procedures, see e.g. [34, 33].

Results

4.1 Toroidal grids

We will now study the dynamic properties of \mathcal{N} on d dimensional toroidal grids. Note that $\text{Var}(\mathcal{N}_0)$ in Eq. (3.1) coincides among all studied algorithms, since it is a property of the stationary measure and does not depend on the details of the underlying Markov-chain. Therefore, in the limit $M \rightarrow \infty$, we have $\frac{\text{Var}_i(\bar{\mathcal{N}})}{\text{Var}_j(\bar{\mathcal{N}})} = \frac{\tau_{\text{int},i}^{(\mathcal{N})}}{\tau_{\text{int},j}^{(\mathcal{N})}}$ where $i, j \in \{\text{P-S, B-S type, irre}\}$.

In Fig. 4.1 we compare the integrated autocorrelation time among the B-S type and lifted worm algorithm (resp. B-S type and P-S worm algorithm). We perform least square fits of the form $A + BL^{-\Delta}$ where A, B, Δ are free parameters. Our conclusion will be that both ratios are approaching constants for $L \rightarrow \infty$, with larger improvements for higher dimensions, see Table 4.1. In two dimensions, our fits lead to the constant improvement $A_{\text{B-S} \rightarrow \text{irre}} = 1.7(2)$, and $A_{\text{P-S} \rightarrow \text{B-S}} = 1.4(1)$ by discarding $L < 40$. For $d = 3$, we find $A_{\text{B-S} \rightarrow \text{irre}} = 8.2(4)$ by discarding $L < 40$, and $A_{\text{P-S} \rightarrow \text{B-S}} = 2.68(9)$ by discarding $L < 20$. In four dimensions our fits lead to $A_{\text{B-S} \rightarrow \text{irre}} = 24(1)$, and $A_{\text{P-S} \rightarrow \text{B-S}} = 3.79(3)$ by discarding $L < 10$. For $d = 5$ we find $A_{\text{B-S} \rightarrow \text{irre}} = 30(1)$, and $A_{\text{P-S} \rightarrow \text{B-S}} = 4.7(1)$. In order to obtain stable fits we fixed $\Delta = 1$ for fitting the ratios of the integrated autocorrelation time of the B-S type and lifted worm algorithm for $d > 2$, and for fitting the ratios of the P-S and B-S type worm algorithm in four and five dimensions.

	P-S \rightarrow B-S	B-S \rightarrow irre	P-S \rightarrow irre
$d = 2$	1.4(1)	1.7(2)	2.4(4)
$d = 3$	2.68(9)	8.2(4)	22(2)
$d = 4$	3.79(3)	24(1)	91(4)
$d = 5$	4.7(1)	30(1)	141(6)

Table 4.1: Improvement factors $\tau_{\text{int},i}^{(\mathcal{N})}/\tau_{\text{int},j}^{(\mathcal{N})}$ by changing from the P-S to the B-S type worm algorithm, B-S type to the irreversible worm algorithm, and P-S to the irreversible worm algorithm on the d dimensional torus

For estimating $\tau_{\text{int,irre}}^{(\mathcal{N})}$ in four and five dimensions we had to choose very large c values outside the common range $c \in [6, 10]$ in the windowing algorithm [34] (see Appendix A.1 for details). In order to understand this, it proves useful to study the autocorrelation function $\rho_{\text{irre}}^{(\mathcal{N})}(t)$ where t is measured in MC hits. For clarity, we will only focus on the five dimensional case. Figure 4.2 shows $\rho_{\text{irre}}^{(\mathcal{N})}(t)$ in the lifted worm algorithm for $d = 5$. $\rho_{\text{irre}}^{(\mathcal{N})}(t)$ exhibits a two-time scaling: For small t , $\rho_{\text{irre}}^{(\mathcal{N})}(t)$ shows a quick exponential decay to a small but bounded value while we observe a much slower decay with a different (larger) exponential scale for larger t . We note that this two-time scaling is absent for $d \leq 3$. Our data suggests that $\rho_{\text{irre}}^{(\mathcal{N})}(t)$ can be described by the ansatz

$$\rho_{\text{irre}}^{(\mathcal{N})}(t) = \alpha_1 \exp(-t/\tau_1) + \alpha_2 \exp(-t/\tau_2) \quad (4.1)$$

where $\alpha_1 + \alpha_2 = 1$, $\tau_1 \geq \tau_2 > 0$. In order to estimate the optimal least-squares parameters for this ansatz we used an improved procedure described in the Appendix A.2. We find that both the ratio α_1/α_2 and τ_2/τ_1 remain bounded as $L \rightarrow \infty$. We estimate the corresponding asymptotic constants using a least squares fitting procedure with a constant and obtain

$$\frac{\alpha_2}{\alpha_1} \stackrel{L \rightarrow \infty}{\sim} 40.6(4) \quad \& \quad \frac{\tau_1}{\tau_2} \stackrel{L \rightarrow \infty}{\sim} 32.4(6).$$

Our numerical observation that $\alpha_1(\tau_2)$ is significantly smaller than $\alpha_2(\tau_1)$ impacts the required choice of parameters in windowing algorithm [34].

4.2 Complete graph

We will now study the integrated autocorrelation time of the B-S type and lifted worm algorithm on the complete graph with n vertices. Our main finding is that \mathcal{N} exhibits critical speeding-up for the lifted process. Figure 4.3 shows $\tau_{\text{int}}^{(\mathcal{N})}/n$ for both algorithms where $\tau_{\text{int}}^{(\mathcal{N})}$ is measured in MC hits. The fitting ansatz $An^z + B$ for $\tau_{\text{int,irre}}^{(\mathcal{N})}$ where A, B, z are free parameters leads to $z = 0.51(1)$ by discarding $n < 2 \cdot 10^5$. Thus,

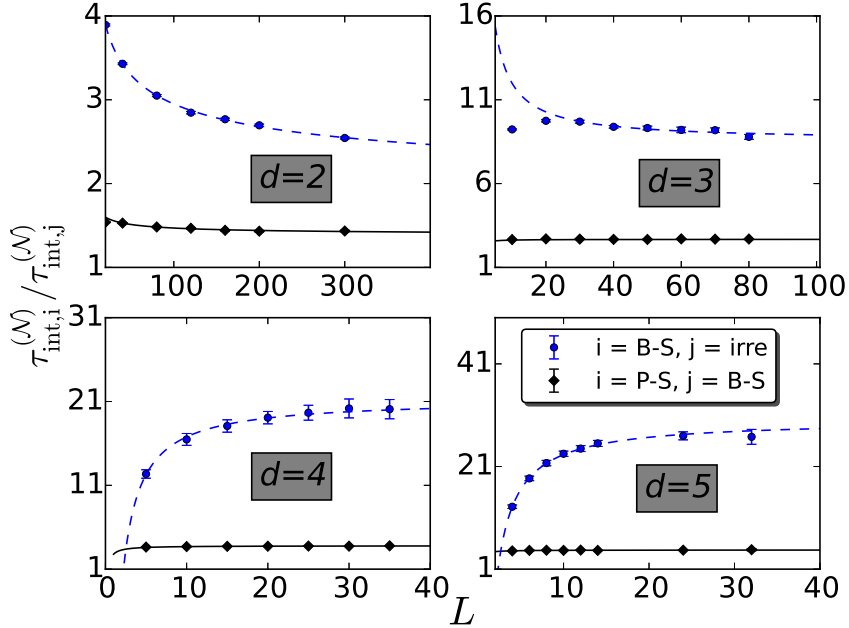


Figure 4.1: Comparison of the integrated autocorrelation time among the P-S, B-S type and lifted worm algorithm. The black diamonds show the ratio of the integrated autocorrelation time of the P-S and B-S type algorithm, while the blue circles compare $\tau_{int}^{(N)}$ among the lifted and the B-S type worm algorithm. The asymptotic improvement factors can be found in Table 4.1. The lines correspond to the fits in Sec. 4.1.

we have $\tau_{int,irre}^{(N)}/n \sim n^{-1/2}$. Note that we had to choose large windowing parameters in agreement to our findings on high-dimensional tori. For the corresponding reversible counterpart (B-S type worm algorithm), it follows immediately from general arguments [36, Cor. 9.2.3] that the integrated autocorrelation time satisfies a Li-Sokal type bound $\tau_{int,B-S}^{(N)} \geq \text{const} \times \text{Var}(\mathcal{N}_0)$ where $\text{const} > 0$. One can, furthermore, calculate [37] that $\lim_{n \rightarrow \infty} \frac{\text{Var}(\mathcal{N}_0)}{n} = \frac{9}{4} - \frac{24\Gamma(5/4)^4}{\pi^2}$ leading to $\tau_{int,B-S}^{(N)}/n \geq \text{const}$. Thus, lifting improves the dynamic critical exponent on the complete graph. Our numerics suggest that this bound is sharp, i.e. $\tau_{int,B-S}^{(N)}/n \sim \text{const}$. More precisely, our fitting ansatz $An^z + B$ for $\tau_{int,B-S}^{(N)}$ leads to $z = 1.00(2)$ by discarding $n < 3000$.

Figure 4.4 shows the autocorrelation function $\rho_{irre}^{(N)}(t)$ for the lifted process where t is measured in MC hits. Our data suggests that $\rho_{irre}^{(N)}(t)$ is well described by the following equation:

$$\rho_{irre}^{(N)}(t) = (1 - \alpha) \exp(-t/\tau_1) + \alpha \cos(\omega t + \phi) \exp(-t/\tau_2). \quad (4.2)$$

Similar ansätze were used in other studies on lifting, see [14, 25]. Our fits lead to $\tau_1 \propto n^{2/3}$, $\tau_2 \propto n^{1/2}$, and $\omega \propto n^{-1/2}$. Moreover, we find that the amplitude of the first

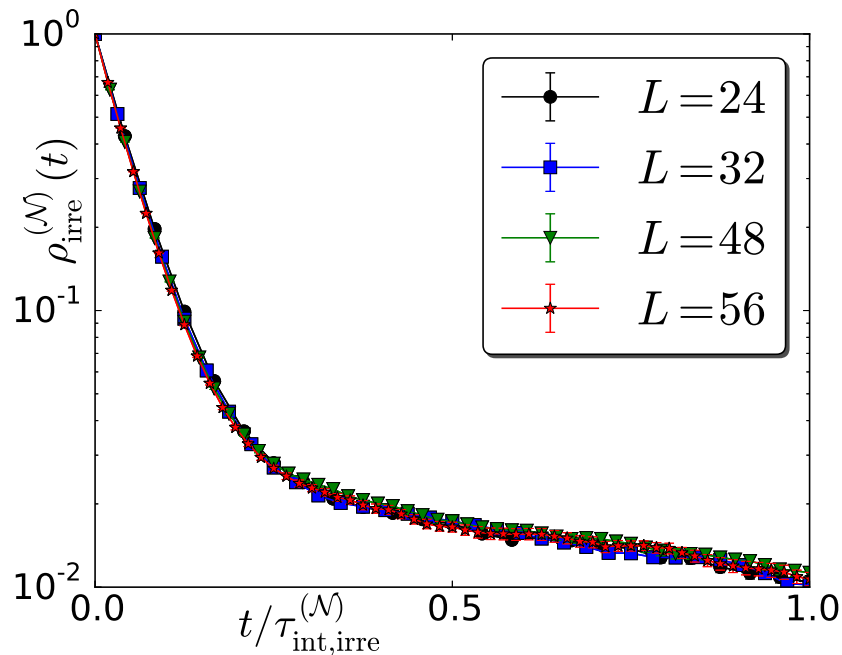


Figure 4.2: Normalized autocorrelation function $\rho_{\text{irre}}^{(\mathcal{N})}(t)$ (t in MC hits) for the irreversible worm algorithm in five dimensions. As stated in Sec. 4.1, $\rho_{\text{irre}}^{(\mathcal{N})}(t)$ is well described by the ansatz in Eq. (4.1).

term vanishes as $n \rightarrow \infty$. We note that the cosine in Eq. (4.2) is motivated by the fact that the eigenvalues of the transition matrix in the lifted process need not be real, unlike the spectrum of reversible chains.

Finally, we numerically observe that the average number of consecutive steps the chain spends in each replica, τ_{intra} , scales as $n^{1/2}$. More precisely, the ansatz $An^z + B$ leads to $z = 0.49(1)$ by discarding $n < 25$. It is interesting to observe that we have thus identified three time scales, i.e. $\tau_{\text{int,irre}}^{(\mathcal{N})}$, τ_2 , τ_{intra} , which scale as $n^{1/2}$.

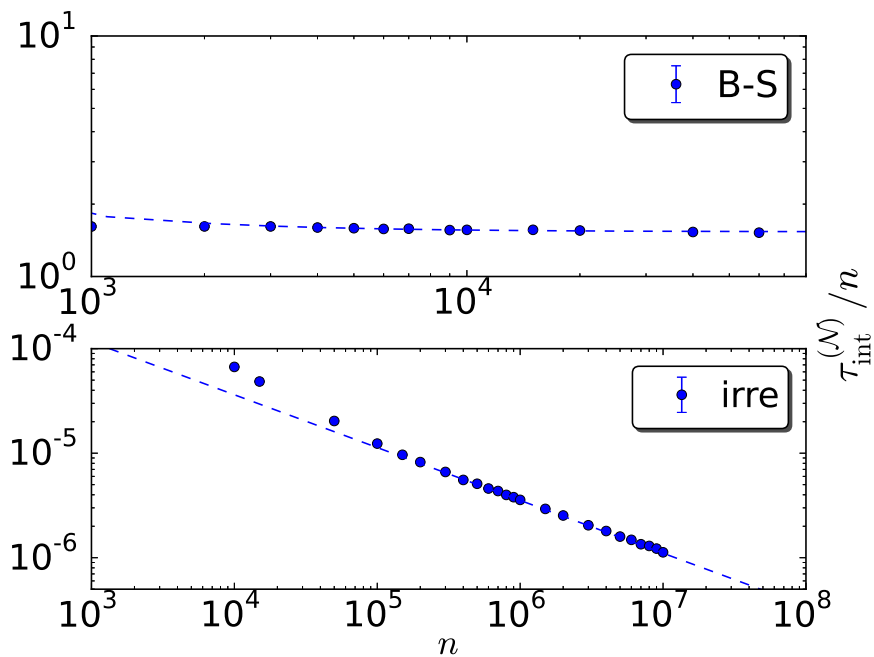


Figure 4.3: Finite-size scaling of $\tau_{\text{int}}^{(\mathcal{N})}/n$ for the B-S type worm algorithm (upper panel) and lifted worm algorithm (lower panel) on the complete graph with n vertices. The dashed lines correspond to the fits in Sec. 4.2.

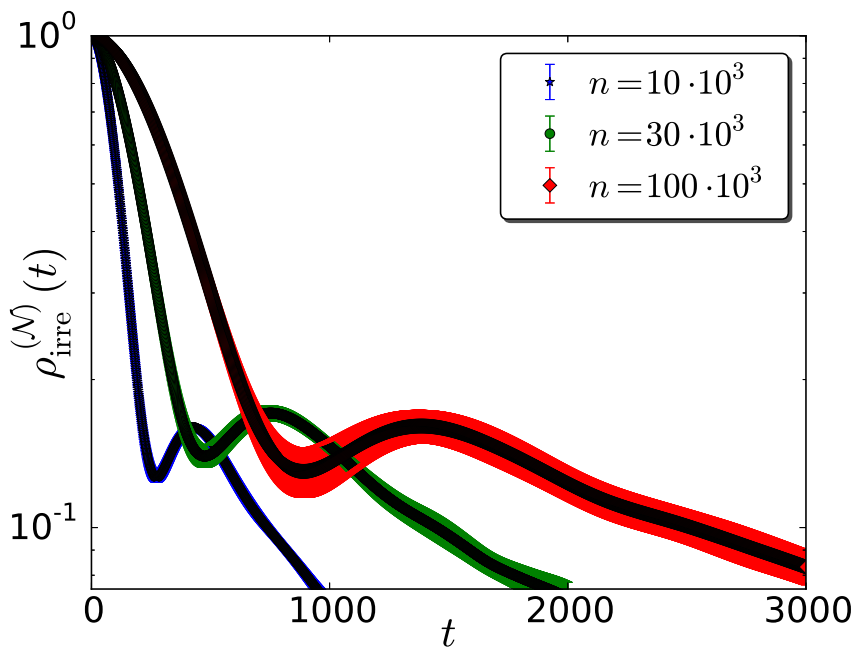


Figure 4.4: Normalized autocorrelation function $\rho_{\text{irre}}^{(\mathcal{N})}(t)$ (t in MC hits) for the lifted worm algorithm on the complete graph with n vertices. The blue (left) curve corresponds to $n = 10 \cdot 10^3$, the green (middle) curve corresponds to $n = 30 \cdot 10^3$, and the red (right) curve corresponds to $n = 100 \cdot 10^3$. As stated in Sec. 4.2, $\rho_{\text{irre}}^{(\mathcal{N})}(t)$ is well described by the ansatz in Eq. (4.2).

Outlook

We constructed an irreversible MCMC worm algorithm for the zero-field ferromagnetic Ising model via the lifting technique. Since it is not obvious how to lift the standard P-S worm algorithm to generate ballistic motion for the number of occupied edges, we first constructed an alternative worm algorithm with different proposals (B-S type) and lifted this chain. We emphasize that this construction can also be used to design lifted worm algorithms for other important models in statistical mechanics such as the XY model. The XY model shares many universal properties of the Bose-Hubbard model [38] which is actively studied in ultracold atom physics. We also emphasize that the lifted worm algorithm for the Ising model can be implemented by changing only a few code lines in the B-S type worm algorithm.

We studied the dynamical critical behavior of the number of occupied edges \mathcal{N} on both the complete graph and toroidal grids in various dimensions. On the complete graph we numerically established $z_{\text{int,irre},\mathcal{N}} \approx -0.5$ for the lifted worm algorithm, while we found $z_{\text{int,B-S},\mathcal{N}} \approx 0$ for the corresponding reversible counterpart. It is interesting to observe that the mixing time of the Swendsen-Wang algorithm scales as $t_{\text{mix}}/n \sim n^{1/4}$ [39]. On the torus we numerically established that the lifted chain leads to a constant improvement with larger improvements for higher dimensions. Even though we did not find a dynamic improvement for $d \leq 5$, it is an open question if \mathcal{N} exhibits critical speeding-up on higher dimensional tori.

We also studied the return time to the Eulerian subspace \mathcal{C}_0 . We find that while

the mean is the same in both the lifted and unlifted processes, the variance is a constant factor smaller in the lifted version.

Finally, we note that a recent study [40] constructed an alternative irreversible worm algorithm which is based on the so-called geometric allocation approach [12]. Similar to our findings, this irreversible worm algorithm does not improve the dynamical critical exponent for \mathcal{N} on the three-dimensional torus, but leads to a significant constant improvement.

Appendix

A.1 Estimation with the Madras-Sokal automatic windowing algorithm and suppressed slow modes

A widely used numerical method to estimate the integrated autocorrelation time of a weakly stationary time series [42] is to consider a truncated version of (3.2), i.e.

$$\widehat{\tau}_{\text{int}}^{(\mathcal{N})}(n) := \frac{1}{2} + \sum_{t=1}^n \rho^{(\mathcal{N})}(t). \quad (\text{A.1})$$

The reason for truncating the time series is well known [42, 34]: The standard deviation of (A.1) is $O(\sqrt{n/M})$, and, hence, (for fixed M) grows with n . The choice of n is, thus, a compromise between bias and standard-error. The Madras-Sokal automatic windowing method determines n self-consistently as the smallest positive integer n that fulfils (numerically)

$$c\tau_{\text{int}}^{(\mathcal{N})}(n) \leq n$$

where c is a free real parameter, typically manually chosen to lie in $[6, 10]$, c.f. [34] for a justification of this particular choice of c .

While analysing the time series for \mathcal{N} for the lifted worm algorithm in $d \geq 4$ we made the observation that the choice $c \in [6, 10]$ significantly underestimates the integrated autocorrelation time. Intuitively, what we implement with (A.1) is a ‘discrete integration’ which we utilise to extract the decay constant (the analogue of the relation $\int_0^\infty dx e^{-x/\tau} = \tau$ in a continuous setting). However, in our setting we only obtain a significant contribution from $\alpha_1 e^{-t/\tau_1}$ to (A.1) when including lags for which the contribution of $\alpha_2 e^{-t/\tau_2}$ to $\rho^{(\mathcal{N})}(t)$ is too small to be separated from noise. The combination of small amplitude and large time scale, thus, requires adjusting c . In Figure A.1 we illustrate this for the particular choice of $L = 56$ of the lifted worm algorithm in $d=5$.

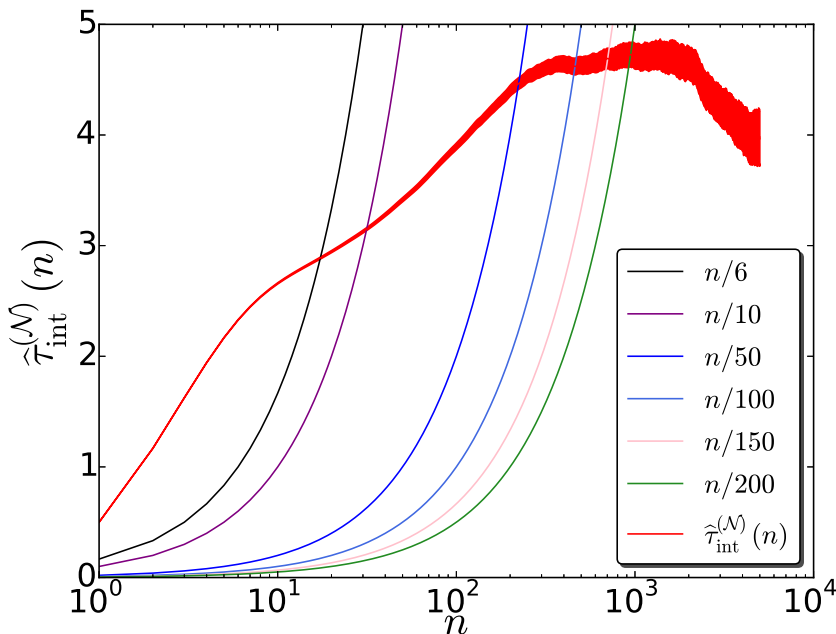


Figure A.1: Dependence on the cut-off time n of the truncated integration autocorrelation time $\hat{\tau}_{\text{int}}^{(\mathcal{N})}(n)$ defined in A.1 for the lifted worm algorithm in five dimensions and $L = 56$ at criticality. The thick red line shows $\hat{\tau}_{\text{int}}^{(\mathcal{N})}(n)$ averaged over 100 independent runs, whereas the surrounding region corresponds to $\pm 1\sigma$. The thin lines correspond to the curves n/c with increasing c from left ($c = 6$) to right ($c = 200$). One clearly sees how $n < 100$ underestimates $\hat{\tau}_{\text{int}}^{(\mathcal{N})}(n)$ and much larger n are required to capture contributions corresponding to the suppressed mode.

A.2 Least square fitting a weighted exponential ansatz

While fitting the normalised autocorrelation function for \mathcal{N} in dimensions four and five we made the observation that it is numerically very hard to obtain reliable

estimates of the parameters involved in a functional model of the two-time scale behavior using the method of least squares. We, therefore, manually analysed the least square conditions. As result of this we were able to reduce the free parameters which we need to numerically minimise from 4 to 2. This significantly improved the numerical precision and stability of the fitting procedure. To this end, our model has free parameters $\alpha_1 > 0, \alpha_2 > 0, 1 > \lambda_1 > 0, 1 > \lambda_2 > 0$ and we would like to minimise the sum of the first T_{\max} squared residuals

$$r_k^2 \equiv \left[\alpha_1 \lambda_1^k + \alpha_2 \lambda_2^k - \rho_{\mathcal{N}}(k) \right]^2,$$

that is our goal is to minimise the function Θ defined as

$$\Theta(\alpha_1, \alpha_2, \lambda_1, \lambda_2) \equiv \sum_{k=0}^{T_{\max}-1} r_k^2$$

A necessary condition for the minimum is

$$\frac{\partial \Theta}{\partial \alpha_1} = \frac{\partial \Theta}{\partial \alpha_2} = \frac{\partial \Theta}{\partial \lambda_1} = \frac{\partial \Theta}{\partial \lambda_2} = 0$$

We start by evaluating the partial derivatives w.r.t. α_1 and α_2 and a consequence of this obtain the following set of two linear equations

$$\begin{aligned} \alpha_1 P(\lambda_1) + \alpha_2 S(\lambda_1, \lambda_2) &= Q(\lambda_1), \\ \alpha_1 S(\lambda_1, \lambda_2) + \alpha_2 P(\lambda_2) &= Q(\lambda_2). \end{aligned}$$

Here we defined the following three polynomials over $(0, 1)$ or $(0, 1)^2$:

$$\begin{aligned} P(\lambda) &\equiv \sum_{k=0}^{T_{\max}-1} \lambda^{2k} = \frac{\lambda^{2T_{\max}} - 1}{\lambda^2 - 1} \\ Q(\lambda) &\equiv \sum_{k=0}^{T_{\max}-1} \lambda^k \rho_{\mathcal{N}}(k) \\ S(\lambda_1, \lambda_2) &\equiv \sum_{k=0}^{T_{\max}-1} \lambda_1^k \lambda_2^k \end{aligned}$$

Note that S is symmetric in λ_1, λ_2 . The above set of linear equations has the unique

solution:

$$\alpha_1(\lambda_1, \lambda_2) = \frac{S(\lambda_1, \lambda_2)Q(\lambda_2) - Q(\lambda_1)P(\lambda_2)}{S(\lambda_1, \lambda_2)^2 - P(\lambda_1)P(\lambda_2)}$$

and $\alpha_2(\lambda_1, \lambda_2)$ is obtained by replacing $1 \rightarrow 2, 2 \rightarrow 1$ in the r.h.s. above. Thus, this allows us to substitute α_1, α_2 as a function of λ_1, λ_2 in Θ and minimise Θ only w.r.t. to λ_1, λ_2 , with the constraints that $\lambda_1, \lambda_2 \in (0, 1)$. We remark, that completely analogous arguments can be used to show that a similar improvement can be achieved for a general ansatz $\sum_{j=1}^n \alpha_j \lambda_j^t$, where one reduces the parameters to numerically minimise from $2n$ to n . The calculations done here generalise the method very recently proposed in [41] for a single exponential ansatz.

Bibliography

- [1] I. Goodfellow, Y. Bengio and A. Courville, *Deep Learning*, MIT press, (2016).
- [2] B. Efron, T. Hastie, *Computer Age Statistical Inference*, Cambridge University Press, Volume 5, (2016).
- [3] N. Metropolis, A. W. Rosenbluth, M. N. Rosenbluth, A. H. Teller, E. Teller, *Equations of state calculations by fast computing machines*, J. Chem. Phys. 21, 1087 (1953).
- [4] W. Janke, *Monte Carlo Methods in Classical Statistical Physics*, in Computational Many-Particle Physics, Lect. Notes Phys., Vol. 739, Springer-Verlag, Berlin (2008).
- [5] N. Prokof'ev, B. Svistunov, *Worm Algorithms for Classical Statistical Models*, Phys. Rev. Lett. 87, 160601 (2001).
- [6] M. Boninsegni, N. Prokof'ev, B. Svistunov, *Worm Algorithm for Continuous-space Path Integral Monte Carlo Simulations*, Phys. Rev. Lett. 96, 070601 (2006).
- [7] U. Wolff, *Collective Monte Carlo Updating for Spin Systems*, Phys. Rev. Lett., 62 (4): 361 (1989)
- [8] R. H. Swendsen, J.-S. Wang, *Nonuniversal critical dynamics in Monte Carlo simulations*, Phys. Rev. Lett., 58(2): 86–88 (1987)
- [9] Y. Deng, T. M. Garoni, A. Sokal, *Dynamic critical behavior of the worm algorithm for the Ising model*, Phys. Rev. Lett. 99, 110601 (2007).
- [10] U. Wolff, *Simulating the all-order strong coupling expansion I: Ising model demo*, Nucl. Phys. B, 810, 491 (2009).
- [11] A. Collecchio, T. M. Garoni, T. Hyndman, D. Tokarev, *The worm process for the Ising model is rapidly mixing*, Journal of Statistical Physics 164, 1082-1102

- (2016).
- [12] H. Suwa, S. Todo, *Markov Chain Monte Carlo Method without Detailed Balance*, Phys. Rev. Lett. 105, 120603 (2010).
 - [13] T. P. Hayes, A. Sinclair, *Liftings of Tree-Structured Markov Chains*, Conference: Approximation, Randomization, and Combinatorial Optimization. Algorithms and Techniques, 13th International Workshop, APPROX 2010, and 14th International Workshop, RANDOM 2010, Barcelona, Spain, September 1-3, (2010).
 - [14] K. Turitsyn, M. Chertkov, M. Vucelja, *Irreversible Monte Carlo algorithms for efficient sampling*, Physica D 240, 410-414 (2011).
 - [15] Y. Sakai, K. Hukushima, *Dynamics of one-dimensional Ising model without detailed balance condition*, J. Phys. Soc. Japan 82, 064003-1-8 (2013).
 - [16] H. C. M. Fernandes, M. Weigel, *Non-reversible Monte Carlo simulations of spin models*, Computer Physics Communications 182, 1856 (2011).
 - [17] E. Bernard, W. Krauth, D. Wilson, *Event-chain Monte Carlo algorithms for hard-sphere systems*, Phys. Rev. E 80, 056704 (2009).
 - [18] M. Engel, J. A. Anderson, S. C. Glotzer, M. Isobe, E. P. Bernard, W. Krauth, *Hard-disk equation of state: First-order liquid-hexatic transition in two dimensions with three simulation methods*, Phys. Rev. E 87, 042134 (2013).
 - [19] S. C. Kapfer, W. Krauth, *Soft-disk melting: From liquid-hexatic coexistence to continuous transitions*, Phys. Rev. Lett. 114, 035702 (2015).
 - [20] M. Michel, J. Mayer, W. Krauth, *Event-chain Monte Carlo for classical continuous spin models*, EPL 112, 20003 (2015).
 - [21] Y. Nishikawa, M. Michel, W. Krauth, K. Hukushima, *Event-chain algorithm for the Heisenberg model: Evidence for $z \sim 1$ dynamic scaling*, Phys. Rev. E 92, 063306 (2015).
 - [22] H. Hu, X. Chen, Y. Deng, *Irreversible Markov chain Monte Carlo algorithm for self-avoiding walk*, Frontiers of Physics, 12:120503, (2017).
 - [23] P. Diaconis, S. Holmes, R. M. Neal, *Analysis of a nonreversible Markov chain sampler*, Ann. Appl. Probab. Volume 10, Number 3, 726-752 (2000).
 - [24] P. Diaconis, *Some things we've learned (about Markov chain Monte Carlo)*, Bernoulli 19 1294–1305, (2013).
 - [25] M. Vucelja, *Lifting - A nonreversible Markov chain Monte Carlo algorithm*, American Journal of Physics 84, 958 (2016).
 - [26] Y. Deng, T. M. Garoni, A. D. Sokal, *Critical Speeding-Up in the Local Dynamics*

- of the Random-Cluster Model*, Phys. Rev. Lett. 98 230602, (2007).
- [27] Y. Pomeau, M. Le Berre, *Critical speed-up vs critical slow-down: a new kind of relaxation oscillation with application to stick-slip phenomena*, arXiv:1107.3331, (2011).
- [28] C. J. Thompson, *Mathematical Statistical Mechanics*, Princeton University Press (1979).
- [29] A. Berretti, A. D. Sokal, *New Monte Carlo method for the self-avoiding walk*, J. Stat. Phys. 40, 483 (1985).
- [30] R. J. Baxter, *Exactly solved models in statistical mechanics*, London: Academic Press Inc. [Harcourt Brace Jovanovich Publishers] (1982).
- [31] Y. Deng, H. W. J. Blöte, *Simultaneous analysis of several models in the three-dimensional Ising universality class*, Phys. Rev. E 68, 036125 (2003).
- [32] P. H. Lundow, K. Markström, *Critical behaviour of the Ising model on the 4-dimensional lattice*, Phys. Rev. E 80, 031104 (2009).
- [33] P. Young, *Everything You Wanted to Know About Data Analysis and Fitting but Were Afraid to Ask*, SpringerBriefs (2015).
- [34] A. D. Sokal, *Monte Carlo Methods in Statistical Mechanics: Foundations and New Algorithms*, Lectures at the Cargèse Summer School on ‘Functional Integration: Basics and Applications’ (1996).
- [35] P. H. Lundow, K. Markström, *Finite size scaling of the 5D Ising model with free boundary conditions*, Nucl. Phys. B, vol 889, p249 (2014).
- [36] N. Madras, G. Slade, *The Self-Avoiding Walk*, Birkhäuser, Boston (1996).
- [37] Eren M. Elçi, Private communications
- [38] B. Svistunov, E. Babaev, N. Prokof’ev, *Superfluid States of Matter*, CRC Press, Boca Raton (2015).
- [39] Y. Long, *Mixing Time of the Swendsen-Wang Dynamics on the Complete Graph and Trees*, Ph.D. Thesis, UC Berkeley (2009).
- [40] H. Suwa, *Directed Worm Algorithm with Geometric Optimization*, arXiv:1703.03136 [cond-mat.stat-mech] (2017).
- [41] Y. Fang, Y. Cao and R. D. Skeel, *Quasi-Reliable Estimates of Effective Sample Size*, arXiv:1705.03831, (2017).
- [42] M. B. Priestley, *Spectral analysis and time series*: Academic Press Inc. (1981)

Glossary

L : Side length of a box.

χ : Susceptibility.

\mathbb{R}^+ : $= \{x \in \mathbb{R} : x > 0\}$.

\mathbb{Z}^+ : $= \{x \in \mathbb{Z} : x > 0\}$.

\mathbb{Z}^- : $= \{x \in \mathbb{Z} : x < 0\}$.

\mathcal{N} : Walk length (part 1), Number of occupied edges (part 2).

\mathcal{W} : Winding number (part 1), lifted state space (part 2).

ρ : autocorrelation function.

τ_{exp} : exponential autocorrelation time.

τ_{int} : integrated autocorrelation time.

\tilde{g} : unwrapped Green's / unwrapped two-point function.

$f(x) = O(g(x))$: Let f, g be real valued functions such that $g(x)$ is strictly positive for large enough values of x . Then, $f(x) = O(g(x))$ if there exists $c > 0$ and $x_0 \in \mathbb{R}$ such that $|f(x)| \leq cg(x)$ for all $x > x_0$.

$f(x) = \Omega(g(x))$: Let f, g be real valued functions such that $g(x)$ is strictly positive for large enough values of x . Then, $f(x) = \Omega(g(x))$ if there exists a $c > 0$ and $x_0 \in \mathbb{R}$ such that $f(x) \geq cg(x)$ for all $x > x_0$.

$f(x) = \Theta(g(x))$: Let f, g be real valued functions such that $g(x)$ is strictly positive for large enough values of x . Then, $f(x) = \Theta(g(x))$ if there exists positive constants $c_1, c_2 > 0$ and $x_0 \in \mathbb{R}$ such that $c_1g(x) \leq f(x) \leq c_2g(x)$ for all $x > x_0$.

$f(x) = \omega(g(x))$: Let f, g be real valued functions such that $g(x)$ is strictly positive for large enough values of x . Then, $f(x) = \omega(g(x))$ if for all $c > 0$ there exists

$x_0 \in \mathbb{R}$ such that $|f(x)| \geq c|g(x)|$ for all $x > x_0$.

$f(x) \asymp g(x)$: $f(x) \asymp g(x)$ if there exists constants $c_1, c_2, x_0 \in \mathbb{R}$ such that $c_1g(x) \leq f(x) \leq c_2g(x)$ for all $x > x_0$.

$f(x) \sim g(x)$: $f(x) \sim g(x)$ if $\lim_{x \rightarrow \infty} f(x)/g(x) = 1$.

$f(x) = o(g(x))$: Let f, g be real valued functions such that $g(x)$ is strictly positive for large enough values of x . Then, $f(x) = o(g(x))$ if for every constant $c > 0$ there exists a constant $x_0 \in \mathbb{R}$ such that $|f(x)| \leq cg(x)$ for all $x > x_0$.

g : Green's / two-point function.

z : fugacity (part 1), dynamic critical exponent (part 2).

B-S algorithm: Berretti-Sokal algorithm.

FBC: Free boundary conditions.

FSS: Finite-size Scaling.

HBC: Holding boundary conditions.

MCMC: Markov-chain Monte Carlo.

P-S worm algorithm: Prokof'ev-Svistunov worm algorithm.

PBC: Periodic boundary conditions.

RBC: Reflective boundary conditions.

RLERW: Random-length Loop-erased Random Walk.

RLRW: Random-length Random Walk.

SAW: Self-avoiding Walk.

List of Figures

2.1	Illustration of a SRW and the corresponding transition probabilities with reflective and holding boundary conditions on a square lattice	11
2.2	Illustration of a SRW on a two-dimensional torus	11
2.3	Illustration of a RLLERW on a two-dimensional torus	12
3.1	Critical PBC scaling of the mean walk length $\langle \mathcal{N}_{\text{SAW}} \rangle$ and susceptibility $\chi_{\text{Ising,SAW}}$ in five dimensions	45
3.2	Critical two-point functions of the SAW and Ising models, and Green's function of a RLLERW with mean walk length $L^{d/2}$ in five dimensions	46
3.3	Average winding number, $\langle \mathcal{W} \rangle$, for Ising and SAW models, and for a RLLERW with mean walk length $L^{d/2}$ on periodic boundaries at criticality	48
3.4	Unwrapped critical two-point function of SAW, and unwrapped Green's function of a RLLERW with mean walk length $L^{d/2}$ on five-dimensional lattices with periodic boundaries	49
3.5	Pseudo-critical two-point functions of the SAW and Ising models for $\lambda = 1, 3/2$, and Green's function of a RLLERW with mean walk length $L, L^{3/2}$	52
3.6	Pseudo-critical two-point functions of the SAW and Ising models for $\lambda = 2$ and Green's function of a RLLERW with mean walk length L^2	53
3.7	FSS behaviour of the mean walk length $\langle \mathcal{N}_{\text{SAW}} \rangle$ and the susceptibility $\chi_{\text{Ising,SAW}}$ on periodic and free boundaries in five dimensions	54
4.1	Illustration: Mapping of a SRW on the torus to a SRW on the box with reflective boundaries	56
4.2	Illustration: Mapping of a SRW on the torus to a SRW on the box with holding boundaries	57
4.3	Critical FBC scaling of the mean walk length $\langle \mathcal{N}_{\text{SAW}} \rangle$ and susceptibility $\chi_{\text{Ising,SAW}}$ in five dimensions	64
4.4	Critical FBC scaling of the two-point functions of the SAW and Ising model on five-dimensional lattices	65

4.5	Green's function of a RLLERW with mean walk length $L^{1.5}$ on five-dimensional hypercubic lattices with free boundaries	66
4.6	Appropriately scaled Green's function of a RLLERW with mean walk length L^2 on five-dimensional hypercubic lattices with free boundaries	67
4.7	Appropriately scaled Green's function of a RLLERW with mean walk length $L^{5/2}$ on five-dimensional hypercubic lattices with free boundaries	67
4.8	Two-point functions of the Ising model and SAW on five-dimensional hypercubic lattices with free boundaries at $z_L = z_c + a(L)L^{-2}$	68
4.9	FBC behaviour of the mean walk length $\langle \mathcal{N}_{\text{SAW}} \rangle$ at $z_L = z_c + a(L)L^{-2}$	69
2.1	Illustration of a worm configuration	83
4.1	Comparison of the integrated autocorrelation time among the P-S, B-S type and lifted worm algorithm	90
4.2	Normalized autocorrelation function $\rho_{\text{irre}}^{(\mathcal{N})}(t)$ (t in MC hits) for the irreversible worm algorithm in five dimensions	91
4.3	Finite-size scaling of $\tau_{\text{int}}^{(\mathcal{N})}/n$ for the B-S type worm algorithm and lifted worm algorithm on the complete graph with n vertices	92
4.4	Normalized autocorrelation function $\rho_{\text{irre}}^{(\mathcal{N})}(t)$ (t in MC hits) for the lifted worm algorithm on the complete graph with n vertices	92
A.1	Dependence on the cut-off time n of the truncated integration autocorrelation time $\widehat{\tau}_{\text{int}}^{(\mathcal{N})}(n)$	96

